NASA/CR—2018–219897

Examining the Conceptual Design Process for Future Hybrid-Electric Rotorcraft

Reed A. Danis, Michael W. Green, and Jeffrey L. Freeman
Empirical Systems Aerospace, Inc.
San Luis Obispo, California

David W. Hall
DHC Engineering
San Mateo, California

May 2018

NASA STI Program ... in Profile

Since its founding, NASA has been dedicated to the advancement of aeronautics and space science. The NASA scientific and technical information (STI) program plays a key part in helping NASA maintain this important role.

The NASA STI program operates under the auspices of the Agency Chief Information Officer. It collects, organizes, provides for archiving, and disseminates NASA's STI. The NASA STI program provides access to the NTRS Registered and its public interface, the NASA Technical Reports Server, thus providing one of the largest collections of aeronautical and space science STI in the world. Results are published in both non-NASA channels and by NASA in the NASA STI Report Series, which includes the following report types:

- TECHNICAL PUBLICATION. Reports of completed research or a major significant phase of research that present the results of NASA Programs and include extensive data or theoretical analysis. Includes compilations of significant scientific and technical data and information deemed to be of continuing reference value. NASA counterpart of peer-reviewed formal professional papers but has less stringent limitations on manuscript length and extent of graphic presentations.

- TECHNICAL MEMORANDUM. Scientific and technical findings that are preliminary or of specialized interest, e.g., quick release reports, working papers, and bibliographies that contain minimal annotation. Does not contain extensive analysis.

- CONTRACTOR REPORT. Scientific and technical findings by NASA-sponsored contractors and grantees.

- CONFERENCE PUBLICATION. Collected papers from scientific and technical conferences, symposia, seminars, or other meetings sponsored or co-sponsored by NASA.

- SPECIAL PUBLICATION. Scientific, technical, or historical information from NASA programs, projects, and missions, often concerned with subjects having substantial public interest.

- TECHNICAL TRANSLATION. English-language translations of foreign scientific and technical material pertinent to NASA's mission.

Specialized services also include organizing and publishing research results, distributing specialized research announcements and feeds, providing information desk and personal search support, and enabling data exchange services.

For more information about the NASA STI program, see the following:

- Access the NASA STI program home page at http://www.sti.nasa.gov

- E-mail your question to help@sti.nasa.gov

- Phone the NASA STI Information Desk at 757-864-9658

- Write to:
  NASA STI Information Desk
  Mail Stop 148
  NASA Langley Research Center
  Hampton, VA 23681-2199

NASA/CR—2018–219897

Examining the Conceptual Design Process for Future Hybrid-Electric Rotorcraft

Reed A. Danis, Michael W. Green, and Jeffrey L. Freeman
Empirical Systems Aerospace, Inc.
San Luis Obispo, California

David W. Hall
DHC Engineering
San Mateo, California

National Aeronautics and
Space Administration

Ames Research Center
Moffett Field, CA 94035-1000

May 2018

Acknowledgments

The work described in this report was performed under a NASA Small Business Innovative Research Phase II contract overseen by Gloria Yamauchi, the Contracting Officer Representative from NASA Ames Research Center. The authors of this report extend their sincere gratitude for her ongoing support during the effort. The authors also thank Wayne Johnson and Chris Silva, also from NASA Ames Research Center, for their technical support and guidance, and for providing several rotorcraft models on which many of the studies were based. The authors also extend their gratitude to the dedicated team members and collaborators who supported this effort including ESAero members Benjamin Pham, Daniel Soto, Daniel Stalters, Colin Wilson, and Frank Zhang, and LaunchPoint Technologies members Brad Paden and Michael Ricci.

Available from:

NASA STI Support Services
Mail Stop 148
NASA Langley Research Center
Hampton, VA 23681-2199
757-864-9658

National Technical Information Service
5301 Shawnee Road
Alexandria, VA 22312
webmail@ntis.gov
703-605-6000

This report is also available in electronic form at
http://ntrs.nasa.gov

Table of Contents

List of Figures iv
List of Tables vi
Nomenclature vii
Summary 1
1. Introduction 1
2. Background 2
2.1 Potential Advantages of Hybrid-Electric Aircraft 2
2.2 Hybrid-Electric Aircraft Design Challenges 3
3. Propulsion Architecture Trade Studies 4
3.1 Trade Study Methodology 4
3.2 Supporting Tools and Concepts Development 6
3.2.1 PANTHER 6
3.2.2 Endurance Indicator and Range Indicator 11
3.2.3 Energy Flow vs. Airspeed Plots 12
3.3 Trade Study Vehicles 13
3.3.1 Development and Calibration of Conventionally Powered Helicopter Models 14
3.3.2 Development and Calibration of Conventionally Powered Tiltrotor Model 18
3.3.3 Modification to Sizing Conditions for Hybrid Helicopter Development 20
3.3.4 Modification to Sizing Conditions for Hybrid Tiltrotor Development 21
3.3.5 Trade Study Design Missions 22
3.3.6 Development of Hybrid-Electric Vehicles 23
3.4 Results 25
3.4.1 Comparison of Configuration A Vehicles 25
3.4.2 Comparison of Configuration B Vehicles 27
3.4.3 Comparison of Tiltrotor Configuration Vehicles 28
3.4.4 Impact of Imposing Redundant Capability Sizing Requirements 29
3.4.5 Impact of Future Technology Improvements 31
3.5 Lessons Learned 34
3.5.1 Design Frontiers for Fixed-Weight and Low-Weight Energy Source Powered Vehicles 34
3.5.2 Impact of Power Distribution Control Methods on Hybrid-Electric Vehicle Design 34
3.5.3 Defining Redundancy Requirements and Regulatory Considerations 39
3.5.4 Impact of Future Hybrid Propulsion Technology 39
4. Demonstrator Vehicle 39
4.1 Concept and Vehicle Selection 41
4.2 Application of Hybrid-Electric Design Methodology 42
4.2.1 Development of Point Performance Requirements 42
4.2.2 Development of Mission Performance Requirements 43
4.3 On-Design Sizing of Demonstrator Vehicle 44
4.3.1 Propulsion Component Sizing 45
4.3.2 Thermal Management System Sizing 46
4.3.3 Weight Statement 49
4.4 Vehicle Performance Simulation 49
4.4.1 Performance Plots 49
4.4.2 Mission Performance 53
4.5 Hybrid-Electric Powertrain Integration 58
4.5.1 Development of Airframe Solid Model 58
4.5.2 Design of Propulsor Nacelles 58
4.5.3 Powertrain and Thermal Management System Integration 62
4.5.4 Completed Hybrid XV-15 Solid Model 64
4.6 Lessons Learned 69
4.6.1 Vehicle Mission Planning Complexity 69
4.6.2 Thermal Management 69
4.6.3 Airframe Integration Challenges 69
5. Conclusion 70
6. References 71

List of Figures

Figure 1. NASA X-57 Distributed Propulsion All-Electric Flight Demonstrator. 2
Figure 2. Flowchart of Trade Study Staged Approach. 5
Figure 3. PANTHER On-Design Framework. 6
Figure 4. PANTHER Off-Design Framework. 7
Figure 5. PANTHER UH-60A Model. 9
Figure 6. PANTHER UH-60 Model Required Rotor Power Compared to NDARC Predictions and Flight Test Data. 9
Figure 7. XV-15 PANTHER Model. 10
Figure 8. PANTHER XV-15 Model Required Rotor Power and Vehicle Pitch Attitude Compared to NDARC Model Predictions and Flight Test Data. 10
Figure 9. Example Energy Flow vs. Airspeed Charts; (a) Conventional Helicopter, (b) Hybrid-Electric Helicopter. 13
Figure 10. Example Endurance Indicator (top) and Range Indicator (bottom) Charts; (a) Conventional Helicopter, (b) Hybrid-Electric Helicopter. 13
Figure 11. Component and Connector Icons. 14
Figure 12. Propulsion Architecture and Group Weights for the Baseline Configuration A Vehicle. 15
Figure 13. Propulsion Architecture and Group Weights for the Baseline Configuration B Vehicle. 15
Figure 14. Configuration A Baseline Vehicle Calibration Mission Profile. 16
Figure 15. Configuration B Baseline Vehicle Calibration Mission Profile. 16
Figure 16. Propulsion Architecture and Group Weights for the Baseline Tiltrotor Vehicle. 18
Figure 17. Comparison of PANTHER Tiltrotor Vehicle Endurance to XV-15 Flight Test Data. 20
Figure 18. Mission Profile Used to Compare Hybrid-Electric Vehicle Performance. 22
Figure 19. Configuration A Battery-Boosted Gas Turbine Vehicle Payload-Range Performance. 25
Figure 20. Configuration A Battery and Fuel Cell Vehicle Payload-Range Performance. 26
Figure 21. Configuration A Diesel Vehicle Payload-Range Performance. 27
Figure 22. Configuration B Vehicle Payload-Range Performance. 28
Figure 23. Tiltrotor Vehicle Payload-Range Performance. 29
Figure 24. Category A Rotorcraft OEI Takeoff Profile. 30
Figure 25. Payload-Range Diagram for C.B-BBT Vehicles With Different Levels of Redundant Capability. 31
Figure 26. Projected Future Configuration A Vehicle Mission Performance. 33
Figure 27. Projected Future Tiltrotor Vehicle Mission Performance. 33
Figure 28. Design Frontier and Specific Design Points for Configuration A Battery and Fuel Cell Vehicles. 35
Figure 29. Energy Flow Diagram of Configuration A Baseline. 35
Figure 30. Endurance and Range Indicators for Configuration A Baseline. 36
Figure 31. Energy Flow in Cruise of Configuration A Battery-Boosted Turbine Hybrid. 37
Figure 32. Endurance and Range Indicators for Configuration A Battery-Boosted Turbine Hybrid. 37
Figure 33. Energy Flow in Cruise of Configuration A Battery-Boosted Turbine Hybrid, Maximum Battery Charge Rate. 38
Figure 34. Hybrid XV-15 Propulsion Architecture Schematic With Component Performance. 46
Figure 35. Hybrid XV-15 Concept Demonstrator TMS Architecture. 48
Figure 36. Hybrid XV-15 Sea Level Energy Flow vs. Airspeed. 50
Figure 37. Hybrid XV-15 Sea Level Endurance and Range Indicators vs. Airspeed. 50
Figure 38. Hybrid XV-15 Cruise Altitude Energy Flow vs. Airspeed. 51
Figure 39. Hybrid XV-15 Cruise Altitude Endurance and Range Indicators vs. Airspeed. 51
Figure 40. Hybrid XV-15 Hover Ceilings. 52

Figure 41. Hybrid XV-15 Maximum Rate of Climb vs. Altitude. 53
Figure 42. Nominal, Maximum-Effort Mission Power and Energy Usage. 54
Figure 43. Contingency—Engine Failure on Takeoff Design Mission Power and Energy Usage. 55
Figure 44. Contingency—Engine Failure During Cruise Design Mission Power and Energy Usage. 57
Figure 45. Contingency—Engine Failure During Cruise Design Mission Port Engine Power Ratings. 57
Figure 46. XV-15 Three-View Drawing Created From Smaller Drawings (ref. 7). 59
Figure 47. XV-15 Nacelle Inboard Profile (ref. 7). 59
Figure 48. XV-15 Inboard Profiles (ref. 7). 60
Figure 49. Side Views of Final Nacelle Iteration (ref. 7). 60
Figure 50. Top (top) and Left Side (bottom) Views of Final Nacelle Iteration With Cooling and Electrical Runs. 61
Figure 51. Isometric View of Final Nacelle Powertrain Iteration. 61
Figure 52. Side View of Integrated Final Nacelle Iteration. 62
Figure 53. Left Side of Fuselage Showing Locations of Powertrain Components. 63
Figure 54. Isometric View of Powertrain Components in Nacelles and Fuselage. 63
Figure 55. Top and Bottom Views of Hybrid XV-15 Solid Model. 64
Figure 56. Left and Right Side Views of Hybrid XV-15 Solid Model. 65
Figure 57. Front and Back Views of Hybrid XV-15 Solid Model. 66
Figure 58. Trimetric and Isometric Views of Hybrid XV-15. 67
Figure 59. Isometric View With Labeling of Components in Fuselage. 68
Figure 60. Screenshot of Hybrid XV-15 Large-Scale Drawing. 68

List of Tables

Table 1. PANTHER and NDARC Configuration A Calibration Mission Performance. 17
Table 2. PANTHER and NDARC Configuration B Calibration Mission Performance. 17
Table 3. Point Performance Sizing Conditions for the Hybrid-Electric Configuration A Vehicles. 21
Table 4. Point Performance Sizing Conditions for the Hybrid-Electric Configuration B Vehicles. 21
Table 5. Point Performance Sizing Conditions for the Hybrid-Electric Tiltrotor Vehicles. 22
Table 6. List of Trade Study PANTHER Vehicles. 23
Table 7. Point Performance Flight Condition Requirements for Sizing Baseline Tiltrotor Vehicle. 30
Table 8. Future Technology Scaling Factors. 32
Table 9. Summary of Hybrid XV-15 Demonstrator Vehicle Compared to the Original NASA XV-15. 40
Table 10. Hybrid XV-15 Design Point. 42
Table 11. Hybrid XV-15 Sizing Flight Conditions. 43
Table 12. Nominal, Maximum-Effort Design Mission Segments. 44
Table 13. Contingency Design Mission Segments. 44
Table 14. Hybrid XV-15 Propulsion Component Performance. 45
Table 15. Conventional and Hybrid-Electric Transmission System Heat Generation Under FC #7. 47
Table 16. Hybrid XV-15 Concept Demonstrator TMS Weight Breakdown. 48
Table 17. Hybrid XV-15 Vehicle Weight Breakdown. 49
Table 18. Nominal, Maximum-Effort Design Mission. 53
Table 19. Contingency—Engine Failure on Takeoff Design Mission. 54
Table 20. Contingency—Engine Failure During Cruise Mission up to Engine Failure Point. 55
Table 21. Contingency—Engine Failure During Cruise, Complete Mission. 56

Nomenclature

AEO	all engines operational
C	c-rate, rate at which an energy source is discharged relative to its design capacity
CAD	computer-aided design
COTS	commercial off-the-shelf (product)
CTO	continued takeoff
ΔT_{amb}	temperature offset from standard atmosphere
DGW	design gross weight
E_{design}	energy source design capacity
$\dot{E}$	energy flow rate (power)
EI_i	endurance indicator of single energy source
$EI_{vehicle}$	endurance indicator of overall vehicle
FAR	Federal Aviation Regulation
FC	flight condition
$fillfrac_i$	ratio of an energy source's current energy to its design energy capacity
fpm	feet per minute
HEx	heat exchanger
HOGE	hover out of ground effect
ID	inside diameter
IRP	intermediate rated power
ISA	international standard atmosphere
KPI	key performance indicator
KTAS	knots true airspeed
MCP	maximum continuous power
MJ	megajoules
MRP	maximum rated power
MTOGW	maximum takeoff gross weight
NDARC	NASA Design and Analysis of Rotorcraft
OD	outside diameter
OEI	one engine inoperative
OML	outer mold line
PANTHER	Propulsion Airframe iNTegration for Hybrid Electric Research
PCM	phase change material
PSFC	power-specific fuel consumption
RI_i	range indicator of single energy source
$RI_{vehicle}$	range indicator of overall vehicle
RTO	rejected takeoff
SBIR	Small Business Innovative Research
SFC	specific fuel consumption
SLS	sea level standard (atmosphere)
TDP	takeoff decision point
TMS	thermal management system
TOGW	takeoff gross weight

UAS	unmanned aircraft system
UL	useful load
V	airspeed
V_{BE}	best-endurance airspeed
V_{BR}	best-range airspeed
VTOL	vertical takeoff and landing
V_v	vertical airspeed, climb rate
$\dot{\omega}$	fuel flow

Examining the Conceptual Design Process for Future Hybrid-Electric Rotorcraft

Reed A. Danis, Michael W. Green, and Jeffrey L. Freeman*

David W. Hall†

Ames Research Center

Summary

Hybrid-electric propulsion systems introduce immense complexity and numerous design challenges not previously encountered in aircraft design. Traditional conceptual-level rotorcraft design approaches may not adequately capture the level of propulsion system detail desired for hybrid-electric vehicle conceptual design. As part of a NASA Small Business Innovative Research (SBIR) Phase II contract, Empirical Systems Aerospace (ESAero) investigated the implementation of several hybrid-electric propulsion architectures onto three rotorcraft configurations. Unique hybrid-electric variants of these configurations were compared against their conventionally powered counterparts using typical metrics such as payload, range, and energy efficiency. The feasibility and performance of these vehicles were also investigated in the +15 and +30-year time frames based on third-party estimations for future component performance. Using the lessons learned during this trade study, ESAero then conducted a conceptual design effort for a hybrid-electric tiltrotor demonstrator based on the XV-15 aircraft. A detailed integration of the hybrid-electric propulsion system into the vehicle airframe was also performed. The hybrid-electric XV-15 concept vehicle was estimated to achieve a 10-percent reduction in cruise fuel consumption, compared to the original NASA XV-15, at the cost of increasing the vehicle empty weight by almost 25 percent. The success of this design effort suggests that the design of a manned, hybrid-electric tiltrotor is technically feasible at current technology levels.

1. Introduction

The era of hybrid-electric aircraft propulsion is evolving at an astonishing rate. With the rapid technological advancement in the fields of electric motors, batteries, conductors, materials, and thermal management, those researching hybrid-electric propulsion for aircraft must continuously devise new and innovative means to study these concepts. Empirical Systems Aerospace, Inc. (ESAero) has performed numerous hybrid-electric propulsion system studies for both fixed-wing and rotary-wing aircraft since 2008. Through these studies, ESAero has continually expanded its suite of tools aimed at quickly and efficiently modeling these systems. However, there are still gaps in the analyses that must be filled, especially for rotorcraft applications.

This contractor report summarizes the work performed during a NASA Phase II SBIR contract (NNX15CA13C) at NASA Ames Research Center. The goal of this effort was to improve on the strengths of the Propulsion Airframe iNTegration for Hybrid Electric Research (PANTHER) program currently in use by several ESAero aircraft design efforts, and then use this tool to further explore the hybrid-electric rotorcraft design space. To realize these goals, the PANTHER tool was expanded to enable the sizing and performance analysis of unique rotorcraft configurations with propulsion system designs heretofore

* Empirical Systems Aerospace, Inc., San Luis Obispo, CA 93401.

† DHC Engineering, San Mateo, CA 94403.

unseen in the vertical lift realm. PANTHER modules were developed for fuel cells, generic energy storage devices, and superconducting motors and generators, as well as both turbine and diesel engines. An advanced Unique Configurations vehicle kinematics tool was also developed to enable the modeling of uncommon configurations such as tilting, compound, and tandem rotorcraft.

ESAero investigated the implementation of several hybrid-electric propulsion architectures onto two rotorcraft configurations provided by NASA Ames, as well as the NASA XV-15 tiltrotor. Starting with these NASA-provided configurations, variants that used unique hybrid-electric propulsion systems were created, and were then compared against their conventional counterparts using typical metrics such as payload, range, and energy efficiency. The feasibility and performance of these vehicles were also investigated in +15 and +30-year time frames using estimations for future component performance.

Using the lessons learned during this trade study effort, ESAero then conducted a conceptual design effort of a hybrid-electric tiltrotor based on the XV-15. This vehicle used a parallel hybrid propulsion architecture that eliminated the mechanical cross-shafting normally required for one-engine-inoperative (OEI) flight and provided a battery-boost capability for improved performance—all while providing a notable improvement in energy efficiency. The sizing and analysis of this vehicle relied heavily on the component modules that were developed earlier in the contract. Detailed integration of the electric propulsion equipment, battery system, traction bus, and thermal management system into the vehicle was also performed, accompanied by solid models and three-view drawings.

2. Background

2.1 Potential Advantages of Hybrid-Electric Aircraft

Hybrid-electric architectures have shown the potential for significant improvements when applied to fixed-wing aircraft. Such improvements include energy consumption, noise, weight, propulsive efficiency, and aero-propulsive interactions, among others. ESAero is the prime contractor on the development of the NASA X-57 Maxwell, an all-electric aircraft that will use distributed electric propulsion to achieve a 500-percent increase in cruise efficiency with zero in-flight carbon emissions and a reduction in ground noise (ref. 1). A depiction of the X-57 distributed propulsion concept is shown in Figure 1.

Figure 1. NASA X-57 Distributed Propulsion All-Electric Flight Demonstrator.

It is expected that hybrid-electric or all-electric architectures will benefit rotary-wing aircraft as well. Several potential qualitative benefits of a hybrid-electric propulsion architecture are listed below:

- The addition of an electric powertrain could provide redundancy in the case of a primary engine failure.
- Relative to turbine and piston engines, electric motors almost instantaneously generate a desired torque in response to throttle input.
- Using a secondary electrical powertrain to provide short-duration boost power allows a primary turbine engine to be sized for high-efficiency operation in cruise.
- The use of power cabling and high-torque motors reduces the need for heavy gearboxes and mechanical power transmission, allowing easier implementation of intensively distributed propulsion systems.
- Electrified systems better enable distributed propulsion to harness aero-propulsive benefits.

Some other benefits of hybrid and all-electric rotorcraft that may be more difficult to quantify include using only electric power to reduce ground noise. Electric power could also be used in situations where a low infrared signature is beneficial. Another benefit could be that electric motors do not ingest air, which allows them to output full power regardless of altitude, unlike an internal combustion engine. Using electric power for takeoff and landing in dusty or sandy conditions could reduce the damage to turbine engines caused by particle ingestion, also reducing engine maintenance costs.

While electric propulsion is ubiquitous at the small unmanned aircraft system (UAS) level, the development of all-electric and hybrid-electric rotorcraft with a takeoff gross weight (TOGW) of more than 100 lbs are only recently reaching the threshold of demonstration flights. For example, the Workhorse Surefly, a 2-passenger gas engine multirotor with battery backup, is planning demonstration flights in the near future (ref. 2). Additionally, subscale all-electric demonstrators of gas-powered, electrically driven designs such as the Aurora XV-24A and NASA Greased Lightning GL-10 have completed flight testing (refs. 3, 4).

2.2 Hybrid-Electric Aircraft Design Challenges

Realization of the full potential of hybrid-electric propulsion systems is currently hampered by several design challenges unique to these types of propulsion architectures. These challenges can be loosely categorized into three domains:

- Developing the capability to size hybrid-electric propulsion architectures.
- Developing the insight to optimally size hybrid-electric propulsion components.
- Developing methods to “fairly” evaluate propulsion architectures against their conventional counterparts.

The first set of challenges deals with how the introduction of hybrid-electric propulsion elements changes many of the fundamental assumptions used in conventionally powered initial vehicle design. As such, the development of design tools that can accommodate propulsion architectures with multiple types of energy sources and/or powerplants must precede any effort to design such a hybrid-electric aircraft.

The second set of challenges addresses a current lack of insight in how to optimally select, size, and operate a hybrid-electric propulsion architecture. The ability of a hybrid-electric propulsion architecture to decouple many of the fundamental relationships exhibited by conventional vehicles is seen as a powerful design tool with significant potential benefits to vehicle performance. The development and optimization of these power and energy management concepts can be a significant challenge for some propulsion architecture designs.

The final set of challenges addresses the development of “fair” trade study key performance indicators (KPIs) when evaluating the relative performance of vehicles with radically different propulsion architectures. Many of the primary benefits of electric and hybrid-electric vehicle designs are indirect performance metrics, such as lifecycle cost or carbon footprint, which require complex, rigorous, and adaptable models in order to apply to an arbitrary set of hybrid-electric propulsion architecture designs. Inappropriate selection of KPIs can result in the selection of a vehicle propulsion architecture design that lacks realizable performance gains.

3. Propulsion Architecture Trade Studies

The massive parameter space encompassing hybrid-electric vehicle design was explored by sizing many different hybrid-electric-powered variants of several vehicle configurations. With such a vast design space to explore, the architecture trade studies used a staged approach to efficiently explore design regions that appeared to provide insight into the impacts of using hybrid-electric propulsion. Each vehicle seeks to answer at least one question about vehicle development within the design space. For example, how does aircraft TOGW or useful load (UL) fraction affect the ideal hybrid-electric system? Can using a diesel engine instead of a turbine result in a more fuel-efficient vehicle despite the added engine weight? Can a hybrid architecture improve vehicle performance by changing the design flight condition that sizes the primary engine? Note that these trade studies are anything but a complete sweep of the vast design space encompassed by all possible hybrid-electric rotorcraft concepts.

Utilizing PANTHER’s capabilities, ESAero investigated the hybridization of two conventionally powered rotorcraft configurations originally developed using the NASA Design and Analysis of Rotorcraft (NDARC) rotorcraft sizing program along with a tiltrotor configuration based on published XV-15 data. The conventional vehicles were reconstructed in PANTHER and calibrated to match their source data to serve as a baseline for the hybrid architecture trade study. Hybrid-electric variants were then created using unique propulsion system configurations that were compared against the conventional vehicle using typical vehicle performance metrics. The impact of predicted future electrical component performance was also investigated. In total, 30 rotorcraft configurations were investigated during this effort.

3.1 Trade Study Methodology

The formalized trade study procedure described in this section was an attempt to streamline the vehicle development process. This methodology helps to maintain a level playing field when sizing vehicles with radically different propulsion systems. The methodology is broken down into four stages and summarized below.

<u>Stage 1: Develop Baseline Configuration and Sizing Conditions/Mission</u>
In the first stage, the vehicle was created in PANTHER and calibrated as close as possible to the source model. NASA’s NDARC Configuration A and B are examples of an existing aircraft model that was adapted for use in the trade study. The XV-15-based tiltrotor vehicle references both NDARC model data and actual flight test performance data.

<u>Stage 2: Re-Engine Baseline Configuration</u>
In the second stage, several variants of the baseline vehicle were created by reconfiguring (or “re-engining”) it with hybrid-electric propulsion architectures. The specific propulsion architectures chosen were selected to investigate interesting areas of the hybrid-electric design space. During the re-engining process, the vehicle’s on-design TOGW and fuel weight are held constant. Variations in propulsion system weight are accommodated by adjusting design payload weight to maintain design gross weight (DGW). The outer mold line (OML) of the vehicle and the vehicle sizing conditions are also held constant.

This is done to ensure the changes in overall performance are solely a result of the hybrid-electric propulsion architecture.

Stage 3: Off-Design Analysis

The re-engined vehicles were then analyzed to determine key performance parameters such as range, radius of action, time on station, best-range speed, best-endurance speed, fuel/energy consumption, etc. These parameters are the primary metrics of comparison between all vehicles. This stage also included the development of energy flow plots, endurance/range plots, and payload-range diagrams. These charts were useful for comparing performance between configurations across a wide range of operating conditions.

Stage 4: Present and Archive Results

The final stage was to present the results in a standardized fashion. All re-engined variants of a baseline vehicle were compared as equivalently as possible using the aforementioned performance metrics. The results were also stored in a formalized manner so that they can be accessed easily in the future along with the relevant PANTHER files.

Figure 2 summarizes these four stages in flowchart form.

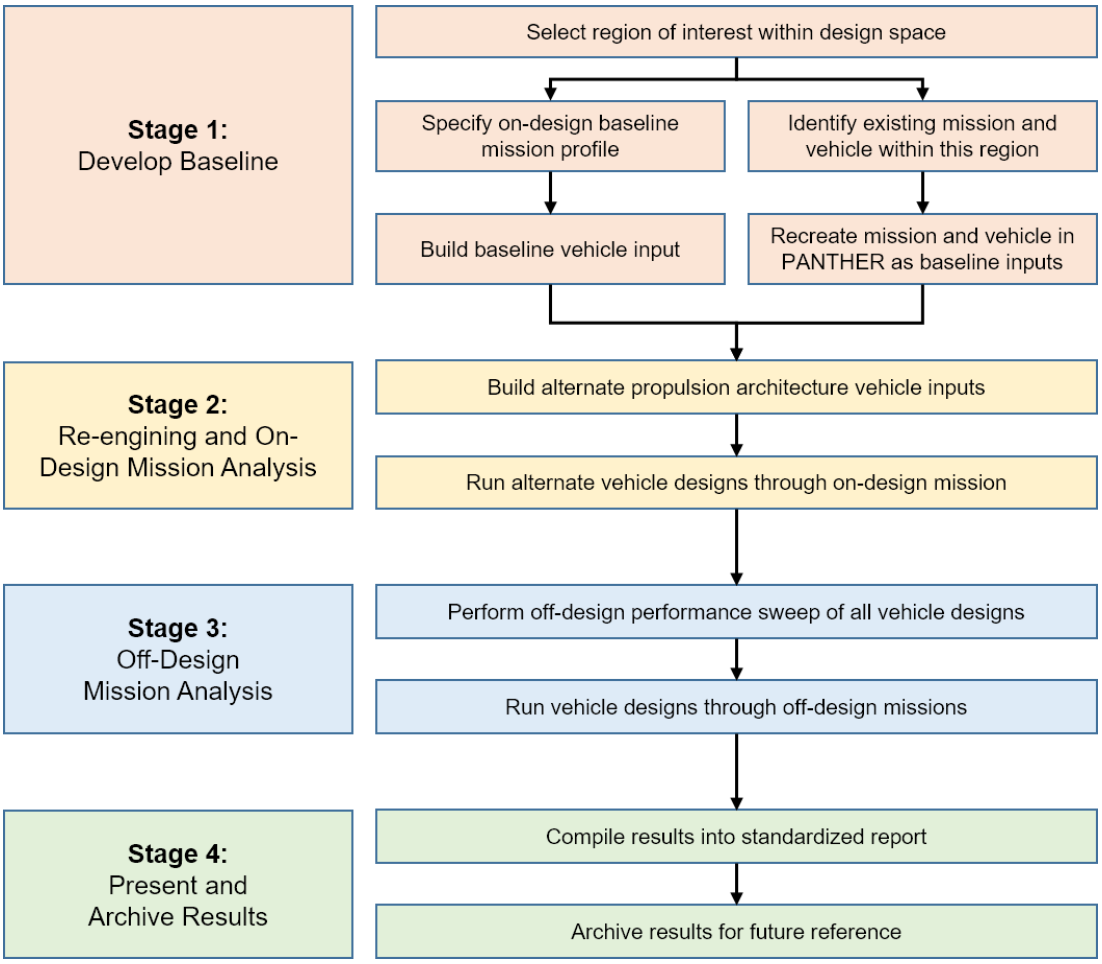

Figure 2. Flowchart of Trade Study Staged Approach.

3.2 Supporting Tools and Concepts Development

Development of the trade study vehicles continually identified a need to modify the tools and methods used. Additionally, the trade study effort required the development of several hybrid-electric vehicle specific design concepts. This section summarizes the primary tools used and unique concepts developed to support the trade study effort.

3.2.1 PANTHER

PANTHER is developed in MATLAB by ESAero for the purpose of investigating the myriad of design opportunities and challenges associated with hybrid-electric propulsion systems in aircraft. PANTHER acts as a framework that allows a user to combine various vehicle configurations, propulsion and thermal management system (TMS) architectures, and analysis methodologies to size and evaluate a design, providing details at the component, system, and aircraft levels. ESAero has developed several empirical- and physics-based component sizing and performance modules that are sufficient for aircraft conceptual design, and purpose-built component modules can be added with relative ease. A multi-point on-design approach allows each module to consider all the user-specified point-performance requirements while sizing each component. Separate off-design analysis routines can test the vehicle's flight envelope, mission performance, and more. PANTHER is in active development, with new features and modules added regularly.

<u>On-Design Vehicle Sizing</u>

At the core of PANTHER is a framework that calls the sizing/analysis modules and solves any unknown parameters, as shown in Figure 3. For on-design operations, the user defines the point-performance sizing flight conditions (FCs), the modules to be called and their architecture relation to one another, and all input parameters required by those modules. Modules are grouped into top-level categories: subsystems, kinematics, powertrain, powerplant, TMS, and vehicle weight. Sub-categories of modules can also be defined to be called by the top-level modules; e.g., a variety of propulsor modules could be called by a kinematics module. The sequence by which the modules are called is coordinated so that sizing requirements created by earlier modules can be referenced by later modules. Unknown parameters are created on-the-fly by the modules. A successive-step iteration process is used to solve these parameters.

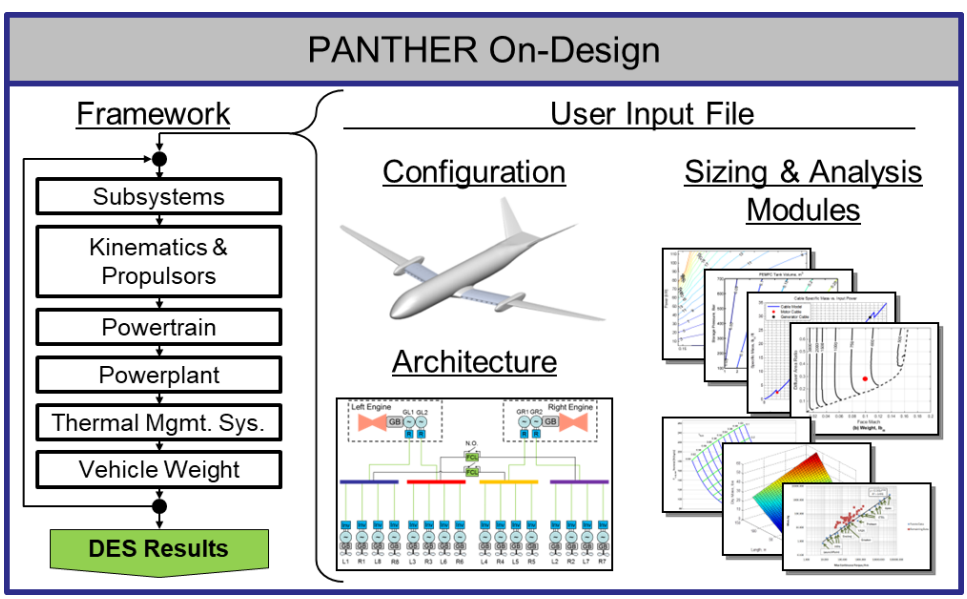

Figure 3. PANTHER On-Design Framework.

Vehicle Performance Simulation

A similar framework is provided for off-design vehicle performance analysis, shown in Figure 4, in which the vehicle and components of known characteristics are evaluated at any off-design test point. Even in off-design, the user can adjust how the vehicle behaves via the Vehicle Control file. Different analysis activities can be completed using the off-design tasks provided in PANTHER, including point performance parameter sweeps, maximum-effort evaluations, time-integrated mission simulations, and more.

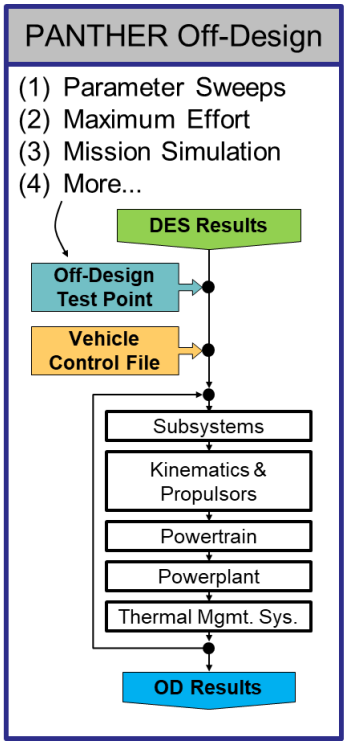

Figure 4. PANTHER Off-Design Framework.

Propulsion Architecture Component Performance Models

PANTHER has the powerful capability to size and simulate a complex vehicle propulsion architecture subsystem through the assembly of preexisting propulsor and powertrain component models. The ability to simulate an arbitrary propulsion architecture allows a user to quickly build and evaluate a large number of propulsion subsystem designs within PANTHER. The propulsion architecture components can be separated into several groups, detailed below:

- *Powertrain components* augment power either by changing the nature of that power or by moving it to a different location. The penalty for these actions comes in the form of weight and losses.
- *Powerplant components* introduce power to the propulsion system. The energy source from which the power originates can be one of two options.
    - Energy is stored in a fuel reservoir that is identified as the powerplant's architecture input (e.g., combustion engines, hydrogen fuel cells).
    - The energy is stored directly within the powerplant. These powerplants are referred to as "EnergyPlants" (e.g., batteries, kinetic energy systems (a.k.a. flywheels)).

- *Subsystem components* represent systems on the vehicle that are not the propulsion system (e.g., avionics, environmental control system). These systems can have mass and may consume power that must be provided by the propulsion system. They might also influence the vehicle's aerodynamics, represented as a drag area.

- *Thermal management system* (TMS) components manage the thermal characteristics of the propulsion system. As with kinematics modules, many parameters within a TMS need to be addressed at a system level. Therefore, each TMS module solves an independent thermal system with multiple sub-modules treating the components contained in that system.

Additionally, the *vehicle weight buildup* modules are responsible for defining the weight of the vehicle and everything in it. All vehicle weight buildup modules collect and summate the weight of the otherwise modeled components in the architecture. A vehicle weight buildup module can also define other line items in a vehicle weight buildup that are not otherwise modeled.

3.2.1.1 Vehicle Kinematics Models

The physics of a PANTHER vehicle are calculated using one of several built-in kinematic modules that determine the thrust required from the vehicle propulsors to achieve a particular flight condition. PANTHER contains several different kinematic modules. Simpler models assume a given aircraft configuration while the more advanced Unique Configurations module allows the implementation of a vehicle with an arbitrary number and location of drag bodies, lifting surfaces, and propulsors. Certain properties of vehicles using the Unique Configuration mode, such as propulsor axis rotation and control surface deflection limits, can be scheduled to automatically adjust with flight condition parameters. This feature allows for the modeling of vehicles that change their configuration in flight.

<u>Unique Configurations Kinematic Model Validation</u>

The UH-60A conventional helicopter model was developed in PANTHER using information from an NDARC validation paper (ref. 5) and the vehicle's operator's manual (ref. 6). The fuselage is modeled as an ellipsoid with slender body theory. The model inputs and a corresponding graphical representation of the aerodynamic model are shown in Figure 5.

Figure 6 shows a comparison of UH-60A rotor power required between the PANTHER model, an NDARC model, and flight test data. The two models and the flight test data show excellent agreement throughout most of the flight envelope. At high airspeeds, the PANTHER model shows better agreement with the flight test data than the NDARC model.

The XV-15 tiltrotor PANTHER model was created using the information in an NDARC validation paper (ref. 5) and a NASA technical document on the vehicle (ref. 7). Figure 7 shows several top-level inputs for each component comprising the XV-15, as well as a graphical representation of the vehicle in PANTHER.

Figure 8 shows results for power and pitch attitude of the XV-15 as predicted by PANTHER and compares them to NDARC and flight test data. PANTHER tends to overestimate power compared to NDARC; however, considering the spread of the flight test data points, PANTHER's results appear to be reasonable and follow the test data well. Similarly, PANTHER also follows the flight test data trend for pitch attitude in helicopter mode. In contrast, NDARC appears to constantly border the upper bound of test data points. In airplane mode, the results for power and pitch between NDARC and PANTHER match closely. Compared to flight test data, both models produce a pitch curve that borders the lower bound of pitch test data points. In all, the Unique Configurations module has shown itself capable of modeling several different configurations, comparing well against both test data and other well validated models.

UH-60A

Main Rotor

Area	2261.9 ft^2
Solidity	0.0825
Hub-Tip Ratio	0.0969
Blade Twist	-18°
# of Blades	4
Flap Frequency (/rev)	1.035
Airfoil	SC1095
RPM	258
Incidence (forward)	-3.0°
Cant	0°

Tail Rotor

Area	95.0332 ft^2
Solidity	0.1875
Hub-Tip Ratio	0.1
Blade Twist	-18
# of Blades	4
Flap Frequency (/rev)	1.14
Airfoil	SC1095
RPM	1190
Incidence (forward)	0°
Cant	-70°

Horizontal Tail

Area	44.65 ft^2
Aspect Ratio	4.63
Airfoil	NACA0015
Twist	0°
Taper Ratio	0.6921
Incidence	0°
Cant	0°
LE Sweep	2.26°

Fuselage

Length	41.33 ft.
Width	7.75 ft.
Height	8.75 ft.

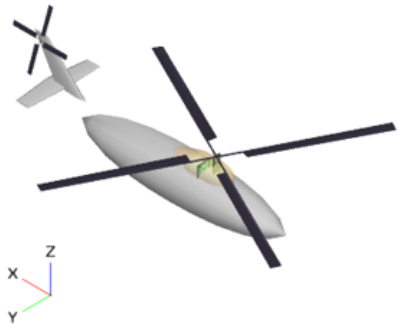

PANTHER Model Representation of UH-60A; Generic drag components modeled as flat plate areas.

Vertical Tail

Area	36.06 ft^2
Aspect Ratio	1.85
Airfoil	NACA0021
Twist	0°
Taper Ratio	0.47
Incidence	0°
Cant	90°
LE Sweep	46.56°

Generic Drag, D/q

MR Hub/Pylon	9.97 ft^2
TR Hub	2.90 ft^2
Engine Nacelle	6.39 ft^2

Vehicle

Weight	16,589 lb.

Figure 5. PANTHER UH-60A Model.

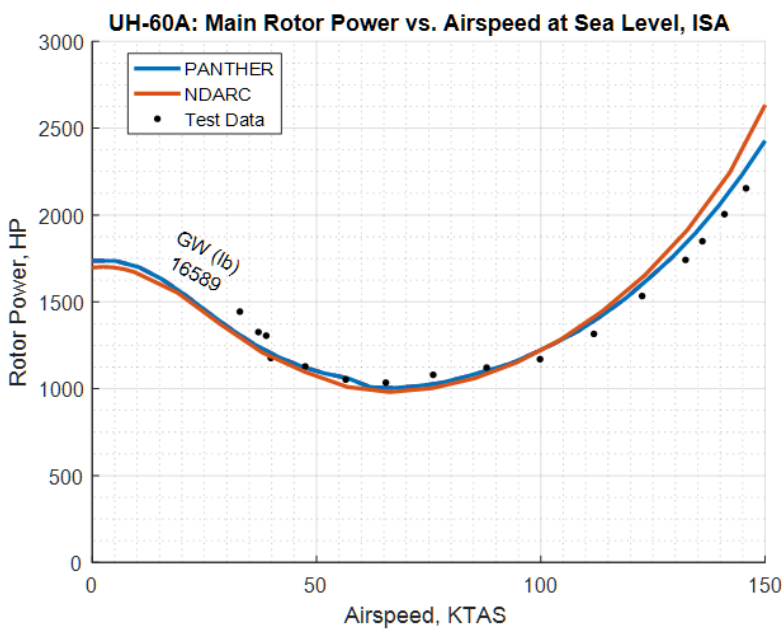

Figure 6. PANTHER UH-60 Model Required Rotor Power Compared to NDARC Predictions and Flight Test Data.

XV-15

Main Wing

Area	169 ft²
Aspect Ratio	6.13
Airfoil	NACA 2412
Twist	0
Taper Ratio	1
Incidence	3°
Cant	0°
LE Sweep	-6.5°
Aileron Chord Fraction	0.25
Flap Chord Fraction	0.25

Horizontal Tail

Area	50.25 ft²
Aspect Ratio	3.28
Airfoil	NACA 0015
Twist	0
Taper Ratio	1
Incidence	0°
Cant	0°
LE Sweep	0°
Flap Chord Fraction	0.30

Vertical Tail

Area	50.50 ft²
Aspect Ratio	2.33
Airfoil	NACA 0012
Twist	0°
Taper Ratio	1
Incidence	0°
Cant	90°
LE Sweep	0°
Flap Chord Fraction	0.25

Generic Drag, D/q

Rotor Pylon (per rotor)	0.76 ft²
Nacelle (per nacelle)	36 ft²

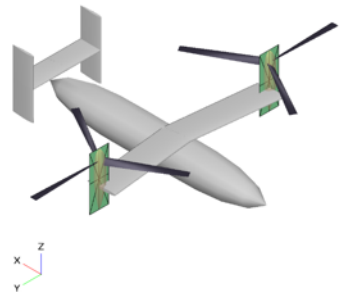

PANTHER Model Representation of XV-15; Generic drag components modeled as flat plate areas.

Rotor

Area	491 ft²
Solidity	0.089
Hub-Tip Ratio	0.10
Blade Twist	-40°
# of Blades	3
Flap Frequency (/rev)	1.020
Airfoil	VR7
RPM (helicopter mode)	565
RPM (airplane mode)	458
Incidence	0°
Cant	0°

Fuselage

Length	41 ft.
Width	5.5 ft.
Height	6.17 ft.

Vehicle

Weight	13,000 lb.

Figure 7. XV-15 PANTHER Model.

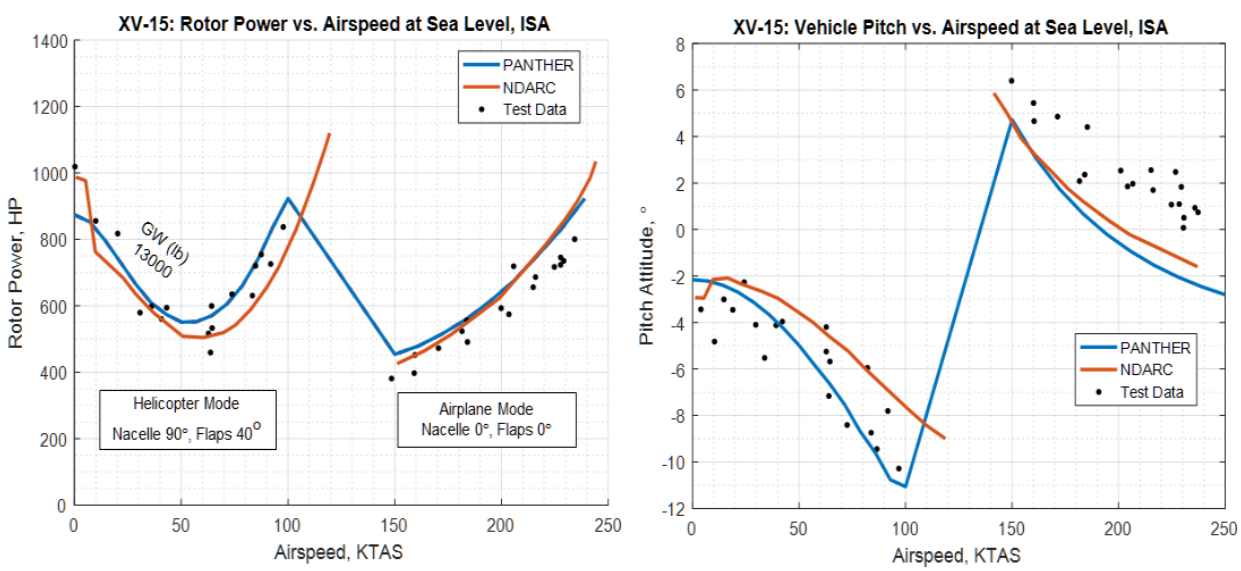

Figure 8. PANTHER XV-15 Model Required Rotor Power and Vehicle Pitch Attitude Compared to NDARC Model Predictions and Flight Test Data.

3.2.2 Endurance Indicator and Range Indicator

The development of initial sizing methods for aircraft over the last century has generally assumed that the vehicle uses only a single energy source. Development of hybrid vehicles requires modification of many sizing methods to properly account for multiple energy sources. Similarly, many key performance metrics commonly used to compare aircraft designs cannot properly account for designs with multiple energy sources. Modified forms of these performance metrics, along with new metrics, will be required to "fairly" compare hybrid-electric vehicles to conventionally powered designs.

For a conventional vehicle, the best-endurance airspeed (V_{BE}) and best-range airspeed (V_{BR}) at a given altitude are calculated from the rate of fuel consumption across a sweep of airspeeds. The commonly accepted maximum-effort airspeed equations are:

$$V_{BE} = \max\left(\frac{1}{\dot{\omega}}\right)$$

$$V_{BR} = \max\left(\frac{V}{\dot{\omega}}\right)$$

where $\dot{\omega}$ is fuel flow and V is the vehicle's airspeed. When analyzing hybrid propulsion systems, several additional complexities must be accounted for:

- The vehicle may have constant-weight energy sources (such as batteries).
- The vehicle may be carrying multiple fuels with different energy densities.
- Some energy sources may have different capacities and depletion rates than others.

As such, these maximum-effort airspeed equations are not applicable to hybrid-electric vehicles because of the decoupling of the vehicle's energy source consumption rate from the rate change in stored energy weight.

The following method provides modified metrics applicable to hybrid-electric propulsion architectures. The discharge rate of a battery is often normalized by the battery's capacity, which results in a specification known as the C-rate. A C-rate of 1C represents a discharge rate that will drain a fully charged battery in 1 hour, a 2C discharge rate would drain the battery in 1/2 hour, etc. This concept can be expanded to encompass fuel-based or any other generic energy sources as well. Thus, the normalized discharge of any energy source can be represented as:

$$C = \frac{\dot{E}}{E_{Design}}$$

where C is the C-rate, $\dot{E}$ is the energy flow rate, and E_{Design} is the design capacity of the energy source.

Since the C-rate of an energy source is always normalized by the same factor, it can be used in a similar manner as fuel flow to find the maximum-effort airspeeds. However, to account for multi-energy-source vehicles, the normalized discharge rate of each energy source is used to calculate an endurance indicator (*EI*) and range indicator (*RI*) specifically for that source:

$$EI_i = \frac{1}{C_i}$$

$$RI_i = \frac{V}{C_i}$$

where the subscript *i* indicates the values are specific to a single energy source.

These equations are the hybrid-electric analogue to the conventional vehicle specific endurance and specific range equations. Since the energy flow of each individual energy source is normalized by its own capacity, the endurance and range indicators of all the energy sources can be compared to determine which would deplete first. At a given flight condition, the overall vehicle endurance indicator and range indicator is thereby set by the energy source with the lowest *EI* and *RI* values, as follows:

$$EI_{vehicle} = \min_i(EI_i)$$

$$RI_{vehicle} = \min_i(RI_i)$$

where the subscript *vehicle* indicates the values that represent overall vehicle performance.

The maximum-effort airspeeds can then be found at the maximum vehicle endurance and range indicator values across a sweep of airspeeds:

$$V_{BE} = V \text{ @ } \max(EI_{vehicle})$$

$$V_{BR} = V \text{ @ } \max(RI_{vehicle})$$

3.2.3 Energy Flow vs. Airspeed Plots

The Energy Flow Plot tool uses PANTHER's off-design modeling capabilities to evaluate the vehicle's energy consumption across a range of airspeeds, vehicle weights, and power distribution schemes. The Energy Flow Plot tool generates Energy Flow vs. Airspeed plots that are analogous to the Fuel Flow vs. Airspeed plots commonly provided in pilot operating handbooks or technical manuals for conventionally powered helicopters. The term "Energy Flow" is used in favor of "Power" to emphasize both the fuel-energy correlation and that the value represents energy source dissipation rates, rather than power output measured at the vehicle's powerplants or propulsors.

The primary output of the Energy Flow Plot tool is the Energy Flow vs. Airspeed plot. Analyzing performance in terms of energy flow rather than fuel flow allows the plots to demonstrate the performance of vehicles with multiple energy sources and non-fuel-based energy sources, such as a hybrid helicopter equipped with both a fuel tank and a battery. The flow from each individual energy source is represented by a set of gross weight isolines. For vehicles with multiple energy sources, a set of net energy flow lines is also generated to represent the net consumption of the vehicle's energy reserves. Examples of the Energy Flow vs. Airspeed plots are shown for both a conventional helicopter and a generic hybrid-electric helicopter with one engine and two constant-weight energy sources in Figure 9. Note that this example hybrid vehicle is using a simple fixed fractional power distribution control scheme, which is not necessarily representative of a feasible hybrid vehicle power distribution concept.

In addition to the energy flow plots, the tool automatically generates Endurance Indicator vs. Airspeed and Range Indicator vs. Airspeed plots. These plots provide feedback on the impact of different flight conditions on the vehicle's range and endurance. They are also useful for comparing the range and endurance capabilities of different vehicles or power distribution control methods. Examples of the Endurance Indicator and Range Indicator plots are shown for the same conventional helicopter and hybrid-electric helicopter in Figure 10.

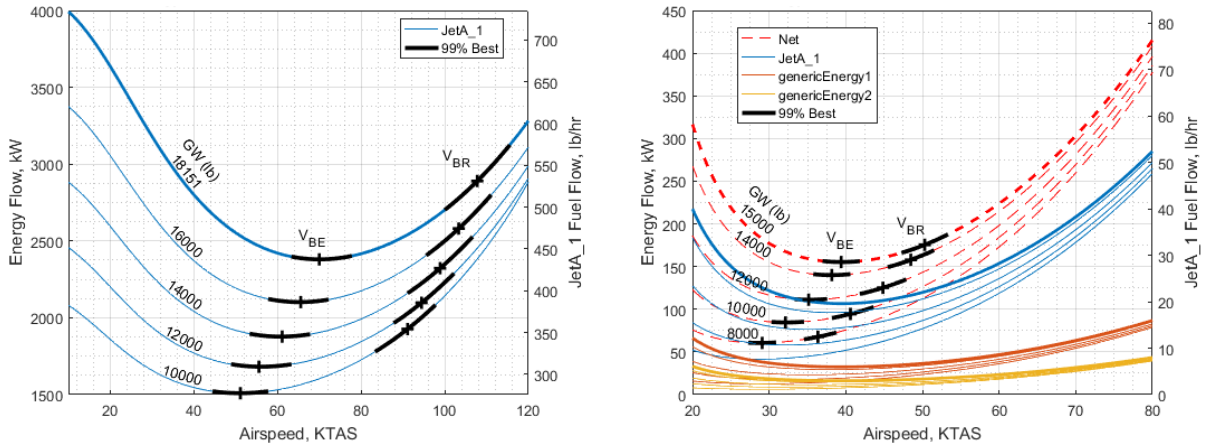

(a) **(b)**

Figure 9. Example Energy Flow vs. Airspeed Charts; (a) Conventional Helicopter, (b) Hybrid-Electric Helicopter.

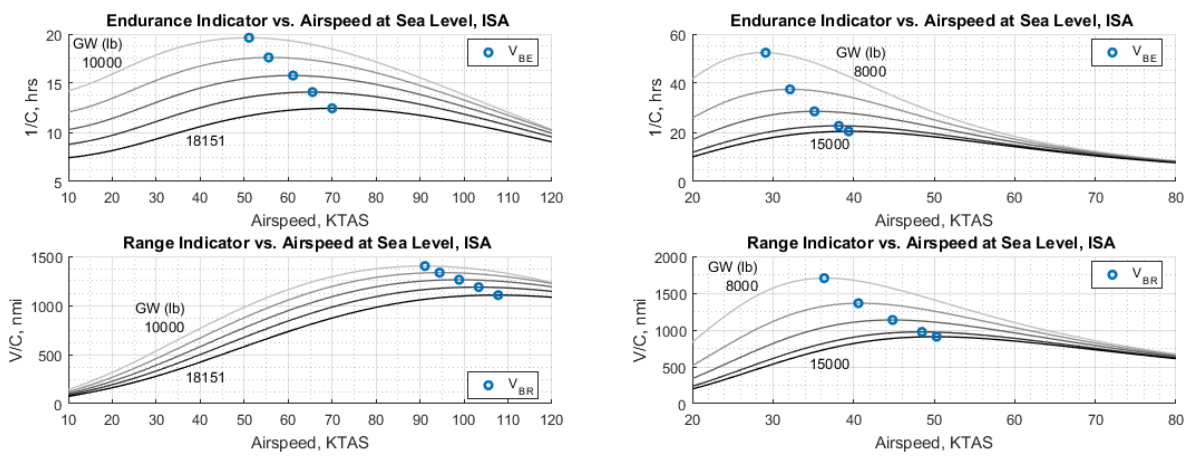

(a) **(b)**

Figure 10. Example Endurance Indicator (top) and Range Indicator (bottom) Charts; (a) Conventional Helicopter, (b) Hybrid-Electric Helicopter.

3.3 Trade Study Vehicles

To aid in visualization of the different types of propulsion system architectures considered in this trade study, a set of graphical icons was created to represent the different PANTHER component models. These icons provide a consistent and visually descriptive means to illustrate the propulsion system being analyzed. The full set of icons is shown in Figure 11.

Component icons are used to represent the primary components that can exist in the vehicle's propulsions system such as rotors, motors, and batteries. Each component that has an icon also has a dedicated module within PANTHER to size and model the component. There are many other ancillary components that make up a propulsion system, but only the main components are considered in these diagrams and within PANTHER.

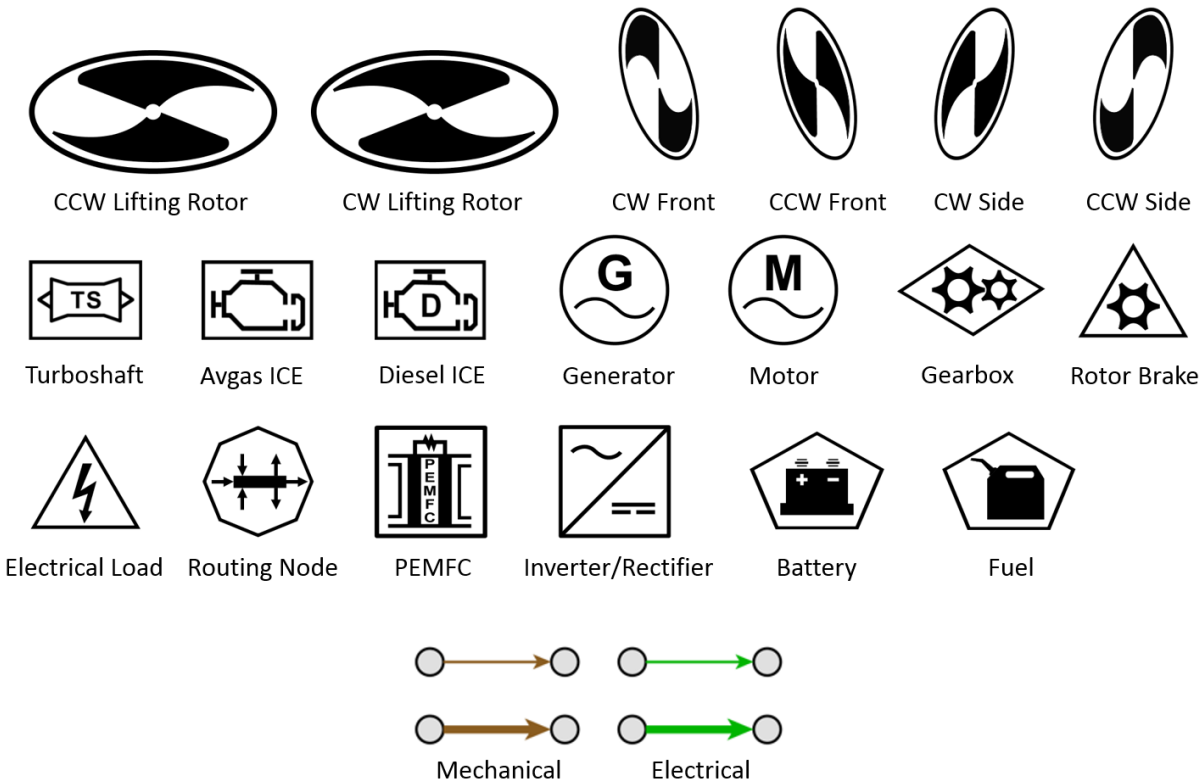

Figure 11. Component and Connector Icons.

Connecting lines convey information about the type of energy being transferred between components (electrical vs. mechanical) as well as the type of modeling approach used in PANTHER. Brown lines correspond to a mechanical power transfer while green lines indicate electrical power. The thickness of the line indicates the handling of this connection within PANTHER. A thin line indicates that the connection is “implied” and is simply representing the flow of energy from one component to another with no losses or weight modeling. A thick line indicates that PANTHER is directly modeling the connection, whether it is an electrical cable or a mechanical shaft, and considering its mass and efficiency.

3.3.1 Development and Calibration of Conventionally Powered Helicopter Models

NASA provided two configurations developed in the NDARC program representing a conventional light helicopter with a design TOGW of 5,781 lbs and a heavy helicopter with a design TOGW of 25,161 lbs, hereafter referred to as Configuration A and Configuration B, respectively. Near-identical configurations were built inside PANTHER in an effort to calibrate PANTHER’s models against NDARC. Particular effort was made to ensure PANTHER’s performance and weight predictions would be reasonably similar to NDARC’s at the given baseline configuration flight conditions. The calibrated PANTHER models are subsequently used to provide a baseline for the hybrid propulsion trade studies

Propulsion systems were developed for Configuration A and B based on available NDARC details. A simple powertrain setup was used in PANTHER and tuned to match the total efficiency of the powertrain system defined in the NDARC input file. A summary of the baseline Configuration A helicopter as modeled in PANTHER is shown in Figure 12. A summary of the baseline Configuration B helicopter is shown in Figure 13.

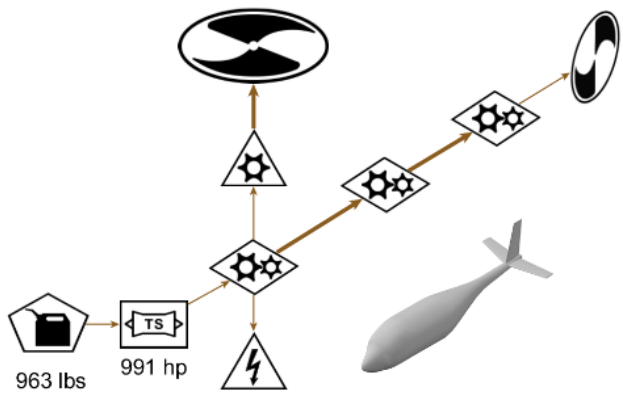

C.A Conventional Weight Summary (lbs)	
Structure Group	**1059**
Fixed Equipment Group	**913**
Propulsion Group	**1356**
Powerplant Total	246
Turbine Engine	246
Empty Weight Margin	**270**
Empty Weight	**3599**
Useful Load Group	**2183**
Payload	1000
TOGW	**5781**

Figure 12. Propulsion Architecture and Group Weights for the Baseline Configuration A Vehicle.

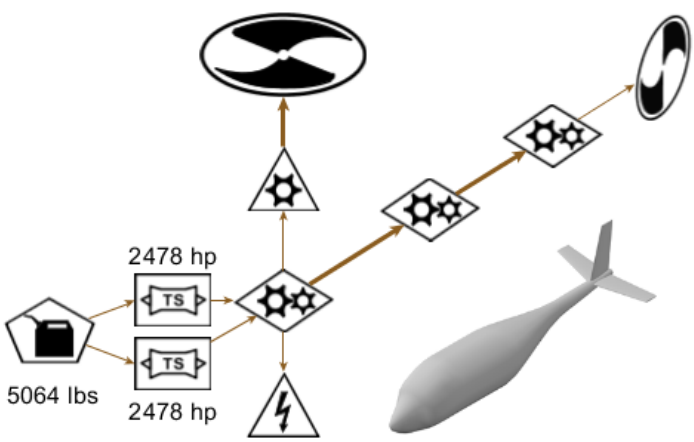

C.B Conventional Weight Summary (lbs)	
Structure Group	**2948**
Fixed Equipment Group	**4335**
Propulsion Group	**5698**
Powerplant Total	978
Turbine Engine 1	489
Turbine Engine 2	489
Empty Weight Margin	**1053**
Empty Weight	**14033**
Useful Load Group	**11128**
Payload	5280
TOGW	**25161**

Figure 13. Propulsion Architecture and Group Weights for the Baseline Configuration B Vehicle.

Sizing Conditions

The original sizing conditions defined in NDARC were recreated as closely as possible in PANTHER.

Sizing Flight Conditions (Configuration A and Configuration B):

FC 1 Hot-High Hover: Hover out of ground effect (HOGE) at 5,000 ft. (International Standard Atmosphere (ISA) +36°F). The vehicle weight fraction in this flight condition is set to 0.995 to account for fuel burn that would occur prior to vehicle liftoff. The maximum allowable throttle setting is intermediate rated power (IRP), a power rating with a 30-minute thermal endurance limit.

FC 2 Top Speed: Vehicle top speed at sea level (ISA) and DGW. The horizontal velocity for either configuration is 150 knots true airspeed (KTAS) for Configuration A and 160 KTAS for Configuration B. The maximum allowable throttle setting is IRP.

Sizing Flight Conditions (Configuration B Only):

FC 3 Vertical Climb Rate: Climb condition at 8,000 ft. (ISA). The vehicle weight fraction is set to 0.948 to match the NDARC gross weight for this condition. The maximum allowable throttle setting is IRP.

FC 4 V_{BR} Cruise: Best-range airspeed at sea level (ISA) and DGW The airspeed is set to the NDARC-derived V_{BR} airspeed of 146.3 KTAS. The maximum available throttle setting is IRP. As a performance-derived, maximum-range airspeed condition this flight condition was not expected to be a design driver of any powertrain components, but was included for posterity.

Mission Performance

The NDARC Configuration A and B on-design sizing mission was modeled in PANTHER using the Mission Analysis tool. Mission segments were modeled as similarly as possible. The idle segment of the NDARC mission was not included in the PANTHER validation missions because the engine deck used for this study was not validated for estimating idle power requirements and fuel consumption. Instead, the PANTHER mission begins with the HOGE segment, with the vehicle fuel and gross weight states initialized to match the NDARC vehicle in this condition. Improved methods for modeling vehicle idle state have since been added to PANTHER. The Configuration A baseline vehicle calibration mission profile is shown in Figure 14. The Configuration B baseline vehicle calibration mission profile is shown in Figure 15.

The results of the mission comparison are shown in Table 1 and Table 2. For both Configuration A and B, there is good agreement across all metrics with the NDARC results, indicating that PANTHER mission simulations are capable of accurately predicting mission performance for a variety of vehicle sizes and performance capabilities.

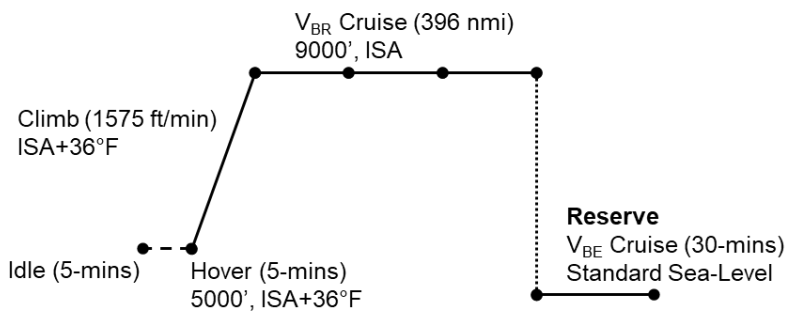

Figure 14. Configuration A Baseline Vehicle Calibration Mission Profile.

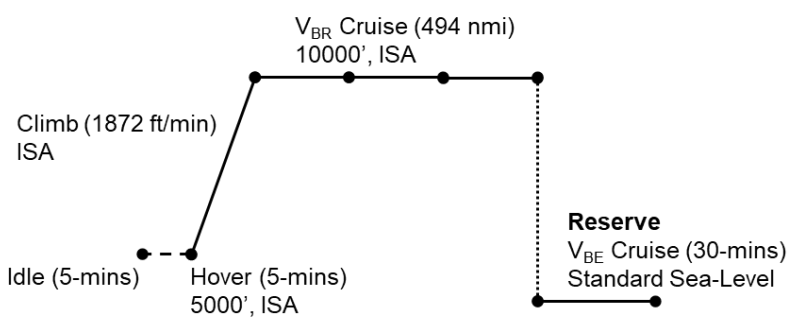

Figure 15. Configuration B Baseline Vehicle Calibration Mission Profile.

Table 1. PANTHER and NDARC Configuration A Calibration Mission Performance.

Configuration A Baseline Mission	Idle	HOGE	Climb	Cruise 1	Cruise 2	Cruise 3	Cruise 4	Reserve
Segment	5 min	5 min		96 nmi	100 nmi	100 nmi	100 nmi	30 min
Altitude (ft.)	5000	5000	5-9000	9000	9000	9000	9000	0
d_{Tamb} (deg. F)								
NDARC	36	36	36	0	0	0	0	0
PANTHER		0	0	0	0	0	0	0
V_h (kts.)	0	0	89	131	130	129	128	69
V_v (ft/min)	0	0	1575	0	0	0	0	0
Total Fuel Burn (lbs.)								
NDARC	10	43	59	257	460	659	855	963
PANTHER		42	57	258	462	661	857	967
percent difference		-3%	-3%	0%	1%	0%	0%	0%
Fuel Burn (lbs.)								
NDARC	10	33	15	198	203	199	196	108
PANTHER		32	15	201	204	199	195	110
percent difference		-4%	-3%	1%	1%	0%	0%	2%
SFC (lbs/hp-hr)								
NDARC	1.012	0.514	0.513	0.531	0.534	0.538	0.542	0.694
PANTHER		0.505	0.505	0.508	0.513	0.520	0.526	0.738
percent difference		-2%	-2%	-4%	-4%	-3%	-3%	6%
Shaft Power (hp)								
NDARC	123	769	698	509	494	479	465	311
PANTHER		756	687	539	518	496	477	298
percent difference		-2%	-2%	6%	5%	4%	3%	-4%

Table 2. PANTHER and NDARC Configuration B Calibration Mission Performance.

Configuration B Baseline Mission	Idle	HOGE	Climb	Cruise 1	Cruise 2	Cruise 3	Cruise 4	Reserve
Segment	5 min	5 min		123 nmi	125 nmi	125 nmi	125 nmi	30 min
Altitude (ft.)	5000	5000	5-8000	8000	8000	8000	8000	0
d_{Tamb} (deg. F)								
NDARC	0	0	0	0	0	0	0	0
PANTHER		0	0	0	0	0	0	0
V_h (kts.)	0	0	83	144	143	143	142	77
V_v (ft/min)	0	0	1872	0	0	0	0	0
Total Fuel Burn (lbs.)								
NDARC	49	196	244	1371	2482	3561	4610	5103
PANTHER		197	242	1367	2464	3529	4563	5074
percent difference		1%	-1%	0%	-1%	-1%	-1%	-1%
Fuel Burn (lbs.)								
NDARC	49	147	48	1127	1111	1079	1049	493
PANTHER		149	45	1125	1097	1065	1034	511
percent difference		1%	-6%	0%	-1%	-1%	-1%	4%
SFC (lbs/hp-hr)								
NDARC	0.8523	0.4621	0.4523	0.474	0.4789	0.4833	0.4883	0.628
PANTHER		0.464	0.462	0.467	0.474	0.480	0.487	0.672
percent difference		0%	2%	-2%	-1%	-1%	0%	7%
Shaft Power (hp)								
NDARC	683	3826	3963	2786	2659	2554	2445	1569
PANTHER		3839	3650	2823	2655	2538	2415	1523
percent difference		0%	-8%	1%	0%	-1%	-1%	-3%

3.3.2 Development and Calibration of Conventionally Powered Tiltrotor Model

The baseline tiltrotor vehicle modeled in PANTHER was extensively referenced to the NASA XV-15 research vehicle. The XV-15 is an excellent validation vehicle because of the large amount of publicly available performance data. Additionally, the Unique Configurations rotor model was previously calibrated against NDARC models of the XV-15. The amount and quality of the XV-15 test data, and their agreement to performance predictions provided by the PANTHER Unique Configurations tool, gave confidence in the validity of the hybridization trade studies.

The tiltrotor propulsion architecture models the primary components of the XV-15 powertrain. Two nacelle-mounted turboshaft engines provide power to the proprotors via large gearboxes. Transverse driveshafts and a central gearbox allow power to be transferred from either engine to both proprotors in the event of an engine failure. The overall gearbox efficiency was set to 98.7 percent, which provided a good correlation to both engine shaft power and rotor shaft power derived from XV-15 flight test data. Engine power takeoff for auxiliary power (hydraulic pump, electrical bus, etc.) is not modeled, but the power loss associated with power takeoff is folded into the gearbox efficiency. A summary of the PANTHER tiltrotor baseline vehicle is shown in Figure 16.

The baseline tiltrotor vehicle was calibrated using published XV-15 test data as a reference for component and group weights (refs. 7, 8). The wing and tail surface unit weights were set such that all had equivalent planform area and weight as the XV-15's. Similarly, the gearbox and shaft weight scaling was set such that the components had weights equivalent to the XV-15's powertrain components. Several vehicle-specific weights such as the landing gear and all the items in the fixed equipment group had their fixed module weights set equivalent to the values provided in the XV-15 weight statement. As with the NDARC configurations, the PANTHER on-design input file fixed the design TOGW equivalent to the XV-15's DGW and floated the design payload. Scaling factors were applied to the original PANTHER output to match the component weights to the actual vehicle data.

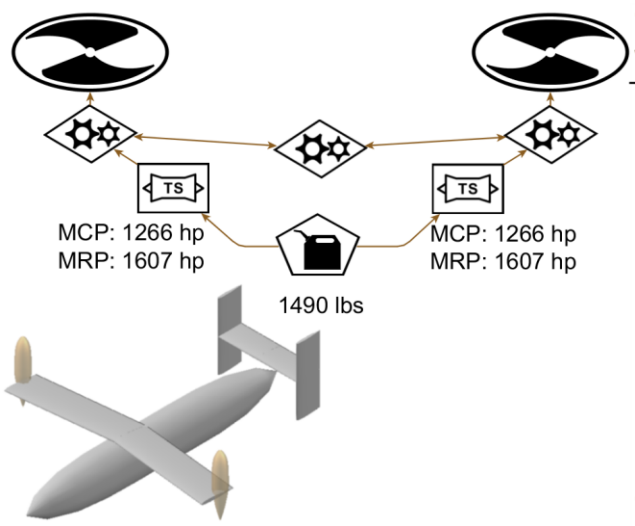

TLT Conventional Weight Summary (lbs)	
Structure Group	**3332**
Fixed Equipment Group	**2243**
Propulsion Group	**3450**
Powerplant Total	1085
Turbine Engine 1	543
Turbine Engine 2	543
Empty Weight Margin	**50**
Empty Weight	**9075**
Useful Load Group	**3925**
Payload	1897
TOGW	**13000**

Figure 16. Propulsion Architecture and Group Weights for the Baseline Tiltrotor Vehicle.

Sizing Conditions

The PANTHER baseline tiltrotor sizing conditions were developed from both XV-15 flight test performance data and sizing conditions used to validate the NDARC XV-15-based tiltrotor vehicle (refs. 5, 7). The point performance flight conditions include both nominal, all-engines-operational (AEO), and contingency, one-engine-inoperative (OEI) performance requirements. The point performance flight conditions are described below:

FC 1 Maximum Weight Hover (AEO): HOGE at sea level at the vehicle's maximum takeoff weight. This flight condition is outside the vehicle's OEI-capable envelope. Derived from NDARC XV-15 model validation Point Design Conditions. The maximum allowable engine rating is IRP, a power rating with a 30-minute thermal endurance limit.

FC 2 Hover Ceiling (AEO): HOGE at 8,000 ft. (ISA) at the vehicle's DGW. This flight condition is outside the vehicle's OEI-capable envelope. Derived from NDARC XV-15 model validation Point Design Conditions. The maximum allowable engine rating is IRP.

FC 3 Maximum Low-Altitude Speed (AEO): Continuous sprint cruise condition at sea level at the vehicle's DGW. This flight condition is outside the vehicle's OEI-capable envelope. Derived from NDARC XV-15 model validation Point Design Conditions. The maximum allowable engine rating is maximum continuous power (MCP).

FC 4 Maximum High-Altitude Speed (AEO): Continuous sprint cruise condition at 12,000 ft. (ISA) at the vehicle's DGW. This flight condition is outside the vehicle's OEI-capable envelope. Derived from NDARC XV-15 model validation Point Design Conditions. The maximum allowable engine rating is MCP.

FC 5 Contingency Level Flight (Engine 1 Inoperative): Cruise condition with the #1 engine inoperative at 12,000 ft. (ISA) at the vehicle's DGW. Derived from NDARC XV-15 model validation Point Design Conditions. The maximum allowable engine rating is MCP.

FC 6 Contingency Level Flight (Engine 2 Inoperative): Mirror of FC #5.

FC 7 Contingency Hover (Engine 1 Inoperative): Hover condition with the #1 engine inoperative at SLS at a vehicle weight of 10,700 lbs. Derived from XV-15 flight test performance data. The maximum allowable engine rating is maximum rated power (MRP), a power rating with a 10-minute thermal endurance limit.

FC 8 Contingency Hover (Engine 2 Inoperative): Mirror of FC #7.

Performance Calibration

Validation of the PANTHER baseline tiltrotor to the actual XV-15 was evaluated using the PANTHER Mission Simulation tool. Figure 17 compares PANTHER vehicle endurance across a range of airspeeds to XV-15 test data. A significant difference in flight endurance is seen when the vehicle is operating in helicopter mode. However, the PANTHER model shows good agreement to the test data when operating above 175 knots in airplane mode. The primary cause of this disparity is the difference between the shape of the rubberized turboshaft engine deck used in PANTHER and the engine performance of the specialized Lycoming LTC1K-4K engines used in the XV-15. Since the majority of fuel consumption was expected to occur during continuous power, airplane-mode flight above 200 knots, the PANTHER XV-15 model was considered an adequate baseline for evaluating hybrid-electric tiltrotor vehicles.

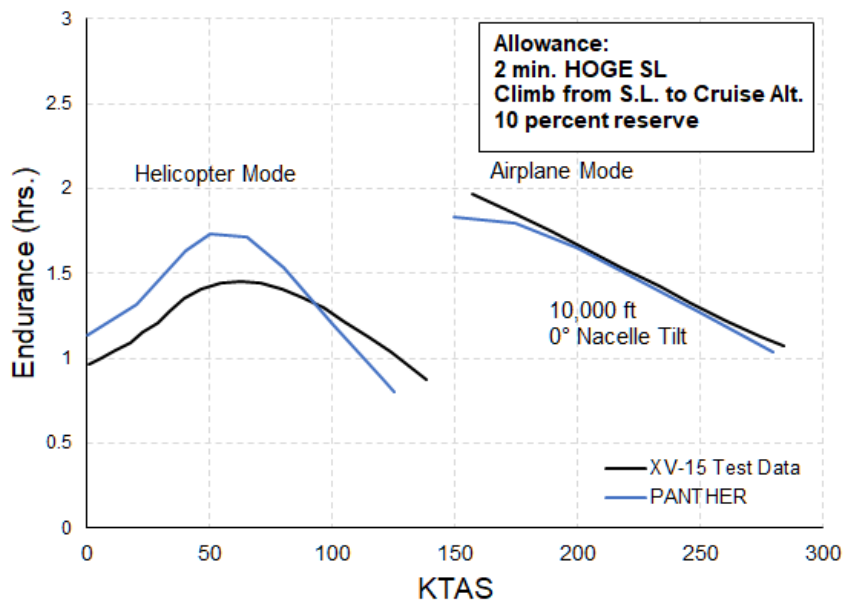

Figure 17. Comparison of PANTHER Tiltrotor Vehicle Endurance to XV-15 Flight Test Data.

3.3.3 Modification to Sizing Conditions for Hybrid Helicopter Development

The development of an additional sizing condition for the baseline configurations was required to set a minimum allowable turbine engine power for the hybrid variants. The airspeeds selected for these new conditions fall within the 99-percent V_{BR} band of the baseline vehicles and were selected as a reasonable first-pass method for evaluating the impact of using a hybrid-electric propulsion architecture to downsize the primary plant.

Hybrid-Electric Specific Sizing Flight Conditions (Configuration A):

> *FC 3 Engine-Only Cruise:* Continuous engine-power-only cruise condition at 9,000 ft. The maximum allowable engine rating is MCP.

Hybrid-Electric Specific Sizing Flight Conditions (Configuration B):

> *FC 5 Engine-Only Cruise:* Continuous engine-power-only cruise condition at 10,000 ft. The maximum allowable engine rating is MCP.

The on-design sizing flight conditions for hybrid-electric Configuration A vehicles are tabulated in Table 3 and the on-design sizing flight conditions for hybrid-electric Configuration B vehicles are tabulated in Table 4.

The following energy scheduling requirement was imposed to size the battery capacity of hybrid-electric helicopter concepts with a secondary battery powerplant. Battery maximum depth-of-discharge is limited to 80 percent of battery capacity to provide some margin and avoid the battery's region of degraded performance at very low charge. Avoiding high depth-of-discharge also improves the battery's cycle life.

- Maximum allowable depth-of-discharge: 80 percent.

Table 3. Point Performance Sizing Conditions for the Hybrid-Electric Configuration A Vehicles.

Sizing Condition	FC #1	FC #2	FC #3
Altitude (ft.)	5000	0	9000
Δ_{Tamb} (F°)	+36	0	0
Weight Fraction	1	1	1
KTAS	0	150	115
V_v (ft/s)	0	0	0
Max Power Rating	IRP	IRP	MCP

Table 4. Point Performance Sizing Conditions for the Hybrid-Electric Configuration B Vehicles.

Sizing Condition	FC #1	FC #2	FC #3	FC #4	FC #5
Altitude (ft.)	5000	0	8000	0	10000
Δ_{Tamb} (F°)	+36	0	0	0	0
Weight Fraction	0.99	1	0.948	1	1
KTAS	0	160	0	146	135
V_v (ft/s)	0	0	1.67	0	0
Max Power Rating	IRP	IRP	IRP	IRP	MCP

3.3.4 Modification to Sizing Conditions for Hybrid Tiltrotor Development

The modification of sizing flight conditions for the hybrid-electric tiltrotor vehicles followed a similar, but slightly different process. The baseline flight conditions were deemed encompassing enough to appropriately size a hybrid version of the vehicle. Decoupling of the engine size from the highest-power flight conditions was managed by adjusting the maximum allowable engine power ratings at each flight condition. Subsequently, hybrid-electric turbine engine size was determined by the highest-power MCP-limited flight condition, with the secondary powerplant sized to provide any additional power needed to achieve the remaining flight conditions. This approach was adequate for the smaller set of tiltrotor designs investigated. The mapping of allowable power rating to each flight condition for the hybrid-electric tiltrotor vehicles is shown in Table 5. Note that this trade study did not investigate battery burst discharge capability; as such, the all-electric vehicle's battery is limited to using only a MCP rating.

The following energy scheduling requirements were imposed to size the battery capacity of the battery backup and battery-boost vehicles. Battery maximum depth-of-discharge is limited to 80 percent of battery capacity to provide some margin and avoid the battery's region of degraded performance at very low charge. Additionally, to prolong battery life the battery must not discharge below 50 percent during the design mission.

For Nominal Flight Conditions (AEO):

- Maximum allowable depth-of-discharge: 50 percent.

For Contingency Flight Conditions (OEI)

- Maximum allowable depth-of-discharge: 80 percent.
- Minimum endurance: 5 minutes.

These requirements were adequate for these vehicles because of the simplicity of their design mission and their fixed power requirements (TOGW and outer mold line (OML) fixed, payload floated). A more complex design effort would require development of a more advanced energy schedule.

Table 5. Point Performance Sizing Conditions for the Hybrid-Electric Tiltrotor Vehicles.

Sizing Condition	FC #1	FC #2	FC #3	FC #4	FC #5	FC #6	FC #7	FC #8
Altitude (ft.)	0	8000	0	12000	12000	12000	0	0
Δ_{Tamb} (F°)	0	0	0	0	0	0	0	0
Weight Fraction	1.154	1	1	1	1	1	0.823	0.823
KTAS	0	0	225	260	172	172	0	0
V_v (kts.)	0	0	0	0	0	0	0	0
Max Allowable Power Rating								
Baseline	IRP	IRP	MCP	MCP	MCP	MCP	MRP	MRP
Battery Backup	IRP	IRP	MCP	MCP	MCP	MCP	MRP	MRP
Battery Boost	MRP	MRP	MCP	MCP	MRP	MRP	MRP	MRP
All Electric	MCP	MCP	MCP	MCP	MCP	MCP	MCP	MCP

3.3.5 Trade Study Design Missions

Mission performance of the trade study vehicles was evaluated using the PANTHER Mission Simulation tool. A simple mission profile was derived from the vehicle sizing flight conditions consisting of a 5-minute HOGE, followed by a climb, and completed with a cruise segment run until primary energy source exhaustion. This simple mission is not intended to represent a realistic design mission, but provides a means to compare hybrid-electric vehicle mission capability as well as observe the performance characteristics of vastly differing propulsion architectures. Climb rate and cruise airspeed varied between vehicles to allow each vehicle to demonstrate its maximum-effort performance. The mission was performed at different payload and fuel loadings for each vehicle to derive payload-range performance. A profile of the comparison mission is shown in Figure 18.

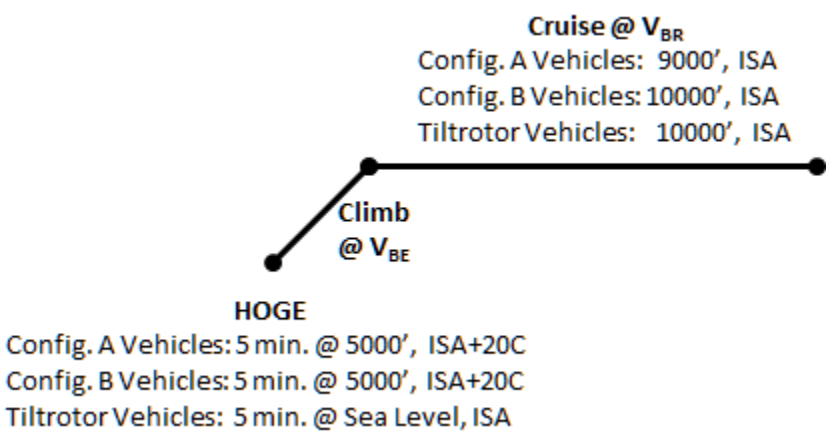

Figure 18. Mission Profile Used to Compare Hybrid-Electric Vehicle Performance.

3.3.6 Development of Hybrid-Electric Vehicles

A list of the vehicles investigated in this trade study effort is shown in Table 6.

Table 6. List of Trade Study PANTHER Vehicles.

	Full Vehicle Name	Abbreviation
NDARC Config. A	Conventional Vehicle	C.A-Conventional
	Task 3.2 - Future Factors: +15 years	C.A-Conventional+15
	Task 3.2 - Future Factors: +30 years	C.A-Conventional+30
	Battery Boosted Gas Turbine Parallel Hybrid	C.A-BBT
	Task 3.2 - Future Factors: +15 years	C.A-BBT+15
	Task 3.2 - Future Factors: +30 years	C.A-BBT+30
	Battery Boosted Gas Turbine Parallel Hybrid – Baseline Payload	C.A-BBT-1000
	Battery Boosted Gas Turbine Series Hybrid	C.A-BBT-S.Hybrid
	Battery All-Electric	C.A-Battery
	Task 3.2 - Future Factors: +15 years	C.A-Battery+15
	Task 3.2 - Future Factors: +30 years	C.A-Battery+30
	Fuel Cell	C.A-Fuel Cell
	Battery Boosted Fuel Cell Series Hybrid	C.A-BBFC
	Diesel	C.A-Diesel
	Twin Diesel	C.A-Twin Diesel
	Battery Boosted Diesel	C.A-BBD
NDARC Config. B	Conventional Vehicle	C.B-Conventional
	Battery Boosted Gas Turbine Parallel Hybrid	C.B-BBT
	Task 3.3 – Failure Modes: Category A Capable, Short Duration	C.B-BBT-Cat.A(5)
	Task 3.3 – Failure Modes: Category A Capable, Long Duration	C.B-BBT-Cat.A(10)
	Battery All-Electric	C.B-Battery
	Fuel Cell	C.B-Fuel Cell
	Battery Boosted Fuel Cell Series Hybrid	C.B-BBFC
XV-15 Tiltrotor	Conventional Vehicle	TLT-Conventional
	Battery Backup Gas Turbine Parallel Hybrid	TLT-BBT-Backup
	Battery Boosted Gas Turbine Parallel Hybrid	TLT-BBT
	Battery All-Electric	TLT-Battery

A brief summary of each vehicle is listed below:

- **C.A-Conventional**—Conventionally powered Configuration A vehicle calibrated to match the corresponding NDARC vehicle.
- **C.A-Conventional+15**—Conventionally powered Configuration A vehicle with component inputs modified to reflect 15 years of technology improvement predictions.
- **C.A-Conventional+30**—Conventionally powered Configuration A vehicle with component inputs modified to reflect 30 years of technology improvement predictions.
- **C.A-BBT**—Hybrid variant of Configuration A featuring a downsized engine and a boost battery using a parallel hybrid propulsion architecture.
- **C.A-BBT+15**—Battery-boosted gas turbine parallel hybrid variant with component inputs modified to reflect 15 years of technology improvement predictions.
- **C.A-BBT+30**—Battery-boosted gas turbine parallel hybrid variant with component inputs modified to reflect 30 years of technology improvement predictions.

- **C.A-BBT-1000**—Battery-boosted gas turbine parallel hybrid variant that maintains the baseline vehicle design payload at the cost of reduced fuel capacity.
- **C.A-BBT-S.Hybrid**—Hybrid variant of Configuration A featuring a downsized engine and a boost battery using a series hybrid propulsion architecture.
- **C.A-Battery**—All-electric, battery-powered variant of Configuration A.
- **C.A-Battery+15**—All-electric, battery-powered variant of Configuration A with component inputs modified to reflect 15 years of technology improvement predictions.
- **C.A-Battery+30**—All-electric, battery-powered variant of Configuration A with component inputs modified to reflect 30 years of technology improvement predictions.
- **C.A-Fuel Cell**—Fuel-cell-powered variant of Configuration A.
- **C.A-BBFC**—Variant of Configuration A featuring a downsized fuel cell and a boost battery using a series hybrid propulsion architecture.
- **C.A-Diesel**—Variant of Configuration A using a large diesel engine instead of the conventional turboshaft engine.
- **C.A-Twin Diesel**—Variant of Configuration A using two diesel engines instead of the conventional turboshaft engine.
- **C.A-BBD**—Variant of Configuration A using two diesel engines and a boost battery using a parallel hybrid propulsion architecture.
- **C.B-Conventional**—Conventionally powered Configuration B vehicle calibrated to match the corresponding NDARC vehicle.
- **C.B-BBT**—Hybrid variant of Configuration B featuring a downsized engine and a boost battery using a parallel hybrid propulsion architecture.
- **C.B-BBT-Cat.A(5)**—Battery-boosted gas turbine parallel hybrid variant with the electric powertrain components scaled up to provide 5 minutes of OEI climb-out capability.
- **C.B-BBT-Cat.A(10)**—Battery-boosted gas turbine parallel hybrid variant with the electric powertrain components scaled up to provide 10 minutes of OEI climb-out capability.
- **C.B-Battery**—All-electric, battery-powered variant of Configuration B.
- **C.B-Fuel Cell**—Fuel-cell-powered variant of Configuration B.
- **C.B-BBFC**—Variant of Configuration B featuring a downsized fuel cell and a boost battery using a series hybrid propulsion architecture.
- **TLT-Conventional**—Conventionally powered tiltrotor vehicle calibrated to match the performance of the XV-15.
- **TLT-BBT-Backup**—Hybrid variant of the tiltrotor configuration featuring downsized engines and a boost battery using a parallel hybrid propulsion architecture. The battery is sized to provide sufficient power for OEI operations.
- **TLT-BBT**—Hybrid variant of the tiltrotor configuration featuring downsized engines and a boost battery using a parallel hybrid propulsion architecture. The battery is sized to provide sufficient power for boosted hover, boosted climb, and OEI operations.
- **TLT-Battery**—All-electric, battery-powered variant of the tiltrotor configuration.

Using the methods discussed previously, the trade study vehicles listed above were assembled and tested in PANTHER. The basic development of each vehicle involved defining the propulsion architecture and point performance sizing conditions in the PANTHER on-design file, then developing the mission profile and power distribution CONTROL files for off-design performance simulation. PANTHER's simulation methods produced a large amount of performance data for each vehicle including many Energy Flow vs. Airspeed plots and mission performance tables and plots. All performance data has been archived and will continue to be a valuable resource in ESAero's development of hybrid-electric vehicle conceptual design methods.

3.4 Results

The primary method of comparing hybrid-electric vehicle performance was through a simple mission profile that was simulated using PANTHER off-design methods. Mission simulation allowed for the generation of payload-range plots for each vehicle. While far from an exhaustive metric of comparison, payload-range performance provides feedback on the quantitative impact of implementing different types of hybrid-electric propulsion systems, power split sizing schemes, and power distribution control methodologies.

3.4.1 Comparison of Configuration A Vehicles

Configuration A Battery-Boosted Gas Turbine Vehicles

The mission performance of the Configuration A–based battery-boosted gas turbine hybrid vehicles is shown in Figure 19. All hybrid vehicles had significantly reduced maximum payload capacity compared to baseline because of the increase in vehicle empty weight. The difference between the similar C.A-BBT and C.A-BBT-1000 vehicles demonstrates the difference in PANTHER results between floating the vehicle design payload or the vehicle design fuel load. The additional reduction in payload exhibited by C.A-BBT is due to the increase in empty weight incurred by the larger capacity fuel system. From a propulsion architecture perspective, the difference between these vehicles is very similar to adding an additional internal fuel tank. For extremely light payloads, C.A-BBT demonstrates slightly increased maximum range over the baseline vehicle.

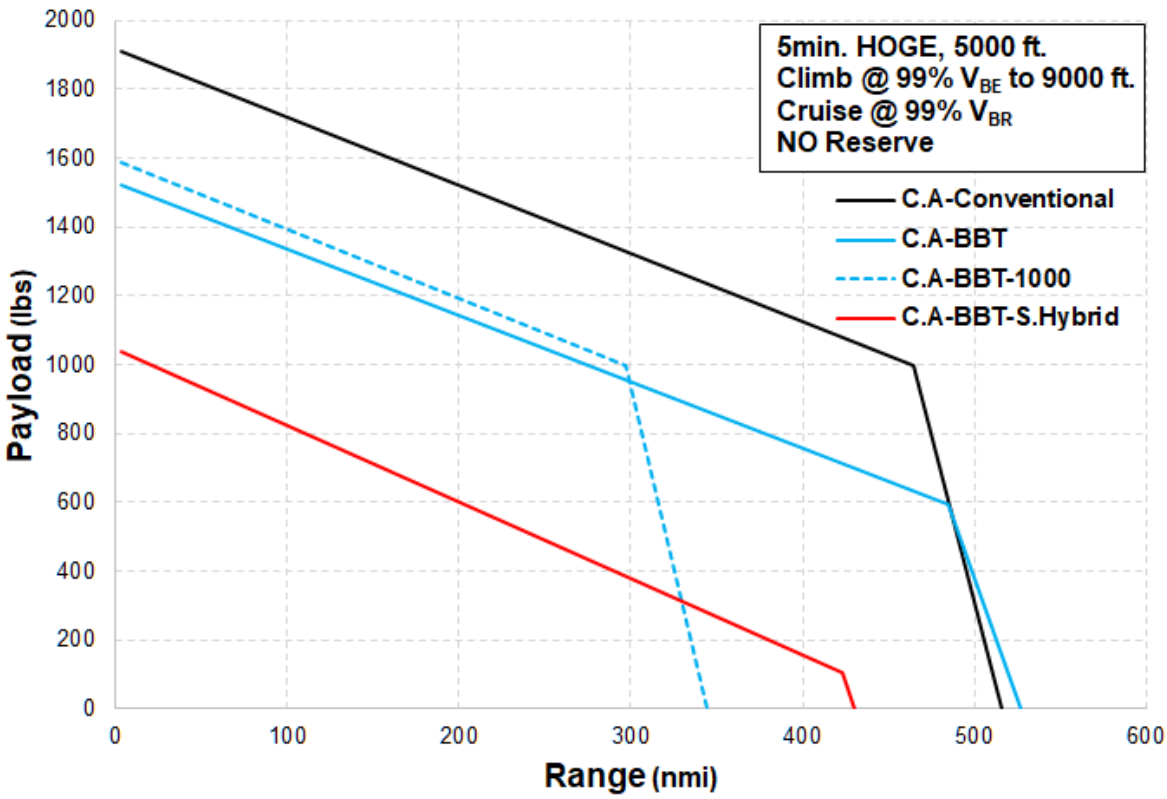

Figure 19. Configuration A Battery-Boosted Gas Turbine Vehicle Payload-Range Performance.

Configuration A Battery and Fuel Cell Vehicles

The mission performance of the Configuration A–based battery and fuel-cell-equipped vehicles is shown in Figure 20. Note that the range of the axes are significantly smaller than shown in the other performance plots because of the poor overall mission performance of these vehicles. The C.A-Battery and C.A-Fuel Cell vehicles are represented by their "design frontiers," which represent the linear trend of the payload-range design point as design energy load is traded for design payload. Section 3.5.1 describes the derivation of the design frontier concept in further detail.

The performance of C.A-BBFC demonstrates how a battery and fuel cell hybrid vehicle can provide a performance improvement over a single-plant battery or fuel-cell-powered vehicle. The fuel cell has poor specific power scaling while the battery is limited by poor specific energy. Use of a supplementary battery to provide boost power for short-duration, high-power maneuvers allowed for a significantly lighter fuel cell system. This indicates that for this propulsion architecture, at a given design point, there is likely some optimal split between the battery and fuel cell power capabilities that minimizes propulsion system weight. Regardless, heavy energy storage components in the form of batteries or hydrogen tanks greatly reduced the mission capability of these types of vehicles. However, these vehicle types may be able to fulfill a low-endurance mission role where cost, noise, and harmful emissions are the paramount concerns.

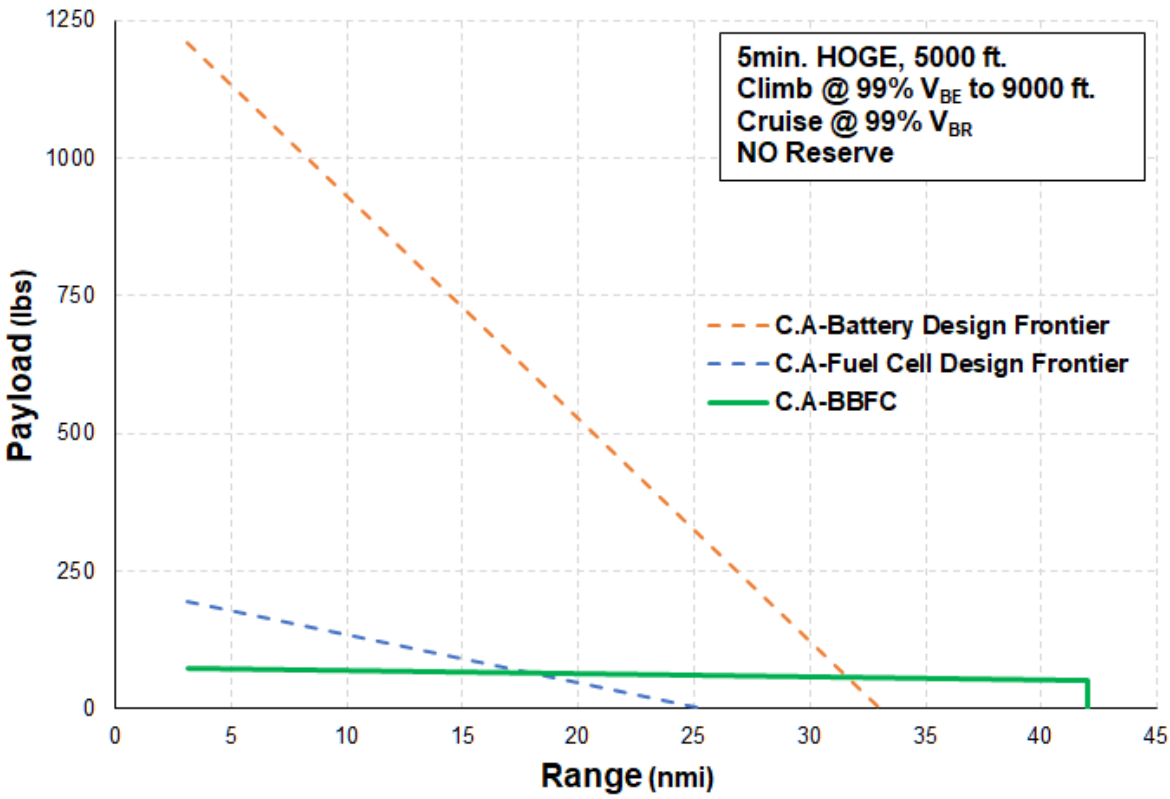

Figure 20. Configuration A Battery and Fuel Cell Vehicle Payload-Range Performance.

Configuration A Diesel Engine Vehicles

The mission performance of the Configuration A–based diesel-engine-equipped vehicles is shown in Figure 21. The improvement in engine efficiency granted the diesel-engine-equipped vehicle a significant range improvement over the baseline turbine-engine-powered vehicle. However, the heavy diesel engine decreased the payload carrying capability. Note that the C.A-Diesel vehicle was equipped with an engine nearly 60 percent more powerful than the most powerful diesel in the aviation diesel engine database used to develop empirical weight and specific fuel consumption (SFC) trends. C.A-BBD and C.A-D2 were both attempts to address the issue of current aviation diesel engines lacking adequate power for the Configuration A vehicle. For both vehicles, the diesel engines were tuned to match the weight, power, and fuel consumption of the most powerful engine in the diesel engine database. In either case, the payload carrying capacity was further limited by the introduction of a heavy secondary powerplant.

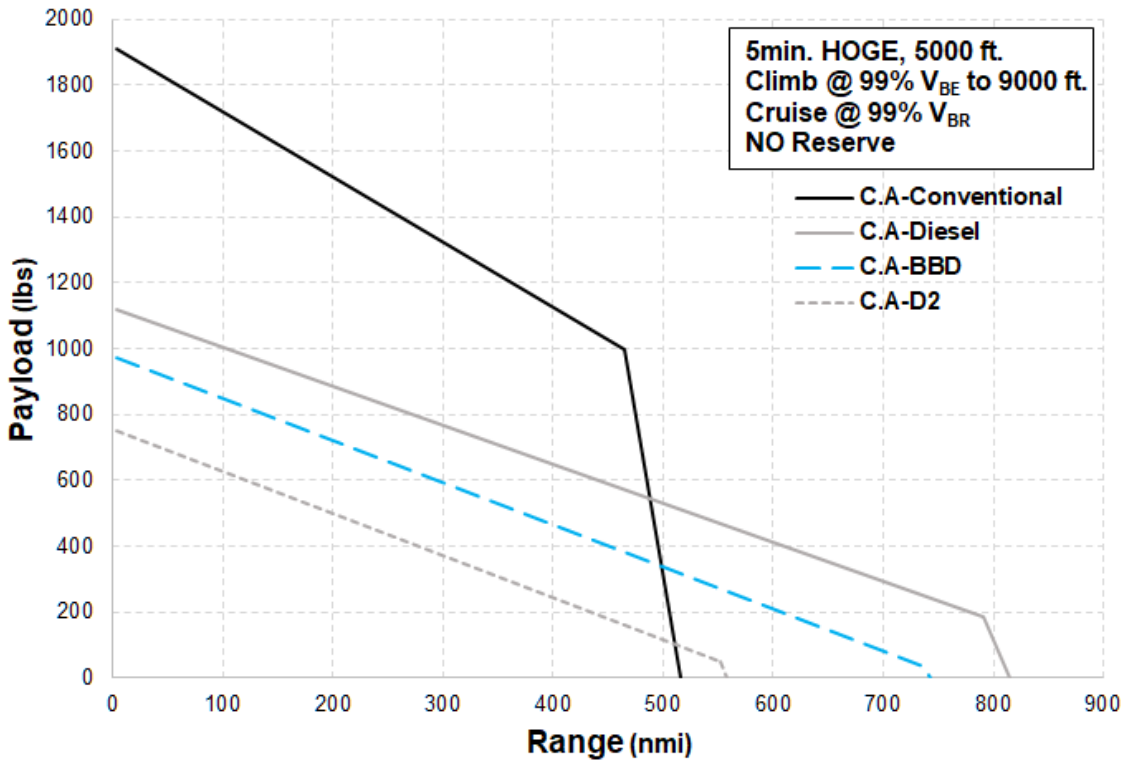

Figure 21. Configuration A Diesel Vehicle Payload-Range Performance.

3.4.2 Comparison of Configuration B Vehicles

Configuration B Vehicles

The mission performance of the Configuration B–based vehicles is shown in Figure 22. C.B-BBT seemed to be more competitive vs. its baseline vehicle than C.A-BBT. The difference was likely a result of the Configuration B hybrid replacing two engines operating at low throttle in cruise with a single engine specifically sized for fuel-efficient cruise performance. The impact of this architecture change on the vehicle's OEI performance is explored in section 3.4.4. The battery and fuel cell vehicles are shown in the far lower corner of the plot. The fuel cell system in particular did not scale well with the increase in vehicle size, and the performance of C.B-Fuel Cell and C.B-BBFC was extremely marginal as a result.

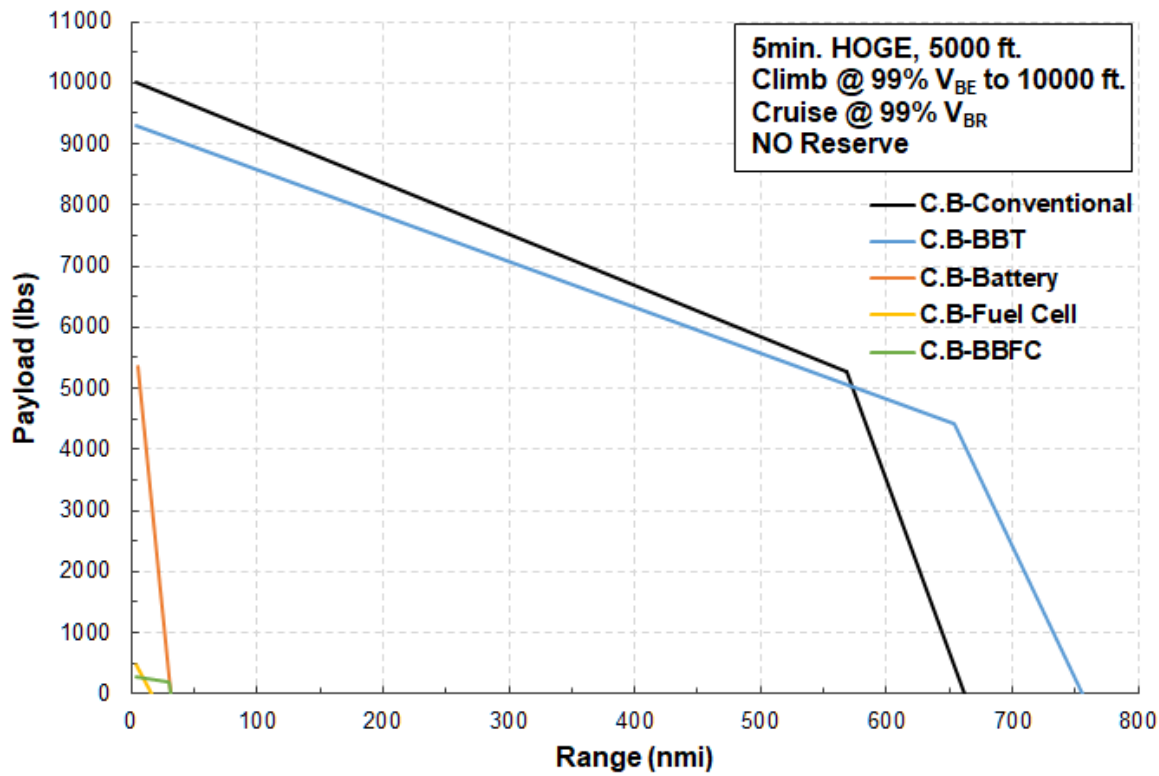

Figure 22. Configuration B Vehicle Payload-Range Performance.

3.4.3 Comparison of Tiltrotor Configuration Vehicles

The design mission payload-range performance of the tiltrotor vehicles is shown in Figure 23. Note that the 13,000 lbs corresponded to the vehicle's OEI-capable gross weight while 15,000 lbs was the non-OEI-capable maximum TOGW specified by the XV-15 reference data. Note also that performance data for the XV-15 indicated that the gearboxes imposed a torque limit while operating in airplane-mode that limited the vehicle's climb rate; this mode-dependent performance limit was not incorporated into the PANTHER XV-15 model. As a result, the maximum takeoff gross weight (MTOGW) line for TLT-Conventional demonstrates the vehicle's engine power limit rather than its vehicle-level performance limit imposed by the powertrain torque limit. The improved point performance fuel consumption of the hybrid-electric vehicles did not result in an overall maximum-effort mission range improvement. This was due to the higher empty weight of the hybrid vehicles resulting in greater overall exertion compared to baseline over the length of the mission. As seen with the NDARC configurations, the all-electric-design frontier provided almost no mission capability. The TLT-Battery vehicle runs out of energy before reaching cruise altitude.

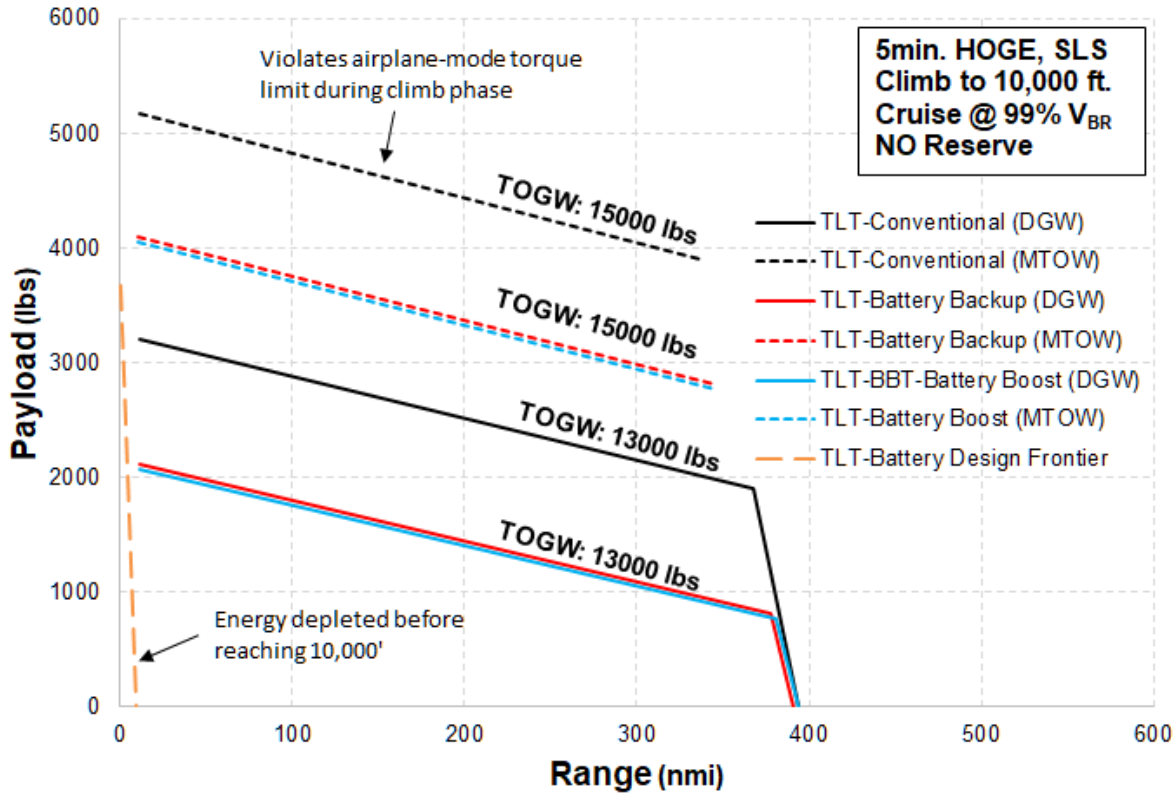

Figure 23. Tiltrotor Vehicle Payload-Range Performance.

3.4.4 Impact of Imposing Redundant Capability Sizing Requirements

As noted in the development and comparison of the Configuration B Battery-Boosted Turbine hybrid-electric vehicle, replacement of the twin turbine engines with a battery-boosted single engine resulted in a notable extension of the vehicle's performance envelope. However, because the sizing conditions for this configuration did not include any failure-mode performance requirements, the propulsion elements were sized solely for nominal operation with no consideration given to potential engine-out scenarios. This gap in analysis arises from the decoupling of engine power requirements from the highest-power-required sizing flight condition. This conceptual problem was investigated by creating a variant of the C.B-BBT vehicle that maintained some of the conventional vehicle's level of powerplant-failure redundant flight capability. Determination of the OEI maneuver requirements was in of itself a challenge—applying the conventional vehicle's method of imposing power parity between the plants would greatly oversize the hybrid's battery powerplant. Initial research indicates that national aviation regulations can be a useful resource for defining hybrid vehicle contingency operation minimum capabilities; however, some creativity is required to adapt these requirements so that they can be applied to hybrid-electric vehicles. A failure-mode sizing flight condition was eventually derived from Federal Aviation Regulation (FAR) 29 Category-A engine failure on takeoff maneuver requirements.

FAR 29.1 states that rotorcraft with a maximum weight greater than 20,000 lbs or 10 or more passenger seats must be type certificated as Category A rotorcraft, whereas rotorcraft of less than 20,000 lbs and carrying seating for less than 10 passengers can be classified as Category B (ref. 9). Based on FAR 29.1, the baseline Configuration A vehicle could be certified as a Category B rotorcraft while the Configuration B vehicle would have to be certified as a Category A rotorcraft to operate at its design TOGW.

Category A certification requires climb-out ability in the event of single engine failure during takeoff and landing maneuvers. The non-vertical FAR 29 Category A takeoff profiles for a rejected takeoff (RTO) and continued takeoff (CTO) are shown in Figure 24. The continued takeoff profile begins at the takeoff decision point (TDP), after which the vehicle can no longer perform an RTO within the required distance. After increasing its airspeed, the helicopter must be capable of a 100-feet-per-minute (fpm) climb up to 200 ft. over the takeoff surface, with the remaining powerplant operating at a 2.5-minute OEI power rating. This is followed by a second climb at 150 fpm at the best climb speed up to 1,000 ft. above the takeoff surface, with the remaining powerplant operating at a 30-minute OEI power rating. The RTO profile was not evaluated as the dynamic nature of this maneuver made it a poor choice for the development of a point-performance sizing condition for this propulsion-power-focused trade study.

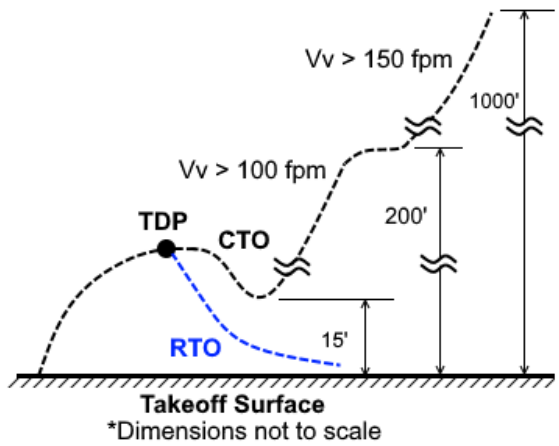

Figure 24. Category A Rotorcraft OEI Takeoff Profile.

The 150-fpm climb requirement was referenced within PANTHER as a flight condition to represent OEI CTO requirements. The 30-minute OEI power setting corresponds to the PANTHER engine model's IRP setting, and the best rate of climb airspeed, V_Y, can be reasonably estimated using PANTHER's performance analysis tools. Implementing this contingency performance requirement for the hybrid-electric vehicle resulted in the modified sizing flight conditions shown in Table 7. Flight conditions #4 and #5 imposed the Category A OEI CTO climb-out power requirements on the battery system and turbine engine, respectively.

Table 7. Point Performance Flight Condition Requirements for Sizing Baseline Tiltrotor Vehicle.

Sizing Condition	FC #1	FC #2	FC #3	FC #4	FC #4	FC #5
Altitude (ft.)	5000	0	10000	8000	6000	6000
Δ_{Tamb} (F°)	+36	0	0	0	0	0
Weight Fraction	0.99	1	1	1	0.99	0.99
KTAS	0	160	135	138.2	81	81
V_v (ft/s)	0	0	0	0	2.5	2.5
Max Power Rating	IRP	IRP	MCP	MCP	Inop.	IRP

The Category A–capable takeoff envelopes for the conventionally powered and battery-boost Configuration B vehicles were evaluated by disabling one of the vehicle's powerplants and enforcing a 150-fpm climb requirement across a sweep of vehicle gross weights and altitudes. The three vehicles evaluated were C.B-Conventional, C.B-BBT, and C.B-BBT-Cat.A, a battery-boosted turbine vehicle with the electrical drivetrain scaled up to provide OEI CTO climb-out capability similar to the baseline vehicle

when performing its design mission takeoff. The Category A–capable hybrid was evaluated with the battery capacity sized for both 5 minutes and 10 minutes of OEI CTO operation; these vehicles were designated as C.B-BBT-Cat.A(5) and C.B-BBT-Cat.A(10), respectively.

The impact on mission performance of scaling up the electric powertrain's power and energy capacity to provide Category A capability is shown in Figure 25. Imposing additional OEI capabilities on the design of Configuration B hybrids had a negative impact on the vehicle's mission capability. The reduction in capability arises from the increase in vehicle powertrain weight from both upscaling the power output of the electrical components and increasing the energy storage capacity of the battery powerplant.

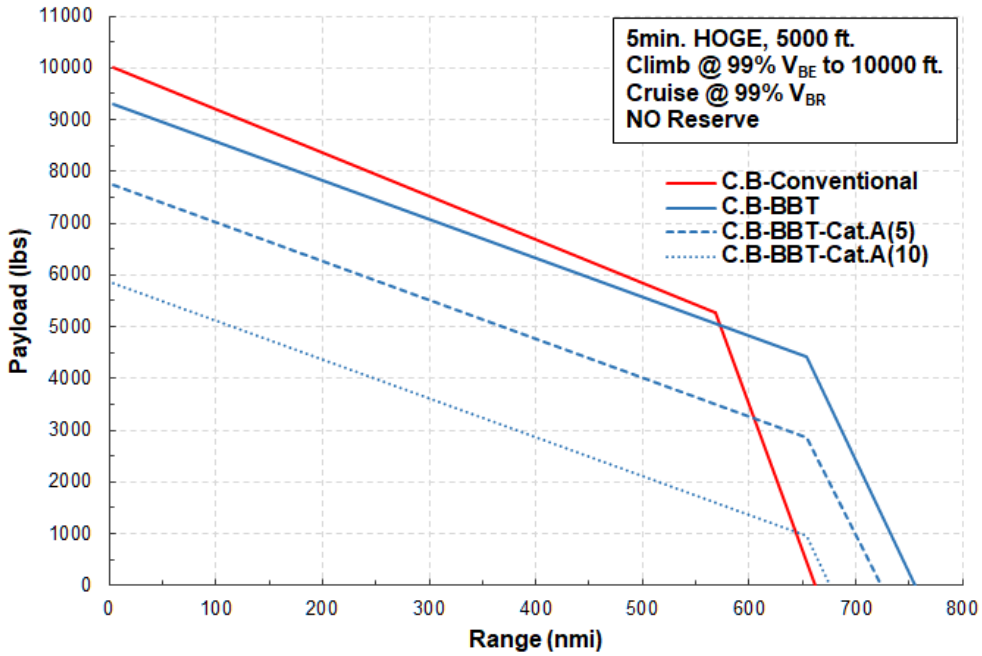

Figure 25. Payload-Range Diagram for C.B-BBT Vehicles With Different Levels of Redundant Capability.

3.4.5 Impact of Future Technology Improvements

Most hybrid-electric propulsion system designs for rotorcraft are not likely to enter service for many years. Therefore, it is important to account for intervening advances in propulsion technology. In an attempt to better understand the impact of technological progression on the feasibility of hybrid-electric rotorcraft designs, future factors were applied to the component performance and sizing factors of several of the propulsion architectures investigated.

Future technology scaling factors were based on a combination of industry projections and constant scaling factors in areas of lesser certainty. Future factors for structural component and conventional, mechanical powertrain components were hard to come by, leading to the use of constant scaling factors across all structural and mechanical powertrain weights. This method was considered acceptable given that these scaling factors were shared between all conventional and hybrid vehicles. Over 15- and 30-year time frames, these weights were modeled as decreasing by 5 and 10 percent, respectively. It is believed that these improvements are neither conservative nor optimistic and should not unduly affect the trends shown in this future factor analysis.

Turboshaft engine SFC was assumed to improve by 7 percent in 15 years and 14 percent in 20 years. This assumption is somewhat more conservative than predictions made by the National Academies of Sciences (ref. 10).This was done in part because it was felt that the trends drawn from historical data may become increasingly marginal as engine technology progresses. Battery-specific capacity was modeled as doubling every 15 years based on a NASA report on future advancements in non-cryogenic electric aircraft propulsion (ref. 11). Current state-of-the-art batteries are predominantly Li-ion, but the specific energy of this chemistry is expected to plateau in the coming years as its theoretical limits are reached. Therefore, to achieve required improvements in specific energy, a change in battery chemistry will be required. Conservative estimates for the performance of these future batteries were made to account for the incomplete understanding of how this technology will mature. Motor and generator performance was scaled in accordance with NASA's projections. A state-of-the-art specific power of 3 hp/lb is projected to increase to 8 hp/lb in the next 15 years and then to 16 hp/lb in the next 30 years. Increases in motor efficiency are expected to improve from current levels of 95 percent to 98 and 99 percent over the same time frames (ref. 11). Table 8 summarizes the scaling factors used in this study.

Table 8. Future Technology Scaling Factors.

Hybrid-Electric Future Factors	State of the Art	+15 years	+30 years
Structure			
Weight Scaling Factor	1	0.95	0.90
Powertrain			
Weight Scaling Factor	1	0.95	0.90
Turboshaft			
Weight Scaling Factor	1	0.95	0.90
SFC scaling factor	1	0.93	0.86
Motor/Generator			
Efficiency	0.95	0.98	0.99
Specific Power (hp/lb)	3	8	16
Battery			
Specific Energy (Wh/kg)	200	400	800

Configuration A was selected for future factor analysis as it saw the most extensive propulsion architecture exploration. The results of applying the future factors to several Configuration A hybrid-electric vehicles are shown in Figure 26. The improvements to electrical component performance are expected to outpace the improvements to gas turbine technology, which resulted in the hybrid-electric vehicle demonstrating performance benefits over the conventional vehicle in the 15- to 30-year time frame. C.A-BBT+30 had similar payload capabilities as the baseline vehicle while exhibiting a notable reduction in fuel burn and subsequent increase in range. The all-electric battery vehicle also exhibited massive future performance improvements. While still rather range-limited, the improved performance perhaps makes it a viable zero-emission, short-range vehicle design.

The results of applying the same future factors to several hybrid-electric tiltrotor vehicles are shown in Figure 27. As with the helicopter, the battery-boosted hybrid exhibited similar payload capacity and improvements to range and fuel consumption at +30-years, with the battery-boosted vehicle showing marginal improvements in maximum range.

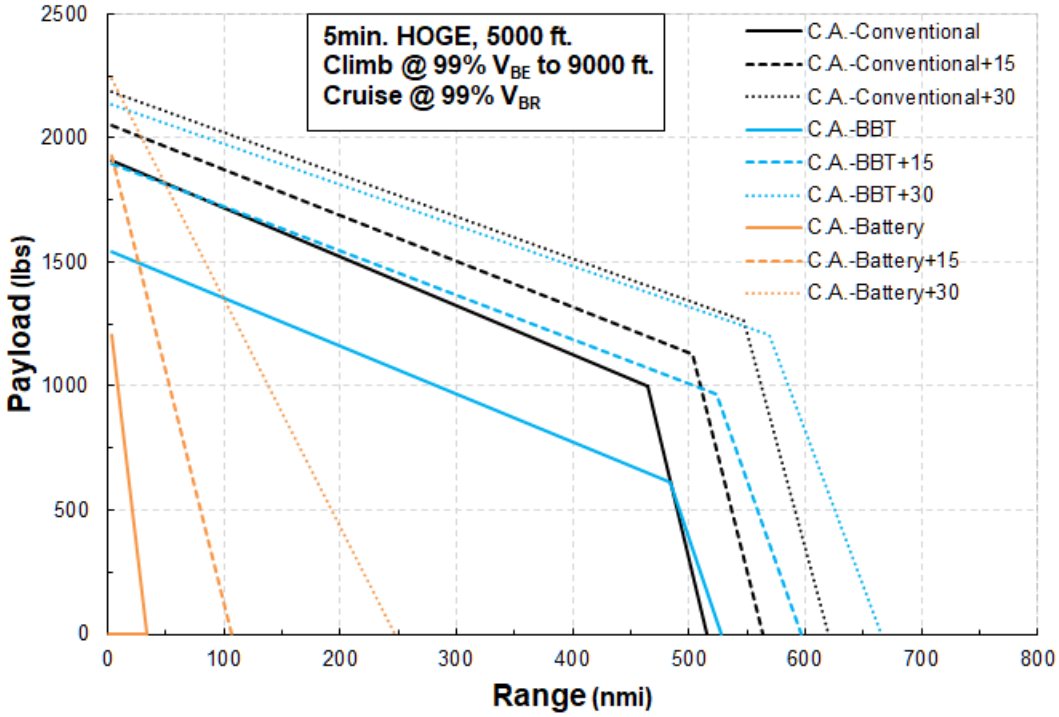

Figure 26. Projected Future Configuration A Vehicle Mission Performance.

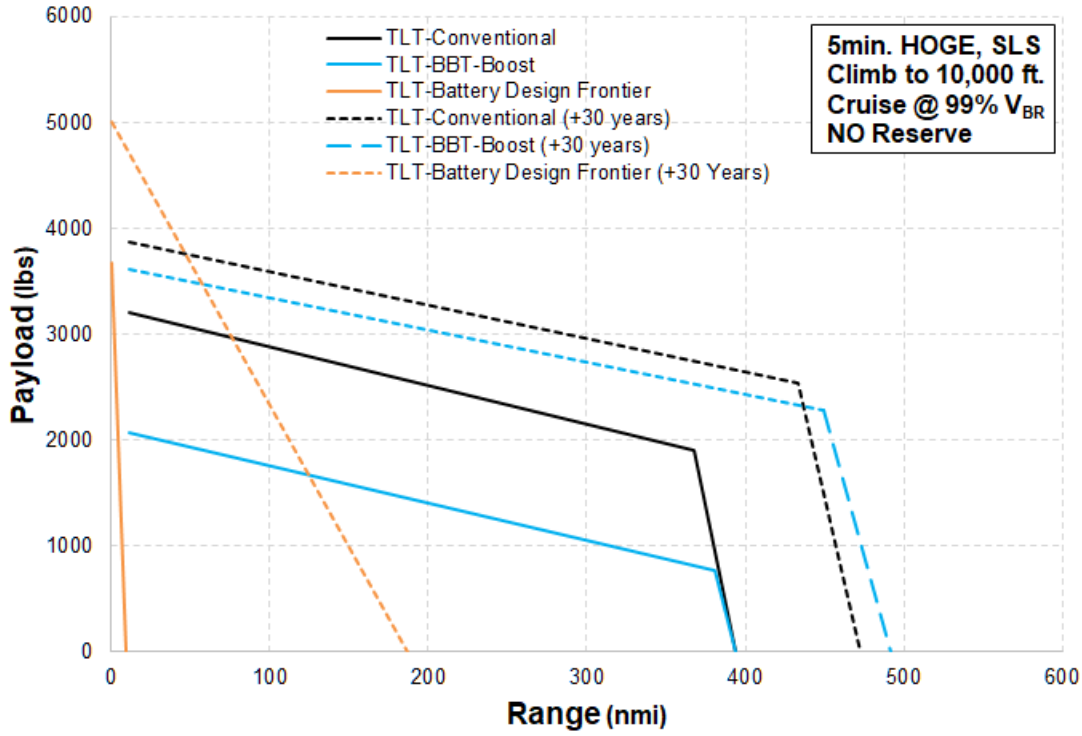

Figure 27. Projected Future Tiltrotor Vehicle Mission Performance.

3.5 Lessons Learned

Aside from the comparative mission performance charts, this project garnered many lessons learned regarding the process for designing and evaluating hybrid-electric rotorcraft. This section lists several of these important lessons.

3.5.1 Design Frontiers for Fixed-Weight and Low-Weight Energy Source Powered Vehicles

Conventional vehicle energy storage systems are comprised of fuel tanks that can usually be filled to nearly any point within their maximum capacity. This design feature allows easy tradeoff between energy weight (fuel) and payload weight to accomplish a wide range of off-design missions. This is demonstrated on a conventional vehicle's payload-range plot by a constant-TOGW line. Constant-weight energy sources do not demonstrate this capability—for example, a battery charged to only half of its energy capacity still has the same weight as a fully charged battery. Additionally, for fuel-type energy sources that have an extremely high specific energy, such as hydrogen, the reduction in fuel weight when operating at partial maximum storage capacity can be insignificant in comparison to the overall vehicle weight. In these cases, the payload-range plot for a given mission profile does not exhibit a significant change in range with payload weight at a fixed TOGW.

However, many conventional vehicles can adjust their overall energy storage capacity by using auxiliary fuel tanks. Some electric or hybrid vehicle designs may be capable of a similar operation, for example by varying the number of battery cells carried between missions. As shown in Figure 28, when multiple fixed-energy-capacity designs for a given vehicle are plotted on the same payload-range diagram, the maximum range at design-TOGW points fall along a line. This line describes the frontier of a vehicle design's energy capacity–payload weight tradeoff. For a constant or near-constant-weight energy source vehicle that allows for variable energy capacity loading, this design frontier is effectively the fixed-TOGW payload-range tradeoff line.

Similarly, the design frontier for the Configuration A fuel cell vehicle is also shown in Figure 28. Because the battery and fuel cell vehicles did not exhibit noteworthy payload-range tradeoffs for a fixed design energy capacity, these vehicles were represented on payload-range diagrams by their design frontiers throughout this report. Note that the design frontier lines shown in this report demonstrate infinitely variable energy capacity loading. This is acceptable for determining the design point of a fixed-energy-capacity vehicle. However, a real-world variable-energy-capacity vehicle would likely demonstrate discrete energy capacity loading options because of effects such as single-pack capacity or packing factors. Additionally, a real-world variable-energy-capacity vehicle might demonstrate a significant non-linear energy capacity–payload weight relationship across its energy loading options.

3.5.2 Impact of Power Distribution Control Methods on Hybrid-Electric Vehicle Design

The Energy Flow vs. Airspeed plot for the conventionally powered Configuration A vehicle at cruising altitude is shown in Figure 29. As expected, it is indistinguishable from a standard fuel flow plot. The corresponding endurance indicator and range indicator sweep plots are shown in Figure 30 and are similarly identical to specific range and specific endurance plots for a conventional vehicle.

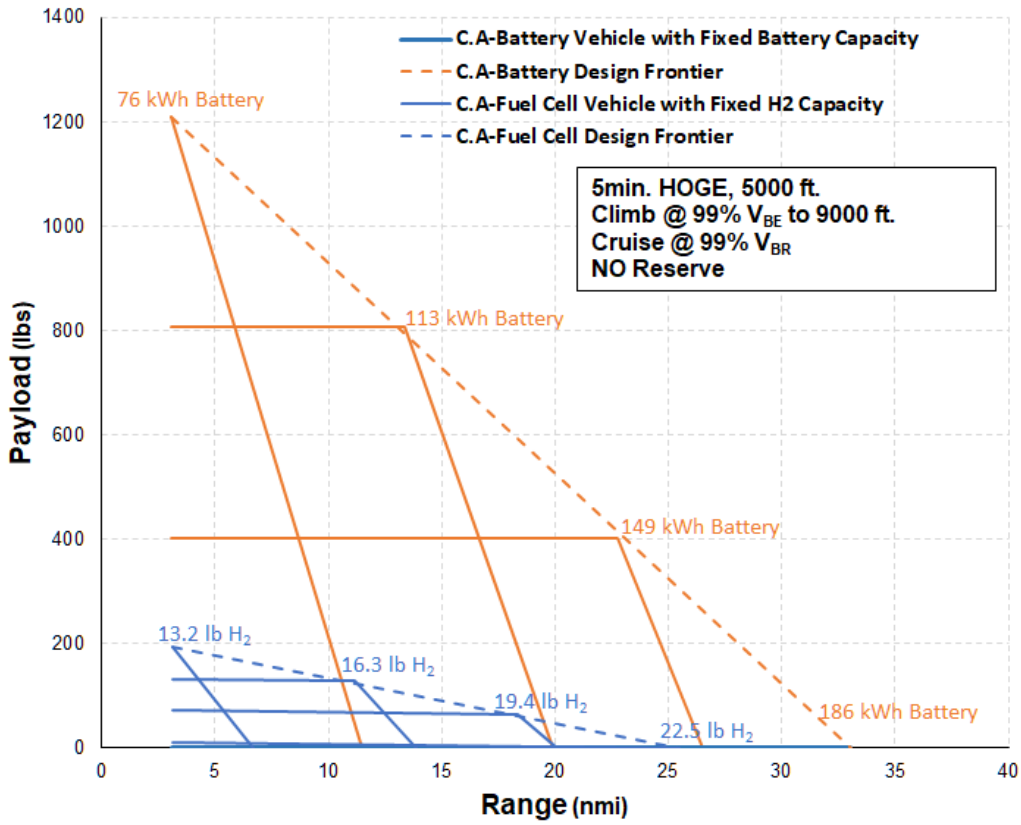

Figure 28. Design Frontier and Specific Design Points for Configuration A Battery and Fuel Cell Vehicles.

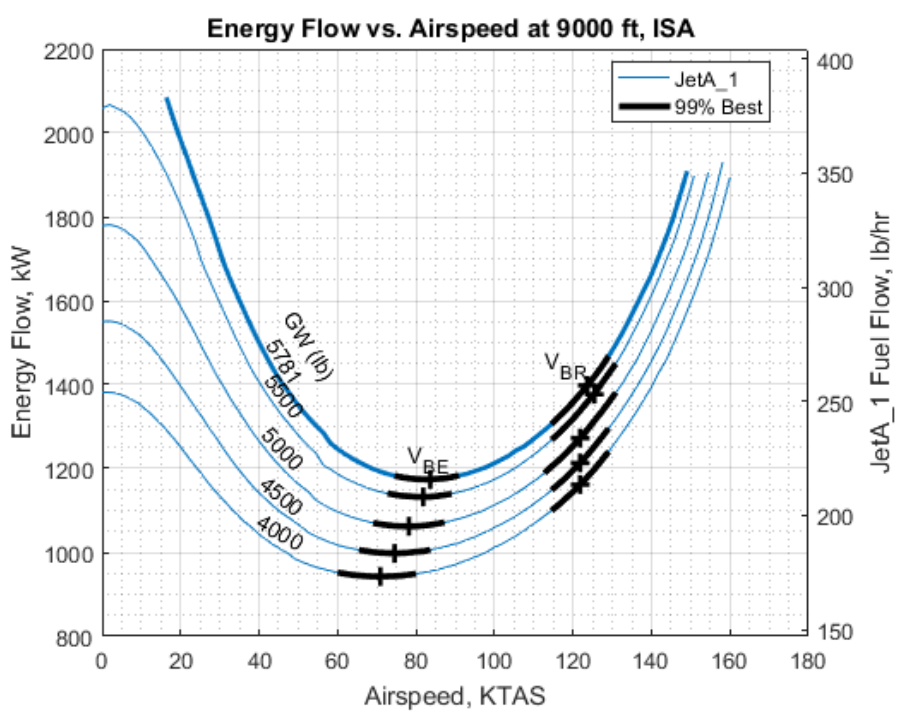

Figure 29. Energy Flow Diagram of Configuration A Baseline.

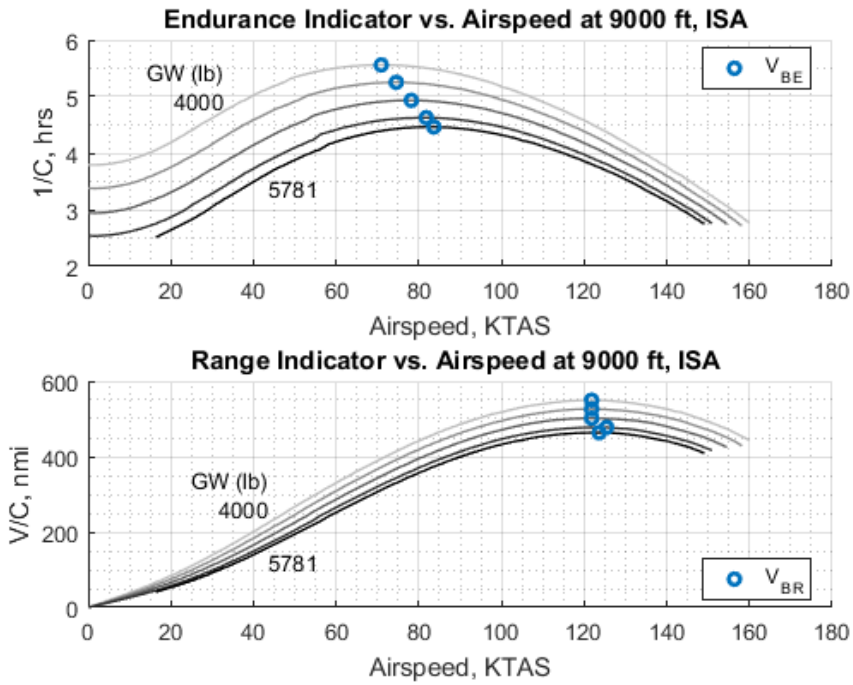

Figure 30. Endurance and Range Indicators for Configuration A Baseline.

The engine of the C.A-BBT hybrid helicopter was sized to operate at a high continuous power setting and subsequent efficiency in cruise, where the conventional vehicle's fuel efficiency suffered from being at a low engine power setting. The effect that this propulsion architecture and power distribution control concept had on the vehicle's energy flow at the cruise altitude is shown in Figure 31. The decoupling of the turbine engine sizing from high-power maneuver requirements can easily be seen by the "flat-rating"–like effect bounding the minimum-required-power bucket. Flight conditions within the flight envelope that exhibit a discrepancy between power required and engine power available were made up for by discharging the battery. The net energy flow from both powerplants is visualized by the dotted "Net" energy flow lines.

The implications these power and energy considerations have on hybrid-electric performance are shown in the behavior of the best-range airspeeds in Figure 31. These values were calculated using the endurance indicator and range indicator metrics derived in section 3.2.2, and account for the lower capacity of the battery when analyzing the vehicle's energy usage rates. The limited battery capacity had the effect of restricting the maximum-effort airspeeds to engine-only operation, as any significant discharge of the battery caused it to drain long before the fuel reserves were depleted. This effect is shown in more detail in the Endurance Indicator vs. Airspeed and Range Indicator vs. Airspeed plots shown in Figure 32. The sharp drop-offs in endurance or range indicator correspond with discharge of the limited capacity battery.

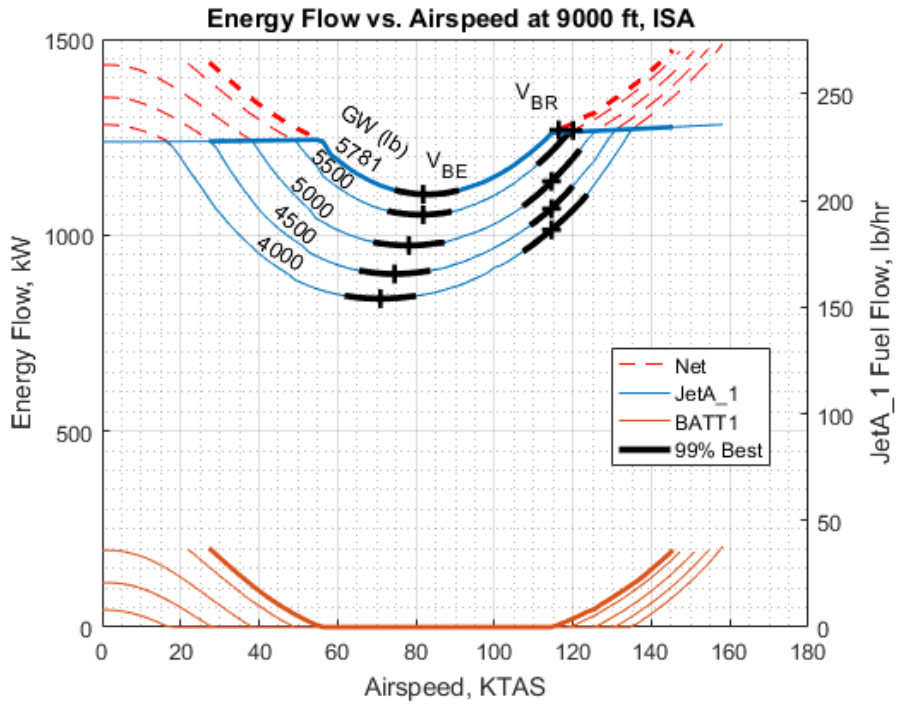

Figure 31. Energy Flow in Cruise of Configuration A Battery-Boosted Turbine Hybrid.

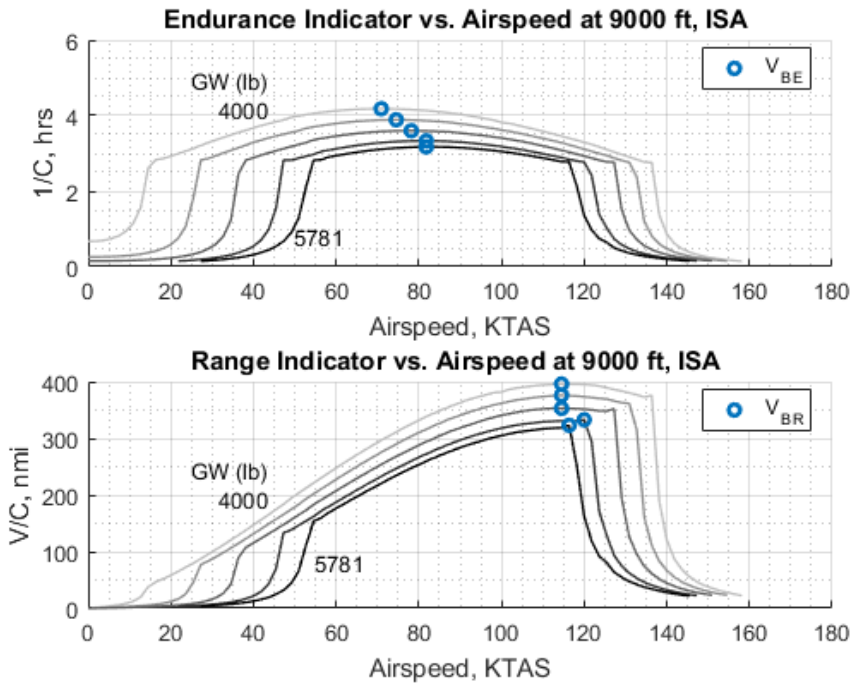

Figure 32. Endurance and Range Indicators for Configuration A Battery-Boosted Turbine Hybrid.

The previous figures represent vehicle performance with no battery charging. Charging the battery requires the production of excess engine power that is distributed internally, which influences the airspeed and energy flow values of the maximum-effort airspeeds. Figure 33 is a sweep of the same hybrid vehicle and flight conditions, but with excess engine power diverted to the battery at its maximum charge rate.

This performance chart is representative of the hybrid vehicle having completed the HOGE and climb segments of the design mission and beginning its cruise segment while charging the battery. Maximum-endurance airspeeds are relatively unaffected, although the fuel flow is increased because of the increase in engine throttle. An interesting effect of distributing engine power internally to charge the battery is that at heavier gross weights, the best-range airspeed is equivalent to the maximum possible airspeed, and under these conditions, throttle would not need to be adjusted to maintain V_{BR} as the vehicle burned fuel.

As shown in the previous energy flow figures, the maximum-effort airspeeds of a hybrid vehicle can be influenced by the internal energy flow, which is dictated by the power distribution control concepts behind the vehicle design. How and when to distribute power within a hybrid vehicle is an important component of the conceptual basis behind the hybrid vehicle. For example, whether to charge a battery at its maximum rate or to charge at a slower rate can affect the overall range and capability of the vehicle. Additionally, a hybrid-electric vehicle expresses unique design metrics, such as the minimum time between high-power maneuvers, which is driven by the vehicle's charging capability.

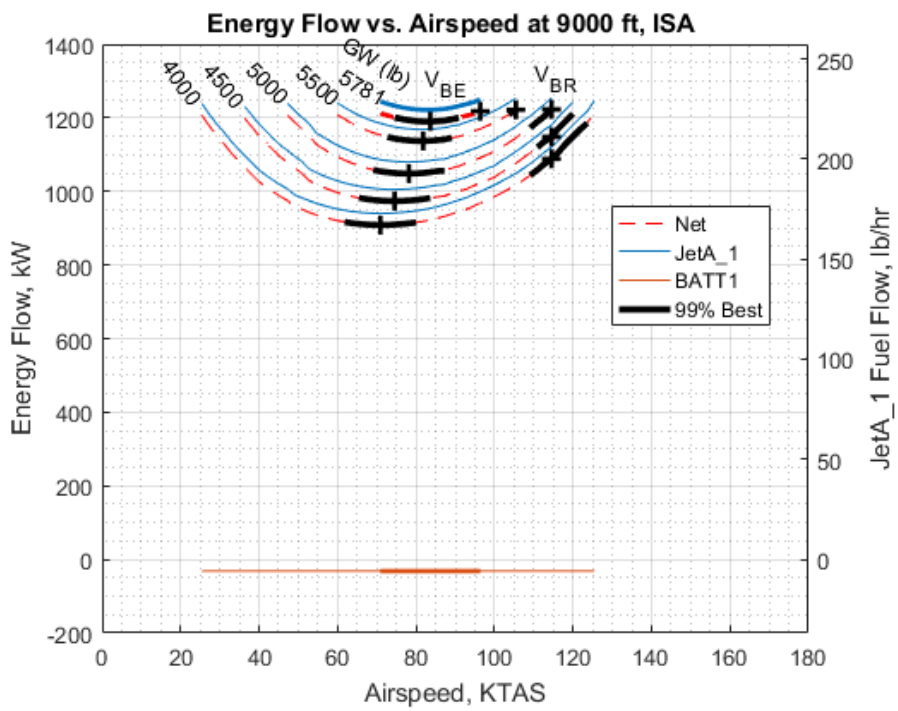

Figure 33. Energy Flow in Cruise of Configuration A Battery-Boosted Turbine Hybrid, Maximum Battery Charge Rate.

3.5.3 Defining Redundancy Requirements and Regulatory Considerations

Initial research indicates national aviation regulations can be a useful resource for defining hybrid-electric vehicle failure-mode performance requirements such as a single engine failure or a battery system failure; however, some creativity is required to adapt these requirements so that they can be applied to hybrid-electric vehicles. The impact of meeting regulatory performance standards on hybrid vehicle design is difficult to establish as most of these regulations are not written to account for the electrical components and operational modes unique to hybrid vehicles. For example, it is not clear exactly how FAR 29.1 would apply to the battery or motor systems of a hybrid-electric vehicle. However, with some intelligent interpretation of how these regulations are likely to one day be applied to hybrid-electric vehicles, their impact on hybrid performance and acceptable failure modes can be investigated.

3.5.4 Impact of Future Hybrid Propulsion Technology

The rate of electrical powertrain component (motors, generators, batteries) performance improvements can be expected to significantly outpace performance improvements to conventional powertrain components (turbine engines, gearboxes) over the next several decades. Even conservative estimates of future electrical component performance relative to current performance can result in astonishing improvements to the competitiveness of hybrid-electric vehicle designs. Since many aircraft designs can be expected to take a decade or longer from inception to production, careful selection of component performance predictions should be made at the initial design stage.

4. Demonstrator Vehicle

Using the lessons learned during the trade study effort, ESAero conducted a conceptual design effort of a hybrid-electric tiltrotor based on the XV-15. This vehicle used a parallel hybrid system that eliminated the mechanical cross-shafting normally required for OEI flight and provided a battery-boost capability for improved performance. The sizing and analysis of this vehicle relied heavily on the component modules that were developed earlier in the contract, except for the TMS module, which was in an immature state at the time. The TMS was instead notionally sized using simplified methods outside of PANTHER, with some TMS component weight estimates being provided by PANTHER TMS modules. Detailed integration of the electric propulsion equipment, battery system, traction bus, and thermal management system into the vehicle was also performed, accompanied by solid models and three-view drawings.

Table 9 summarizes the converged Hybrid XV-15 demonstrator vehicle design and compares it to the conventionally powered NASA XV-15. The vehicle features downsized engines sized for nominal cruise flight. A secondary battery powerplant provides the boost power needed for high-power maneuvers such as climb and hover, as well as for emergency maneuvers in the event of a single engine failure. A DC electrical bus serves in lieu of the original XV-15's mechanical cross-shafting to transfer power between the propulsor nacelles. The hybrid vehicle's powertrain weight is significantly heavier than the conventional powertrain, but was sized to allow for a greater OEI-capable hover gross weight. The hybrid vehicle is capable of limited duration, high-performance sprint and climb through the use of battery-boosting. Additionally, sizing the engines for cruise conditions significantly lowered the hybrid vehicle's fuel consumption compared to the oversized engines of the conventionally powered XV-15 (ref. 7).

Table 9. Summary of Hybrid XV-15 Demonstrator Vehicle Compared to the Original NASA XV-15.

	NASA XV-15	ESAero Hybrid XV-15
Energy Sources	JP-5	JP-5 Li-Ion Battery
Power Sources	Twin Turboshaft	Twin Turboshaft Li-Ion Battery
Powertrain Architecture	Mechanical	Parallel Hybrid-Electric
Nacelle Interconnect	Cross-shafting	DC Electrical Bus
Vehicle Weights (lbs)		
Propulsion Group	3450	5594
Empty Weight	9075	11262
Design		
Useful Load	3925	1738
TOGW	13000	13000
OEI Capable		
Useful Load	1625	1738
TOGW	10700	13000
Airspeeds at DGW, 10,000' (KTAS)		
V_{BE}	160	170
V_{BR}	218	216
$V_{Max,Continuous}$	280*	292
$V_{Max,Sprint}$	280*	324†
Hover Ceiling at Min. Operational GW / Design GW (ft.)		
Max	17400 / 8500*	17800† / 14500†
Engine Power Only	17400 / 8500*	11500 / 8033
OEI	2800 / Incapable	5200† / 0†
Sea-Level Rate of Climb (ft/min)		
Engine-Only	2850*	3938
Boosted		5400†
Cruise Fuel Consumption (lbs/hr)		
at V_{BE}	703	623
at V_{BR}	820	732

**Torque limited*

†Endurance limited by battery capacity

4.1 Concept and Vehicle Selection

A parallel hybrid-electric tiltrotor aircraft was selected to serve as the concept demonstrator vehicle. Several characteristics of the tiltrotor configuration make it an interesting testbed for hybrid-electric rotorcraft design, including the use of multiple lifting devices, demanding OEI performance requirements, and a broad span of power levels required throughout a standard vertical takeoff and landing (VTOL) mission. The concept vehicle demonstrated the following hybrid-electric-vehicle design concepts:

1. **Decoupled power and energy management**
   The turbine engines of the vehicle served as the primary powerplant. A secondary battery powerplant provided limited-duration boost power. This decoupled engine sizing from the high-power sizing flight conditions and allowed them to be sized for optimal performance in cruise. The capability to design propulsion components for specific sizing conditions demonstrates the potential for hybrid vehicles to offer improved performance.

2. **Fault-tolerant hybrid-electric propulsion architecture design**
   Safe operation of a tiltrotor requires the ability to continue providing power to both rotors in the event of a single engine failure. A demonstration of power distribution reconfiguration in the event of a component failure shows how hybrid-electric propulsion architectures can be designed to be fault tolerant.

3. **Distributed propulsion via electrical bus**
   The dual-rotor design and redundancy requirements of tiltrotor vehicles result in a complex and heavy mechanical drivetrain system. The inclusion of an electrical bus allowed for the removal of mechanical cross-shafting. Demonstration of electrical power distribution schemes aids in the design of aircraft with highly distributed propulsion systems.

4. **Battery-boosted turbine propulsion**
   The secondary battery powerplant provides short-duration boost power to expand the vehicle's performance envelope. The battery powerplant did not suffer the power lapse that affects the turbine engines at high altitude. The capability to supplement turbine engine power with battery-boost power demonstrated the potential for high-altitude performance improvements, such as higher cruise ceilings or increased dash speeds.

The Hybrid XV-15 concept demonstrator used the NASA XV-15 tiltrotor vehicle as the baseline design for the development of a hybrid-electric propulsion architecture. The XV-15 provided an excellent baseline for initial design of a hybrid-electric tiltrotor because of the large amount of available flight test data, its incorporation into other vehicle design tools such as NDARC, and its pedigree as a test vehicle for many successful tiltrotor designs.

The Hybrid XV-15 used the trade study tiltrotor vehicles' OML and DGW. Use of this vehicle design provided a validated aerodynamic model but constrained the Hybrid XV-15's sizing criteria to being XV-15–like. The vehicle was intended to primarily serve as a testbed for testing the concepts listed previously. As such, the vehicle design payload was expected to consist entirely of instrumentation for recording flight test data. A set of key performance requirement metrics for the concept demonstrator was derived from the XV-15 and the associated trade study tiltrotor vehicles. This basic design point is summarized in Table 10.

Table 10. Hybrid XV-15 Design Point.

Performance Metric	Value	Units
Payload	200	lbs
Mission Radius	100	nmi
Mission Endurance	1	hour

Selection of propulsion architecture was based off the trade study results and the selection of concepts to be demonstrated. The Tiltrotor Battery-Boosted Gas Turbine (TLT-BBT) parallel hybrid design was selected as the most capable of demonstrating all of the selected concepts. Given the lessons learned from the trade study and the goals of the concept demonstrator vehicles, several changes were made to the original TLT-BBT propulsion architecture to increase the fidelity of the Hybrid XV-15 concept demonstrator vehicle model.

4.2 Application of Hybrid-Electric Design Methodology

Many of the methods developed and lessons learned during the earlier trade study effort were applied to the design approach of the Hybrid XV-15. As with the trade study tiltrotors, the design concept's point performance sizing conditions were developed from the sizing conditions used to develop the conventionally powered XV-15 baseline vehicle. The design missions were further developed to represent a more realistic conceptualization of vehicle operation.

4.2.1 Development of Point Performance Requirements

The Hybrid XV-15 point performance sizing conditions were based off the trade study XV-15 tiltrotor sizing conditions. A shortfall of the tiltrotor designs in the trade study was an extremely poor OEI-capable useful load (UL), because of a significant increase in vehicle empty weight. To mitigate this, the OEI HOGE gross weight was increased to the vehicle DGW of 13,000 lbs. The Hybrid XV-15 point performance sizing criteria are listed below:

FC 1 Maximum Weight Hover (SLS, AEO): HOGE at sea level at the vehicle's maximum takeoff weight of 15,000 lbs. This flight condition is outside the vehicle's OEI-capable envelope. Derived from NDARC XV-15 model validation Point Design Conditions.

FC 2 Hover Ceiling (8,000 ft., AEO): HOGE at 8000 ft. (ISA) at the vehicle's DGW of 13,000 lbs. This flight condition is outside the vehicle's OEI-capable envelope. Derived from NDARC XV-15 model validation Point Design Conditions.

FC 3 Maximum Low-Altitude Speed (SLS, AEO): Continuous sprint cruise condition at sea level at the vehicle's DGW of 13,000 lbs. This flight condition is outside the vehicle's OEI-capable envelope. Derived from NDARC XV-15 model validation Point Design Conditions.

FC 4 Maximum High-Altitude Speed (12,000 ft., AEO): Continuous sprint cruise condition at 12,000 ft. (ISA) at the vehicle's DGW of 13,000 lbs. This flight condition is outside the vehicle's OEI-capable envelope. Derived from NDARC XV-15 model validation Point Design Conditions.

FC 5 Contingency Level Flight (12,000 ft., Engine 1 Inoperative): Cruise condition with the #1 engine inoperative at 12,000 ft. (ISA) at the vehicle's DGW of 13,000 lbs. Derived from NDARC XV-15 model validation Point Design Conditions.

FC 6 Contingency Level Flight (12,000 ft., Engine 2 Inoperative): Mirror of FC #5.

FC 7 Contingency Hover (SLS, Engine 1 Inoperative): Hover condition with the #1 engine inoperative at SLS at the vehicle's DGW of 13,000 lbs.

FC 8 Contingency Hover (SLS, Engine 2 Inoperative): Mirror of FC #7.

FC 9 Gearbox and Rotor Sizing Condition:* HOGE at sea level (ISA) at a gross weight of 18,903 lbs. This condition properly sized the gearboxes and rotors to handle maximum engine output power. It was included to mitigate a minor issue within PANTHER that affects component sizing in some cases when power flow is reversed. It was not considered reflective of actual vehicle mission capability. The vehicle was considered to have an MTOGW of 15,000 lbs, imposed by structural limits.

These flight conditions are tabulated in Table 11.

Table 11. Hybrid XV-15 Sizing Flight Conditions.

Sizing Condition	FC #1	FC #2	FC #3	FC #4	FC #5	FC #6	FC #7	FC #8	*FC #9**
Altitude (ft.)	0	8000	0	12000	12000	12000	0	0	*0*
Δ_{Tamb} (F°)	0	0	0	0	0	0	0	0	*0*
Gross Weight (lbs)	15000	13000	13000	13000	13000	13000	13000	13000	*18903*
KTAS	0	0	225	260	172	172	0	0	*0*
V_v (kts.)	0	0	0	0	0	0	0	0	*0*
Max Power Rating	MRP	MRP	MCP	MCP	MRP	MRP	MRP	MRP	*MRP*

As with the trade study tiltrotors, boost power from the battery was required to provide a minimum of 5 minutes of operation under the most demanding OEI flight condition. Battery maximum depth-of-discharge was limited to 80 percent of battery capacity to provide some margin and avoid the battery's region of degraded performance at very low charge. Additionally, to prolong battery life the battery must not discharge below 50 percent during the design mission.

For Nominal Flight Conditions (AEO):

- Maximum allowable depth-of-discharge: 50 percent.

For Contingency Flight Conditions (OEI)

- Maximum allowable depth-of-discharge: 80 percent.
- Minimum endurance: 5 minutes.

4.2.2 Development of Mission Performance Requirements

The sizing criteria of the Hybrid XV-15 incorporated two design missions. The nominal maximum-effort mission was designed to reflect the key performance requirement metrics and the XV-15 derived flight conditions. To demonstrate the concept of battery-boosted gas turbine propulsion, the battery boost was used to perform both a maximum-effort climb and a maximum-effort sprint. Engine-only cruise segments provide time to recharge the battery between high-power maneuvers. Table 12 shows the incorporation of the vehicle design point and sizing flight conditions into this mission profile. A 10-minute-reserve section is included to provide fuel margin; this is a small reserve relative to operational vehicles, but was sized proportionally to the vehicle's design endurance.

The Engine Failure on Takeoff Contingency Design Mission verifies that the vehicle met all sizing criteria under the most demanding contingency flight condition. As shown in Table 13, it consisted of a 5-minute AEO hover followed by 5 minutes of OEI hover.

Table 12. Nominal, Maximum-Effort Design Mission Segments.

	Nominal, Max Effort Mission - OEI-Capable	GW (lbs)	Payload	Fuel Load	Start Alt. (ft)	End Alt. (ft)	Airspeed	Distance (nmi)
1	**Takeoff (HOGE)**	13000	200	1000	0	0	0	
2	**Climb**				0	10000	99% V_{BE}	100
3	**Cruise**				10000	10000	V_{BR}	
4	**Sprint**				10000	10000	V_{Max}	
	Return to Base							
5	**Cruise**				10000	10000	V_{BR}	
6	**Descend**				10000	0	V_{BR}	-100
7	**Land (HOGE)**				0	0	0	
	Reserve Loiter		*200*	*111*	*0*	*0*	*150 KTAS*	
							Total	**0**

Table 13. Contingency Design Mission Segments.

	Contingency Mission - Engine Failure (Takeoff)	GW (lbs)	Payload	Fuel Load	Start Alt. (ft)	End Alt. (ft)	Airspeed	Distance (nmi)	Duration (min)
1	**Takeoff (HOGE)**	13000	200	1000	0	0	0	0	5
	Engine Failure!								
2	**Land (OEI HOGE)**				0	0	0	0	5
							Total	**0**	**10.0**

4.3 On-Design Sizing of Demonstrator Vehicle

Several improvements were made to the TLT-BBT propulsion architecture prior to sizing the vehicle. The improvements sought to develop a more realistic model of a vehicle developed with current cutting-edge technology.

Fuel Load as Float Variable

The trade study vehicles floated payload and kept fuel capacity constant across applicable vehicle designs. For this task, the Hybrid XV-15 concept demonstrator design payload and range was known. As such, the design fuel load was floated within PANTHER to absorb changes to powertrain weight. Man-in-the-loop adjustments were made to the fuel load as the vehicle design progressed to keep the design mission range near the target value. Empty weight margin was also increased from baseline and adjusted to provide fine-tuning of vehicle weight as the design closed.

Engine Modernization

While the use of the NASA XV-15 as the reference vehicle for the trade study tiltrotors provided ample performance data for calibrating the vehicle, it resulted in those tiltrotors being calibrated to a vehicle using over-40-year-old technology. This was an acceptable drawback for the trade study as performance comparisons were made to other vehicles similarly calibrated. However, to increase the accuracy of the Hybrid XV-15 concept demonstrator vehicle model, the engine scaling was updated to reflect the last half-century of turboshaft engine development. While the Hybrid XV-15 concept demonstrator uses the same TPE331 rubberized engine deck as before, the scaling factors were adjusted to bring the Hybrid XV-15's engines in-line with the trends exhibited by modern engines from the turboshaft engine database. The

“modernization” of the TLT-BBT engines results in a 30-percent decrease in engine weight and a 12-percent improvement in power-specific fuel consumption (PSFC).

Motor Stacking

Sizing of the TLT-BBT resulted in motors with a power output of 771 hp, far exceeding the continuous power limit of any current aviation-capable electric motors. For the Hybrid XV-15 concept demonstrator, a new sizing scheme was employed in which maximum allowable motor power was fixed to about 200 hp, reflecting the power limits of the EMRAX 348, one of the most powerful axial flux synchronous motors available (ref. 12). Higher power requirements were met by stacking multiple motors, coupled together via common driveshaft. Initial sizing efforts established that a stack of five motors would meet the power requirements at the desired power-per-motor. Similarly, inverter-rectifier controller volumetric scaling was adjusted to 80 lbs/ft^3 to match the EMRAX-compatible emDrive 500 (ref. 13). Each motor was equipped with its own controller box.

The use of multiple stacked motors and controllers increased the overall chance of component failure but also provided partial redundancy in the case of both single and multiple failures. Additional non-dimensional components were added to the PANTHER model to control routing of power from the main gearboxes and power cables to the individual motor-generators and rectifier-inverter controller boxes. This allowed the model to simulate individual failures among these components and subsequent power flow reconfiguration.

Accessory Power Takeoff

Accessory power takeoff was reintroduced to the tiltrotor model for the Hybrid XV-15 concept demonstrator. The overall power takeoff for the vehicle was fixed at 66 hp. This value was selected from a trend of vehicle subsystem power vs. DGW that included both the NDARC helicopter configurations and rotorcraft of similar gross weight as the XV-15, such as the UH-60. Power takeoff was simulated using the PANTHER subsystem module. An accessory box was incorporated into each nacelle, powered off the main gearbox. The current implementation was sufficient for itemizing accessory power requirements without further complicating vehicle power control methods. Future developments may instead implement a centralized accessory power box fed via the electric bus.

4.3.1 Propulsion Component Sizing

Imposing the vehicle sizing criteria defined in section 4.2 on the propulsion system architecture detailed in the previous section resulted in the component-level performance requirements shown in Table 14.

Table 14. Hybrid XV-15 Propulsion Component Performance.

Engines	Value	Units
Continuous Power (MCP)	1032	hp
Military Power (IRP)	1223	hp
Takeoff Power (MRP)	1310	hp
Engine Volume	11	ft^3
Rectifier-Inverter Boxes		
Max Continuous Power	211	hp
Motor-Generators		
Max Continuous Power	207	hp
Fuel Tanks		
Fuel Capacity	1000	lbs
Energy Capacity	5410	kWh

Battery Pack	Value	Units
Max Power	568	kW
Energy Capacity	59.8	kWh
Pack Volume	290	L
Pack Specific Energy	150	Wh/kg
Pack Specific Power	1426	W/kg
Power Distribution		
Max Gearbox Power	1665	hp
Max Bus Power	1061	hp
Accessory Power Boxes		
Take-off Power	33	hp

These values are graphically mapped to the propulsion architecture in Figure 34.

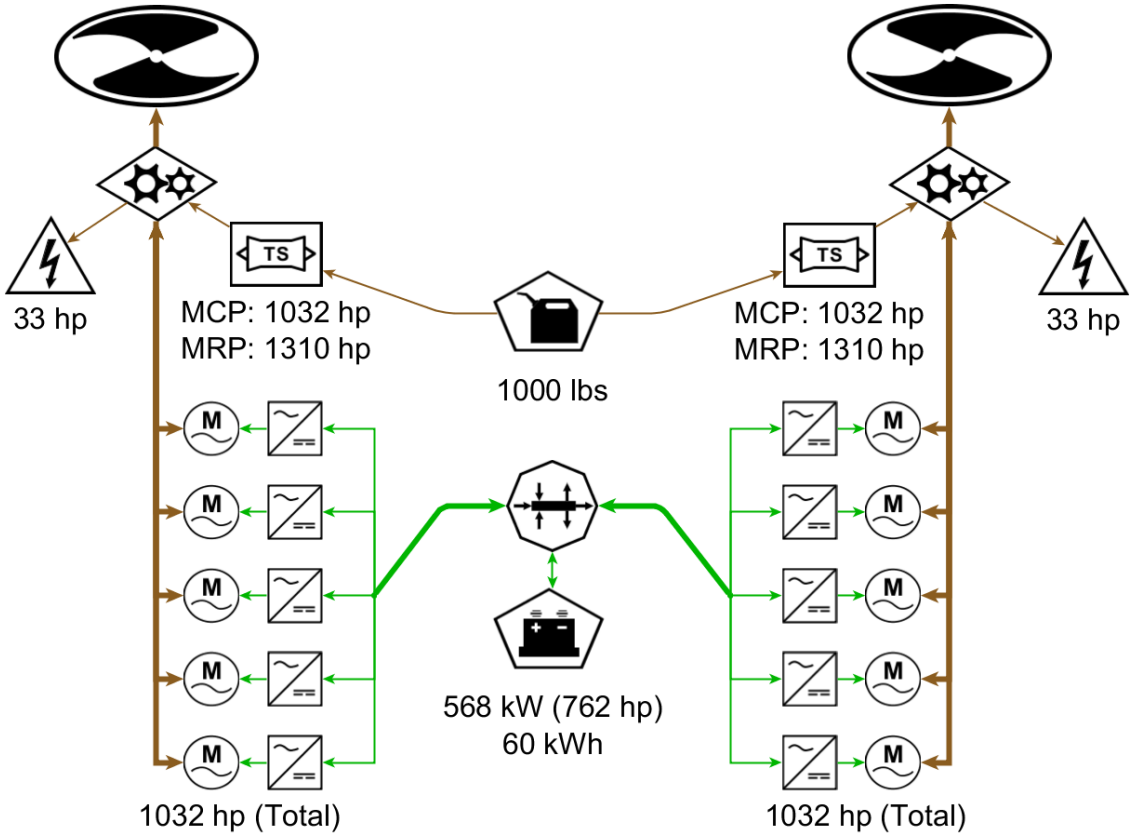

Figure 34. Hybrid XV-15 Propulsion Architecture Schematic With Component Performance.

4.3.2 Thermal Management System Sizing

The PANTHER TMS module and sub-modules were not ready for full integration into the concept demonstrator sizing effort; however, elements of them were used to aid in the initial sizing and design of the thermal management system of the concept demonstrator. An estimate of the concept demonstrator's powertrain cooling requirements relative to baseline was made by comparing the waste heat generation of both vehicles under the strenuous OEI HOGE flight condition. As shown in Table 15, the hybrid-electric vehicle produced waste heat at almost three times the rate of the baseline vehicle because of a reduction in the overall efficiency of the hybrid-electric powertrain. The total amount of heat generated in a worst-case scenario was calculated by multiplying the heat generation rate by the 5-minute maximum endurance of that flight condition.

The increase in the heat generated by the hybrid-electric propulsion architecture was exacerbated by the hover flight condition, which greatly limits the heat rejection possible through a conventional radiator design. Attempts at sizing a suitable radiator in PANTHER for zero airflow conditions resulted in unrealistically large designs. Cooling airflow can be forced across a radiator by using either vehicle propwash or active blowers, but either method negatively impacted vehicle performance.

Table 15. Conventional and Hybrid-Electric Transmission System Heat Generation Under FC #7.

	Bell XV-15	Concept Demonstrator
	Waste Heat Generation (hp)	
Port Nacelle		
Gearbox	19.6	12.9
Motors		41.3
Controllers		21.1
Starboard Nacelle		
Gearbox	9.6	12.9
Motors		12.7
Controllers		6.1
Transmission	9.8	7.7
Total (hp)	39.0	114.7
Total (kW)	**29.1**	**85.5**
	Total Waste Heat (kJ)	
At 5-Minutes	8724.6	25662.0

An interesting aspect of the tiltrotor design is the massive power requirement difference between its high-power helicopter maneuvers and its low-power aircraft maneuvers. This results in a massive difference in cooling requirements between the two flight modes—with a similar discrepancy in cooling capability, a result of the difference in airspeeds. Sizing a thermal management system for the concept demonstrator to operate continuously while under the high-power conditions would have a significant, negative impact on both the vehicle empty weight and aircraft-mode aerodynamics. This observation spurred an initial investigation into a conceptual approach towards cooling in which the TMS was sized for continuous operation during aircraft mode but could absorb transient heat spikes during short-duration, high-power helicopter maneuvers.

An assumption was made that by increasing the baseline heat exchanger volume to 0.6 ft^3 per nacelle, along with increasing the nacelle cooling inlet area and blower power, about half of the heat generated during OEI hover could be exhausted from the system. To handle the other 12.9 MJ of heat generated during 5 minutes of OEI hover, a central cooling loop with an oversized coolant reservoir could absorb the excess heat, acting as a thermal capacitor. Assuming an ambient hot day temperature of 35°C and an electronics temperature limit of 80°C, this amount of heat could be stored by 160 lbs of water. During contingency operations, this 5-minute window matches the battery endurance, after which the vehicle was expected to land. If the vehicle managed to fill the coolant system to its heat storage capacity during nominal operation, it must transition to a lower-power flight state, after which the stored energy could be gradually dumped through the air-cooled radiators. A schematic of this cooling system is shown in Figure 35.

Initial weight estimates were derived for the primary components of the TMS, resulting in a system weight of 317 lbs. The weight breakdown is shown in Table 16. These weights should be considered extremely preliminary. As a means of rough validation, applying the STARC-ABL hybrid-electric vehicle TMS scaling assumption of 0.68 kW_{th}/kg to the Hybrid XV-15 concept demonstrator gave an estimate of 277 lbs, a 12.5-percent difference (ref. 14).

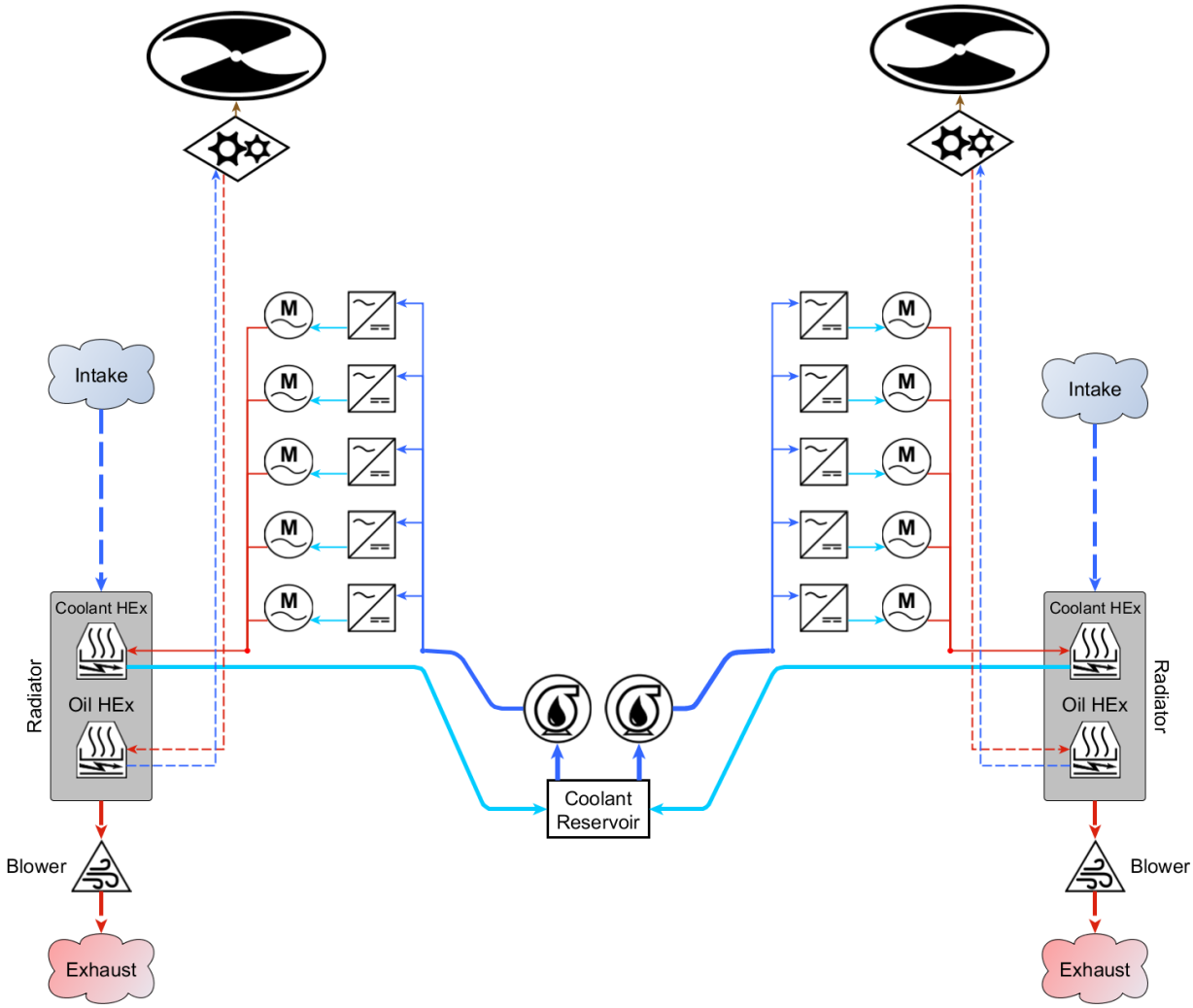

Figure 35. Hybrid XV-15 Concept Demonstrator TMS Architecture.

Table 16. Hybrid XV-15 Concept Demonstrator TMS Weight Breakdown.

Component	Weight (lbs)	Sizing Method
Coolant	160	Used heat capacity formula to determine req. volume
Reservoir	23	COTS research into aluminum 20-gal tanks
Pumps	20	COTS research into pumps with required flow rate
Radiators	82	PANTHER radiator model
Piping	32	PANTHER Ducting Model
Total	**317**	

4.3.3 Weight Statement

The group weight statement for the converged Hybrid XV-15 design is shown in Table 17. The vehicle was of significantly greater empty weight than the trade study vehicles, largely because of the impact of increasing the OEI-capable hover weight. Other additions to the vehicle empty weight arise from the inclusion of TMS, an increased empty weight margin, and adoption of baseline structure group weights. However, the vehicle was capable of OEI sea level hover up to its design weight, resulting in a greater OEI-capable design mission payload than any of the trade study tiltrotors.

Table 17. Hybrid XV-15 Vehicle Weight Breakdown.

Group Weight Statement *XV-15 Test Data Derived Fixed Weight	lbs	
Structure Group*	**3316**	
Fixed Equipment Group*	**2243**	
Propulsion Group	**5593**	
Rotors		897
Powertrain	1857	
Gearboxes		1023
Shafts		109
Rectifier-Inverters		422
Power Cables		244
Power Control Elec.		59
Powerplant	1511	
Turboshaft Engines		667
Exhaust System		14
Air Induction*		17
Lubrication*		22
Engine Accessories		103
Motor-Generators		688
Battery Packs		879
Fuel System		133
Thermal Management		317
Empty Weight Margin	**110**	
Empty Weight	**11262**	
Useful Load	**1738**	
Fuel		1000
Payload		200
Fixed Useful Load*		538
DesignTOGW*	**13000**	

4.4 Vehicle Performance Simulation

With the Hybrid XV-15 sized via PANTHER on-design methods, the PANTHER off-design methods were used to evaluate the point performance and mission performance of the vehicle design.

4.4.1 Performance Plots

<u>Energy Flow vs. Airspeed</u>

The sea level energy flow of the Hybrid XV-15 is shown in Figure 36 for both helicopter and aircraft-mode flight. At sea level, most of the flight envelope could be reached without battery-boost power, with the

maximum airspeed set by rotor performance limits. The associated endurance indicator and range indicator plots are shown in Figure 37. Note that these plots do not account for vehicle endurance limits imposed by engine power rating endurance.

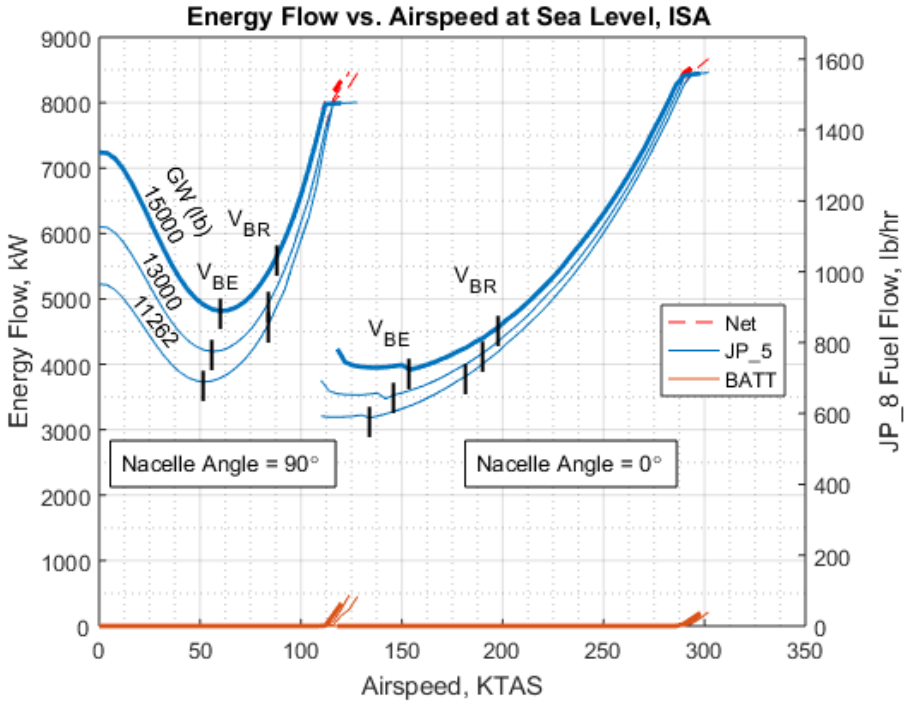

Figure 36. Hybrid XV-15 Sea Level Energy Flow vs. Airspeed.

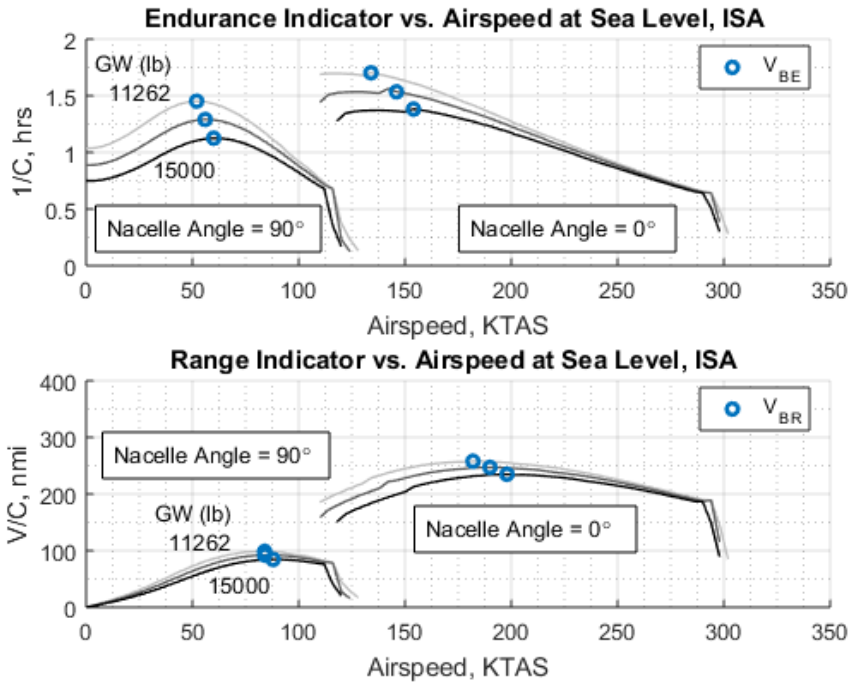

Figure 37. Hybrid XV-15 Sea Level Endurance and Range Indicators vs. Airspeed.

Energy flow at cruise altitude is shown in Figure 38. With the engines experiencing power lapse because of altitude, battery-boost power was required to reach more of the flight envelope. The associated endurance indicator and range indicator plots are shown in Figure 39.

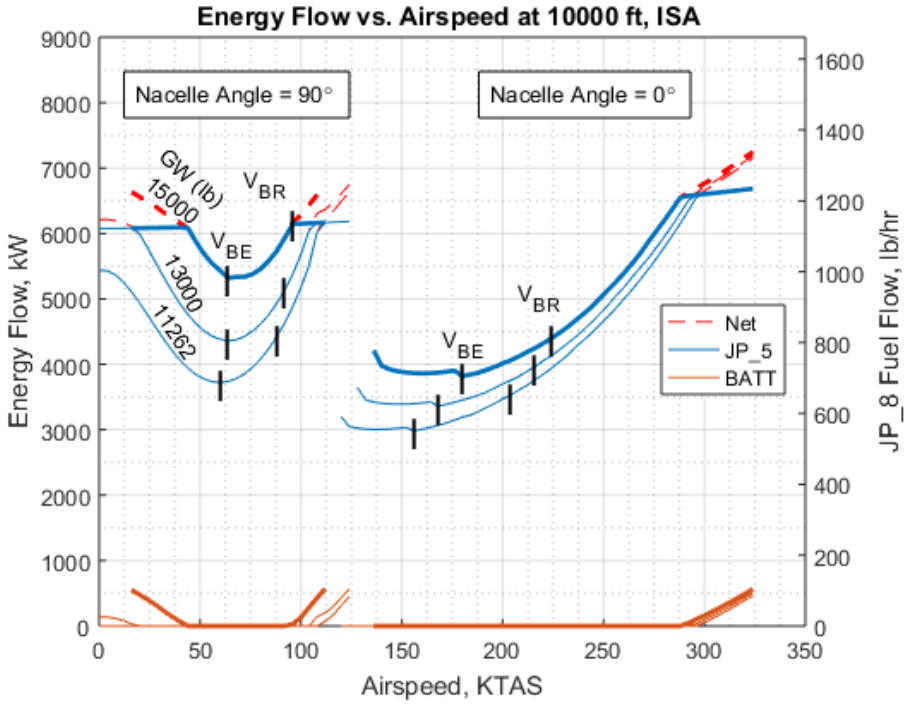

Figure 38. Hybrid XV-15 Cruise Altitude Energy Flow vs. Airspeed.

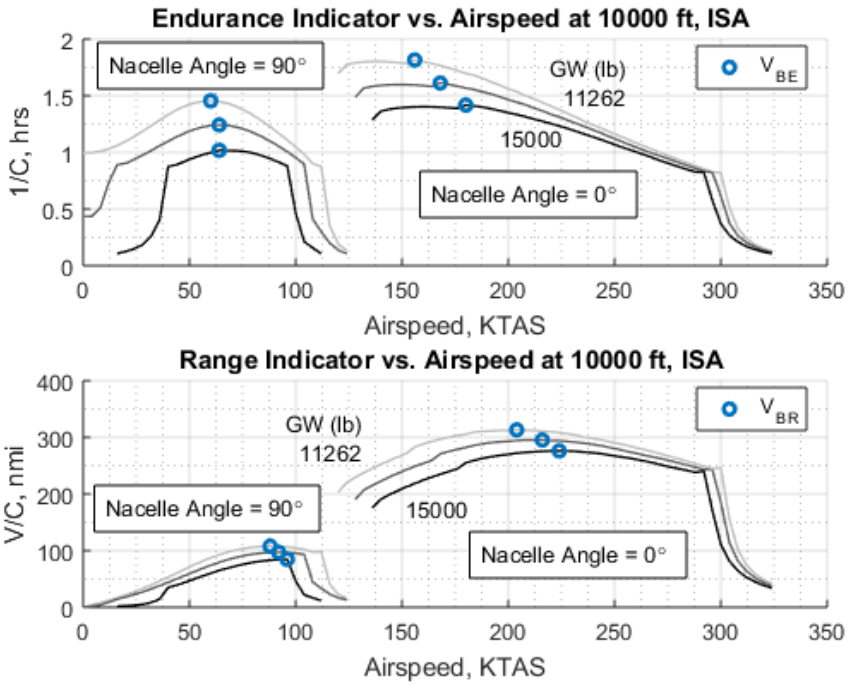

Figure 39. Hybrid XV-15 Cruise Altitude Endurance and Range Indicators vs. Airspeed.

Hover Ceiling

Off-design sweeps were performed to determine the Hybrid XV-15's hover ceilings. Being a multi-powerplant vehicle, several distinct ceilings existed for the different power distribution modes, as shown in Figure 40. Note the small red markers correspond to flight conditions evaluated in the performance sweeps that determined vehicle capability. Use of battery-boost greatly expanded the hover ceiling, although the vehicle was only capable of performing this maneuver for 5 minutes at the maximum power limit. OEI hover also represented a battery-capacity-limited endurance limit of 5 minutes.

Maximum Rate of Climb

The vehicle's airplane-mode maximum rate of climb across a range of altitudes is shown in Figure 41. As with the hover ceiling, the vehicle had different limits depending on how the three powerplants were used. The boosted climb rate was extremely rapid, with a simulated time to climb to 10,000 feet of less than 2.5 minutes. At lower altitudes, battery-boosted maximum power climb rate was limited by the ability of the control surfaces to trim the vehicle.

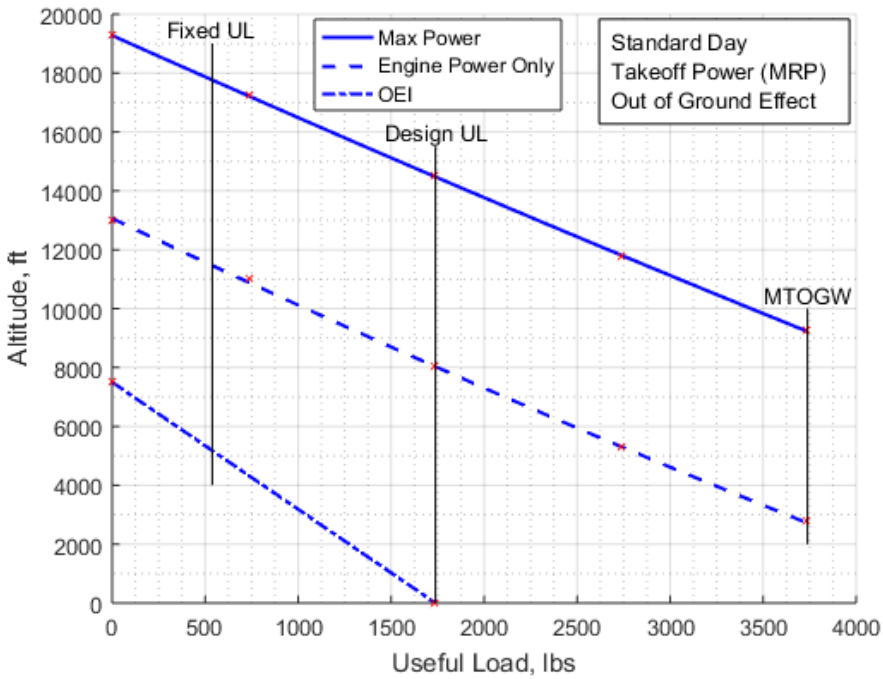

Figure 40. Hybrid XV-15 Hover Ceilings.

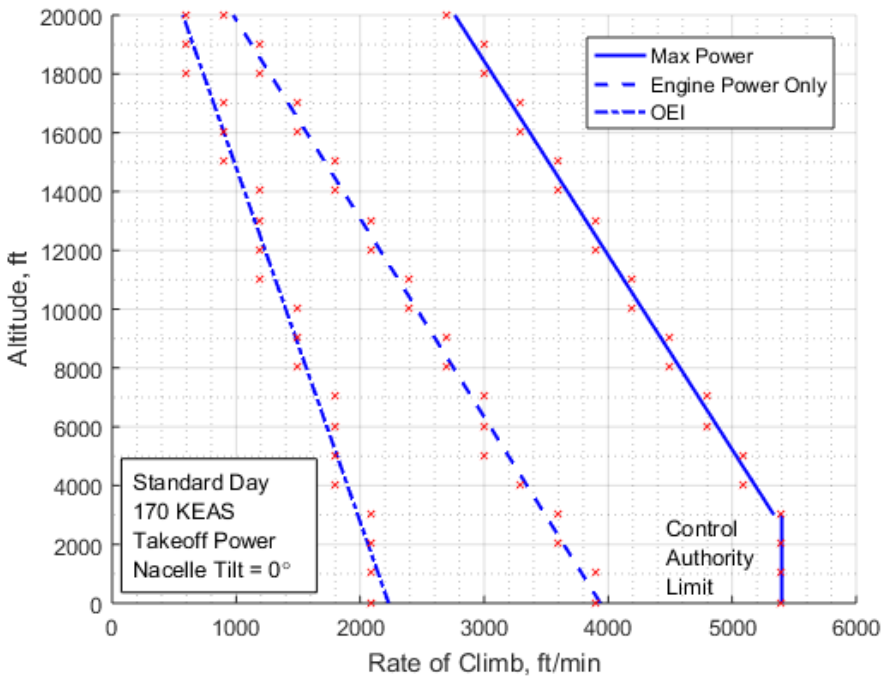

Figure 41. Hybrid XV-15 Maximum Rate of Climb vs. Altitude.

4.4.2 Mission Performance

The converged Hybrid XV-15 vehicle design was able to meet the design goals discussed in section 4.2.2 when performing the nominal, maximum-effort mission. Table 18 lists the details of the mission segments. The battery provided adequate energy for a 2.8-minute sprint at 325 KTAS.

Vehicle powerplant power and energy bucket fill fraction throughout the mission are shown in Figure 42. The vehicle used battery-boost power during the climb and sprint segments. The battery maximum depth-of-discharge limits were not violated, and the cruise segments were adequate to recharge the battery between high-power maneuvers.

Table 18. Nominal, Maximum-Effort Design Mission.

		GW (lbs)	Payload	Fuel Load	Start Alt. (ft)	End Alt. (ft)	Airspeed	Distance (nmi)	Duration (min)
	Nominal Operation - OEI-Capable								
1	**Takeoff (HOGE)**	13000	200	1000	0	0	0	0	5.0
2	**Climb**				0	10000	187 KEAS	7	2.2
3	**Cruise**				10000	10000	218 KTAS	78	21.5
4	**Sprint**				10000	10000	325 KTAS	15	2.8
	Return to Base								
5	**Cruise**				10000	10000	218 KTAS	-66	18.2
6	**Descend**				10000	0	218 KEAS	-34	10.0
7	**Land (HOGE)**				0	0	0	0	5.0
	Reserve Loiter		*200*	*111*	*0*	*0*	*150 KTAS*	*0*	*10.0*
							Total	**0**	**64.6**

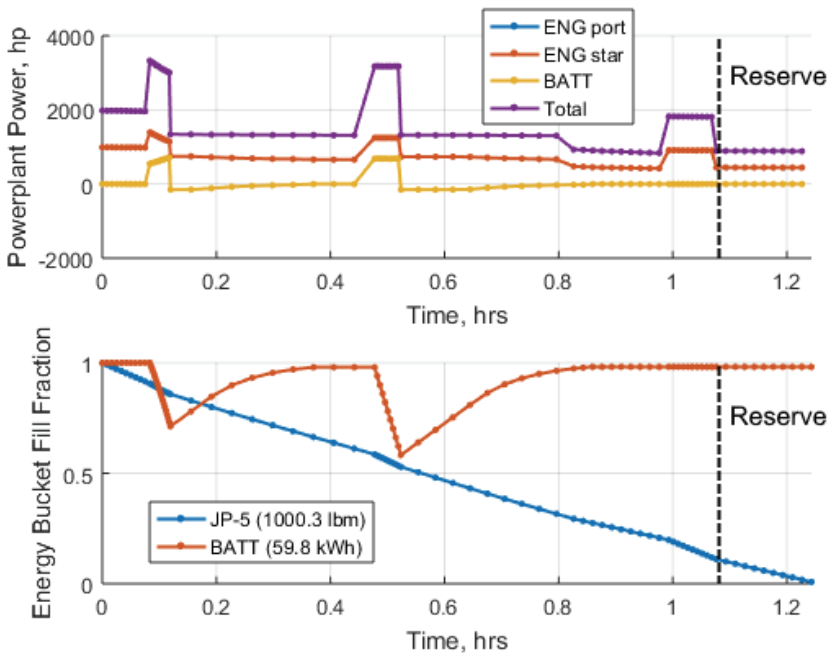

Figure 42. Nominal, Maximum-Effort Mission Power and Energy Usage.

<u>Contingency Mission—Engine Failure on Takeoff</u>

Table 19 summarizes the engine failure on takeoff mission. The vehicle's power and energy state are shown in Figure 43. The vehicle ended the mission without the battery violating the maximum allowable contingency maneuver depth-of-discharge limit of 80 percent.

Table 19. Contingency—Engine Failure on Takeoff Design Mission.

	Contingency Mission - Engine Failure (Takeoff)	GW (lbs)	Payload	Fuel Load	Start Alt. (ft)	End Alt. (ft)	Airspeed	Distance (nmi)	Duration (min)
1	**Takeoff (HOGE)**	13000	200	1000	0	0	0	0	5
	Engine Failure!								
2	**Land (OEI HOGE)**				0	0	0	0	5
							Total	**0**	**10.0**

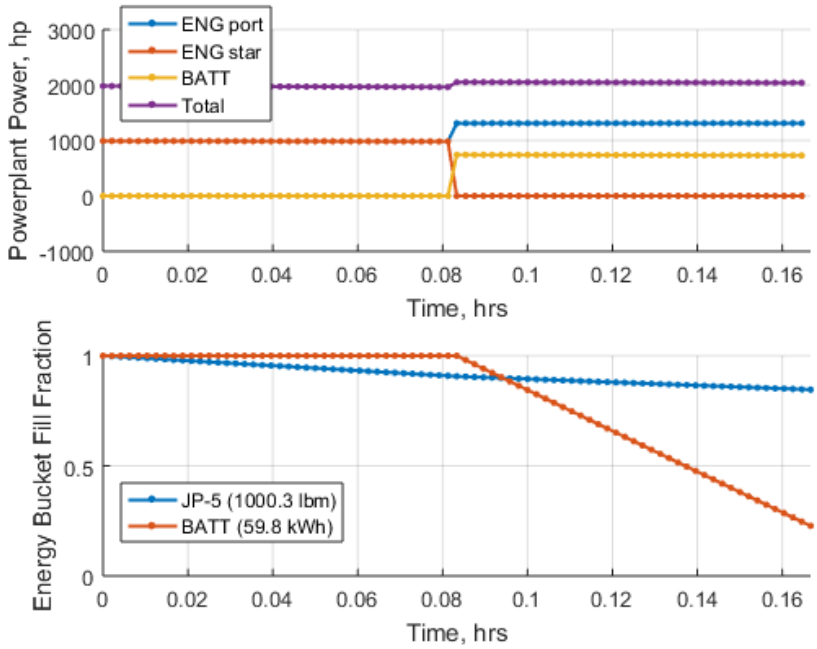

Figure 43. Contingency—Engine Failure on Takeoff Design Mission Power and Energy Usage.

<u>Contingency Mission—Engine Failure During Cruise</u>

In addition to the design missions, an additional mission was formulated to explore concepts of hybrid-electric-vehicle energy management and flightpath planning. A question not addressed by the prior missions was the vehicle's capability for contingency operations when a failure was encountered partially through a mission. A near-worst-case scenario was chosen to analyze the vehicle's ability to return to base. The first half of the resulting mission profile remained identical to the nominal, maximum-effort mission up through the boosted sprint segment. However, shortly after returning to base, when the battery was near its minimum nominal charge state and both the engine and motors were near their thermal limits, the vehicle experienced an engine failure. The state of the vehicle up to this point is shown in Table 20.

Table 20. Contingency—Engine Failure During Cruise Mission up to Engine Failure Point.

	Contingency Mission - Engine Failure (Cruise)	GW (lbs)	Payload	Fuel Load	Start Alt. (ft)	End Alt. (ft)	Airspeed	Distance (nmi)	Duration (min)
1	**Takeoff (HOGE)**	13000	200	1000	0	0	0	0	5.0
2	**Climb**				0	10000	187 KEAS	7	2.2
3	**Cruise**				10000	10000	218 KTAS	78	21.5
4	**Sprint**				10000	10000	325 KTAS	15	2.8
	Return to Base								
5	**Cruise**				10000	10000	218 KTAS	-5	1.4
	Engine Failure!								
6	**Cruise (OEI)**				10000	10000	218 KTAS	-4	1.0
							Total	**91**	**33.8**

The vehicle had to establish a new flight plan that allowed it to return the remaining 91 nmi back to base before it ran out of fuel. In addition, assuming the landing zone is a helipad rather than an airstrip, the vehicle also had to charge its battery to a level capable of providing the adequate energy for the 5-minute landing maneuver. Finally, the thermal state of the engine could not be neglected, as the return cruise and battery charge maneuver would have to allow the engine to cool to a state where it could perform at MRP for the 5-minute landing maneuver without overheating.

A possible solution to this dilemma was a multi-stage return transit, in which the vehicle performed several descents to reduce the flight power requirements and allow the powerplant components to cool. This flightpath is summarized in the complete mission shown in Table 21.

The energy and power output of the vehicle's powerplants throughout the entire mission are shown in Figure 44. The vehicle was able to return to base before running out of fuel and had enough energy to perform the landing maneuver. Additionally, as seen in Figure 45, the descent stages provided the engines with time to cool at a reduced power setting between high-power maneuvers.

As shown in this contingency mission, flightpath planning of a hybrid-electric vehicle can be extremely complex when operating near the margins of vehicle capability. There is a need for improved hybrid-electric mission planning tools that can provide insight into the relationship between vehicle energy storage states, component thermal limits, and flightpath restrictions.

Table 21. Contingency—Engine Failure During Cruise, Complete Mission.

		GW (lbs)	Payload	Fuel Load	Start Alt.	End Alt.	Airspeed	Distance	Duration
	Contingency Mission - Engine Failure during cruise								
1	**Takeoff (HOGE)**	13000	200	1000	0	0	0	0	5.0
2	**Climb**				0	10000	187 KEAS	7	2.2
3	**Cruise**				10000	10000	218 KTAS	78	21.5
4	**Sprint**				10000	10000	325 KTAS	15	2.8
	Return to Base								
5	**Cruise**				10000	10000	218 KTAS	-5	1.4
	Engine Failure!								
3	**Cruise (OEI)**				10000	10000	218 KTAS	-4	1.0
4	**Descend (OEI)**				10000	5000	170 KEAS	-16	5.0
3	**Cruise (OEI)**				5000	5000	160 KTAS	-61	22.7
4	**Descend (OEI)**				5000	0	170 KEAS	-15	5.0
5	**Land (HOGE, OEI)**				0	0	0	0	5.0
	Reserve (OEI)		*200*	*143.2*	*0*	*0*	*150*	*0*	*10.0*
							Total	**0**	**71.5**

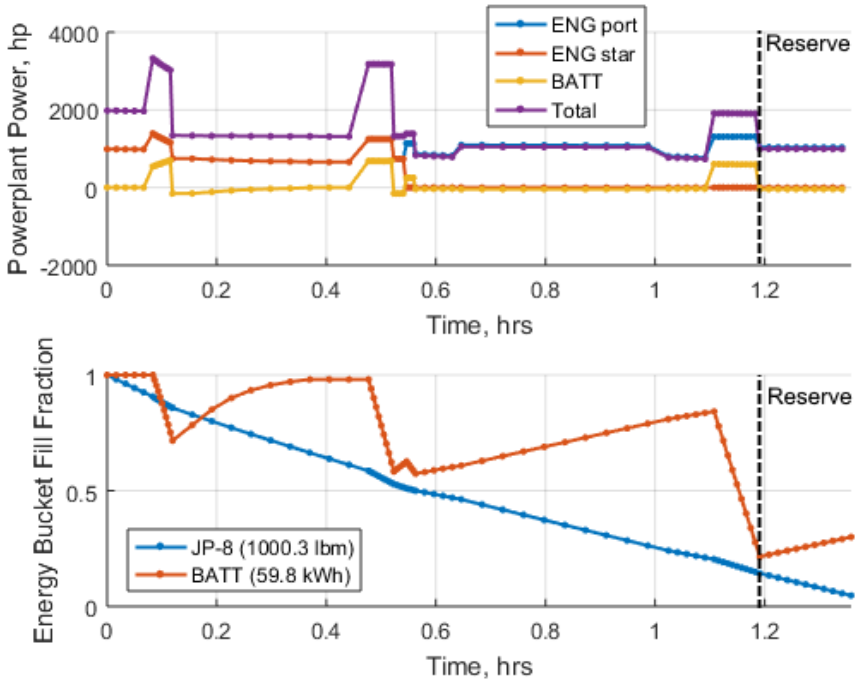

Figure 44. Contingency—Engine Failure During Cruise Design Mission Power and Energy Usage.

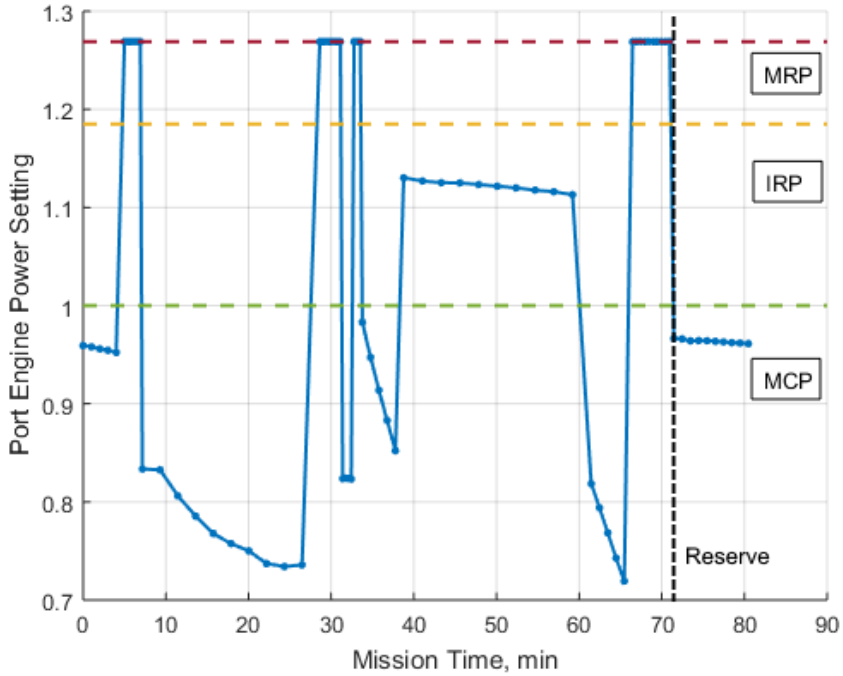

Figure 45. Contingency—Engine Failure During Cruise Design Mission Port Engine Power Ratings.

The concept demonstrator vehicle was able to meet all of the conceptual and performance design goals. Vehicle component performance was within cutting-edge technology levels, with a propulsion architecture that accounts for commercial off-the-shelf (COTS) products electronic power limitations. TMS sizing was preliminary, but several concepts for handling electronics waste heat were explored. The vehicle was able to meet its mission performance goals and demonstrated single-fault redundancy throughout both of its design missions. Analysis of a mission scenario featuring a “worst-case” engine failure demonstrated the vehicle’s capability to redistribute power to balance the energy and thermal states of its multiple powerplants.

4.5 Hybrid-Electric Powertrain Integration

The focus of this effort was on the modeling of the hybrid-electric XV-15 to demonstrate the installation of the electric propulsion system components and to assess feasibility from an integration perspective. A goal of this effort was for this demonstrator vehicle to closely resemble the existing conventional vehicle such that it could be compared to an extensive set of wind tunnel and flight test data to show the advantages and disadvantages of hybrid-electric propulsion.

4.5.1 Development of Airframe Solid Model

Development of an integration model for the concept demonstrator began with a computer-aided design (CAD) recreation of the baseline XV-15 airframe and primary structural elements. Several reference drawings were obtained from various reports, but these drawings were neither accurate enough nor large enough in scale to reverse engineer the aircraft. However, when combined with the many publicly available photographs of the aircraft, they served as an excellent starting point for creating the computer model of the aircraft. The various pictures and three-view drawings could be enlarged, traced, and compared to one another to effectively arrive at a shaping consensus for the OMLs as illustrated in Figure 46. These were combined with the larger-scale scrap views to add necessary details and flesh out component shaping and locations of primary and secondary structure.

4.5.2 Design of Propulsor Nacelles

The historical XV-15 nacelle inboard appears in Figure 47 and Figure 48. Modeling of the nacelles took five iterations to arrive at a workable compromise between OML and internals.

Modeling of nacelle components started with sizing and placement of the motor stacks and controller boxes. The design team iterated on component physical size until everything fit reasonably well in a streamlined nacelle. Airflow to the heat exchangers required a more sizable duct than in the original XV-15 nacelle. The redesigned duct dominates the upper portion of the nacelle, as shown in Figure 49. The cooling air duct incorporates a fan aft of the heat exchanger to force air through it during VTOL operations. Note also the cooling provided to the accessory gearbox with a small bulge on the nacelle underside. In these figures, the blue cylinders represent the motors and the yellow boxes represent each motor’s controller/inverter box.

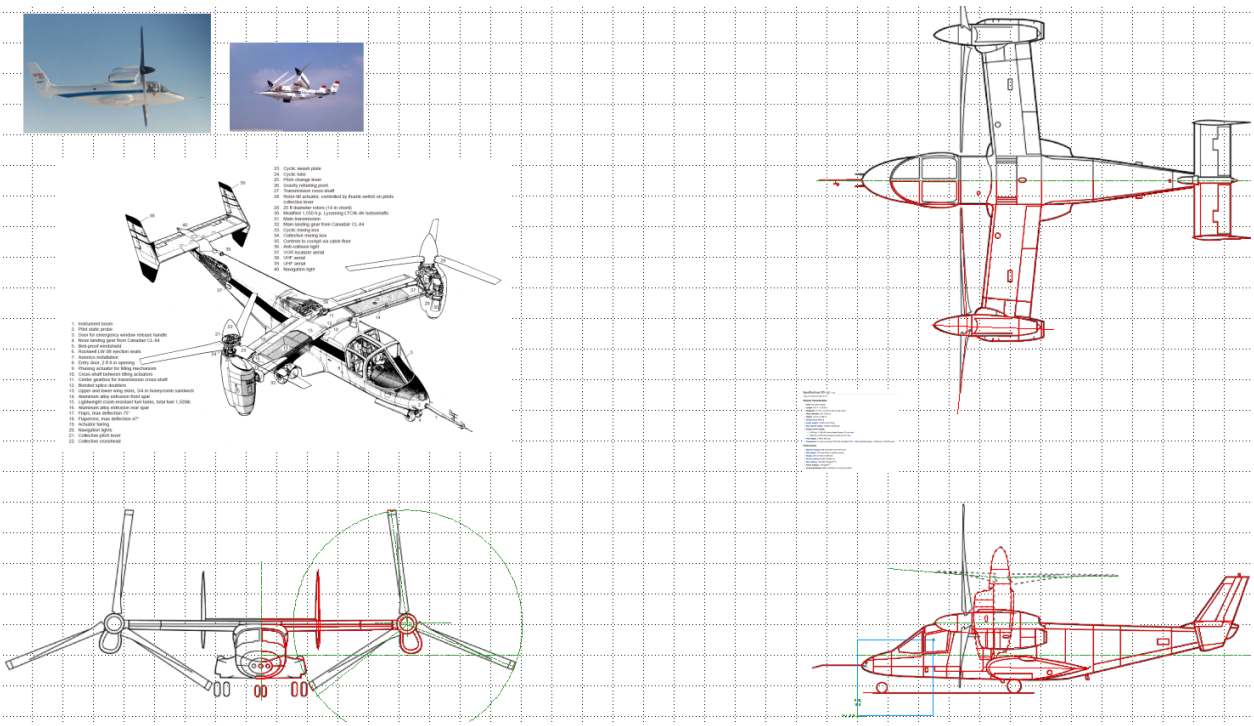

Figure 46. XV-15 Three-View Drawing Created From Smaller Drawings (ref. 7).

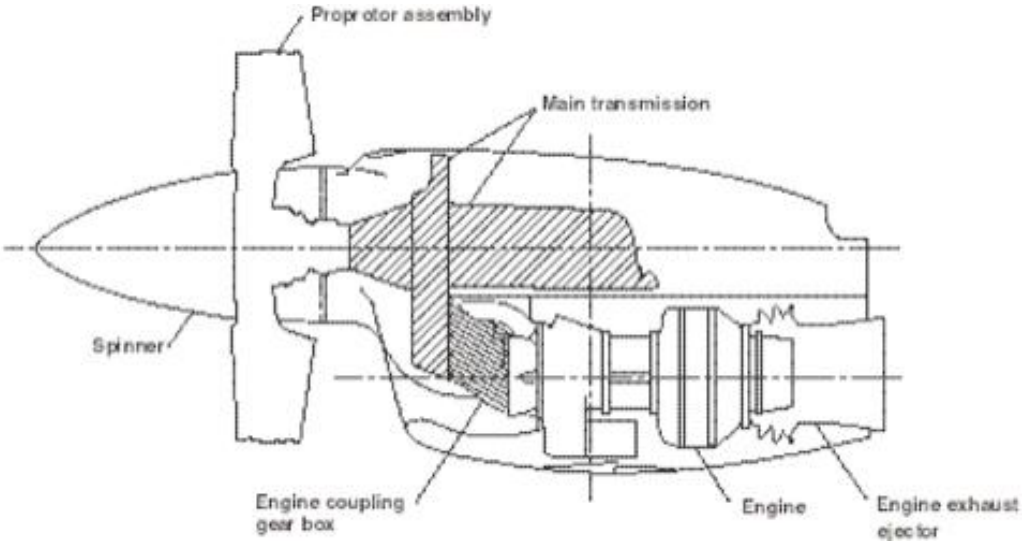

Figure 47. XV-15 Nacelle Inboard Profile (ref. 7).

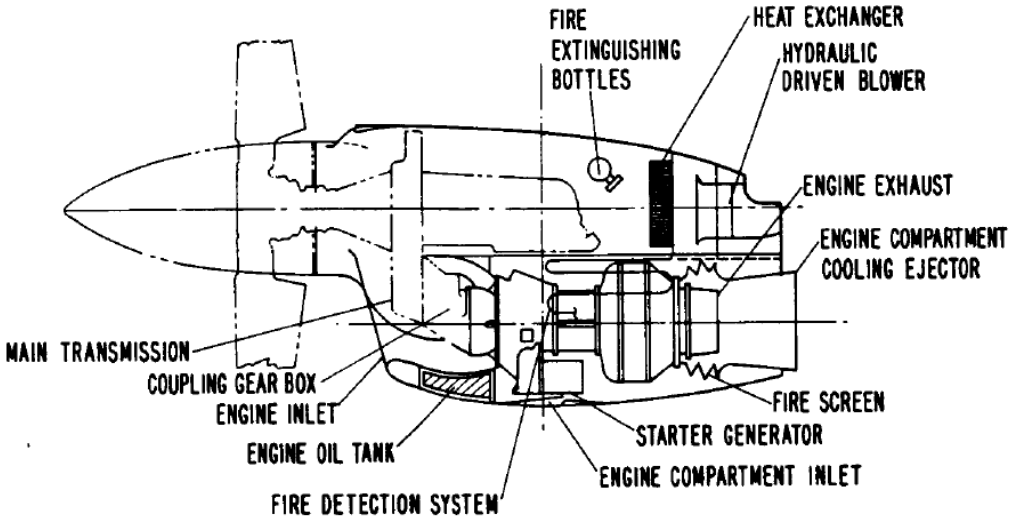

Figure 48. XV-15 Inboard Profiles (ref. 7).

Coolant and oil runs to/from the heat exchangers are shown in Figure 50 and Figure 51 along with a gearbox and engine power transmission based on the XV-15. Oil coolant lines from the sump to the heat exchanger are also shown.

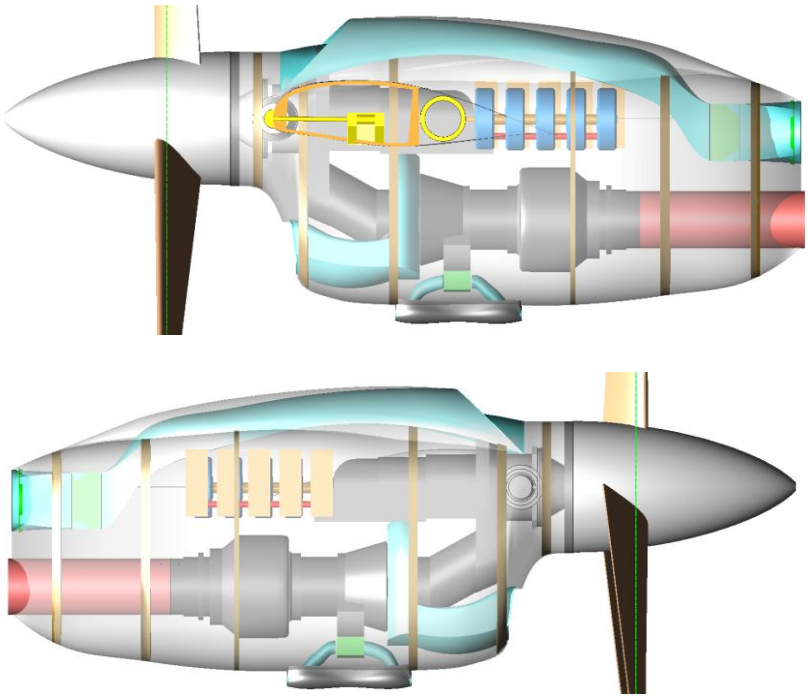

Figure 49. Side Views of Final Nacelle Iteration (ref. 7).

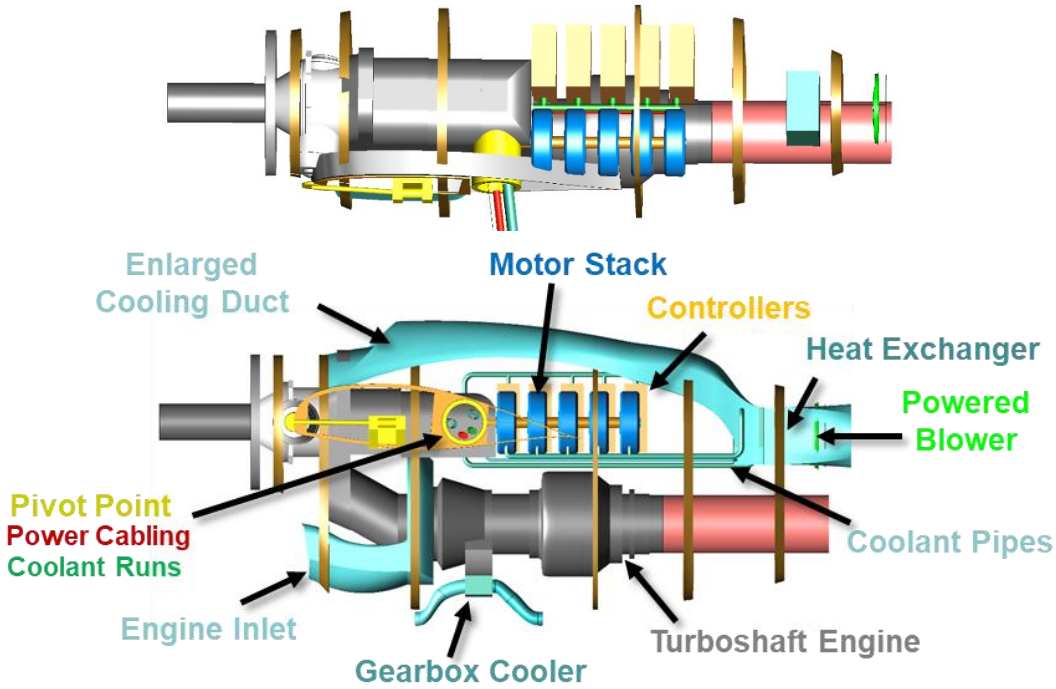

Figure 50. Top (top) and Left Side (bottom) Views of Final Nacelle Iteration With Cooling and Electrical Runs.

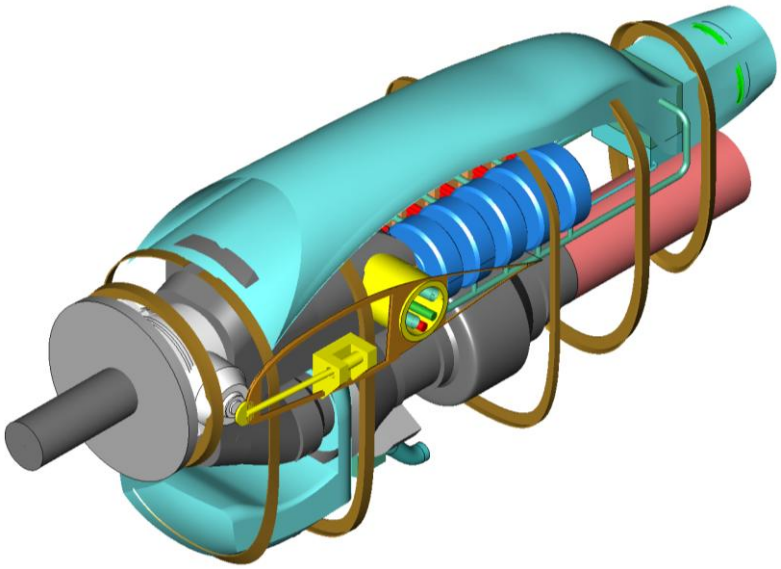

Figure 51. Isometric View of Final Nacelle Powertrain Iteration.

The bright yellow cylinder in Figure 52 is the tilting pivot, which has a 10-inch outside diameter (OD) and an 8-inch inside diameter (ID). Routing the various subsystems in a manner that prevents twisting or excessive strain throughout a full VTOL flight will be a major challenge. Power and coolant are run through the pivot, but control runs and housekeeping functions that require power will have to be run through it as well. Therefore the pivot diameter may increase, resulting in either a thicker aft-loaded airfoil or a gentle spanwise bump along the wing.

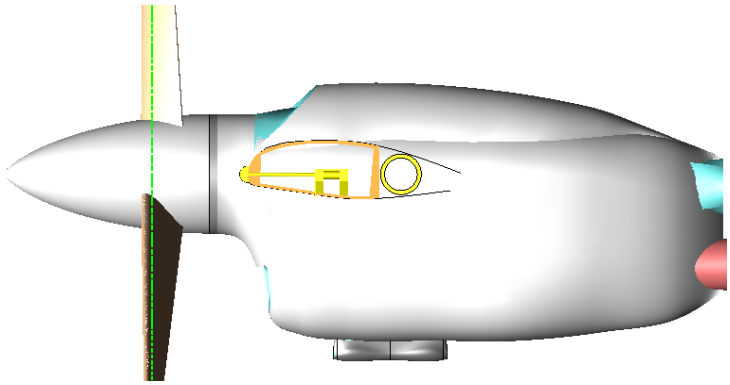

Figure 52. Side View of Integrated Final Nacelle Iteration.

4.5.3 Powertrain and Thermal Management System Integration

The final step in modeling the full powertrain was incorporating all electrical and coolant plumbing runs. Electrical cables and cooling lines are shown in Figure 53 running through the conversion pivot (bright yellow) to and from the nacelles and cabin. The electrical power out (bright red), electrical power return (dark green), and coolant out (blue-green) lines are also shown. The coolant reservoir (teal) is located on the cabin centerline and is 2.6 cubic feet, which holds 73 liters of coolant. The oil cooling lines are light blue and run to and from the transmission and gearbox to the lower 30 percent of the heat exchanger. Figure 53 and Figure 54 show various views of the powertrain components that run through the wing, fuselage, and nacelles. Much structure is left out for simplicity and clarity. The olive-colored box is power management and the salmon-colored box is design payload.

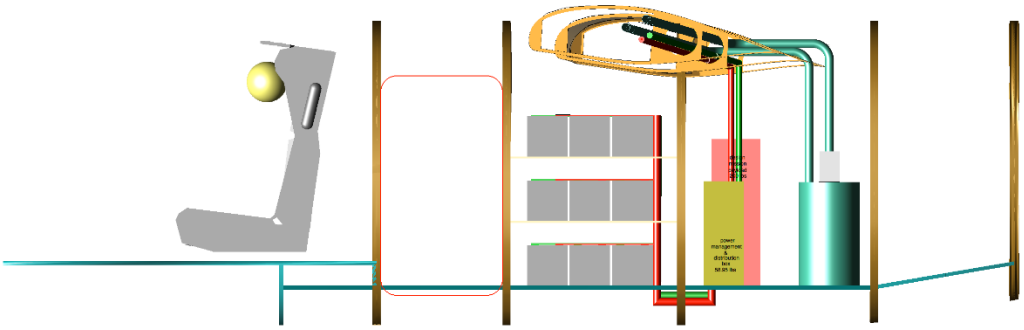

Figure 53. Left Side of Fuselage Showing Locations of Powertrain Components.

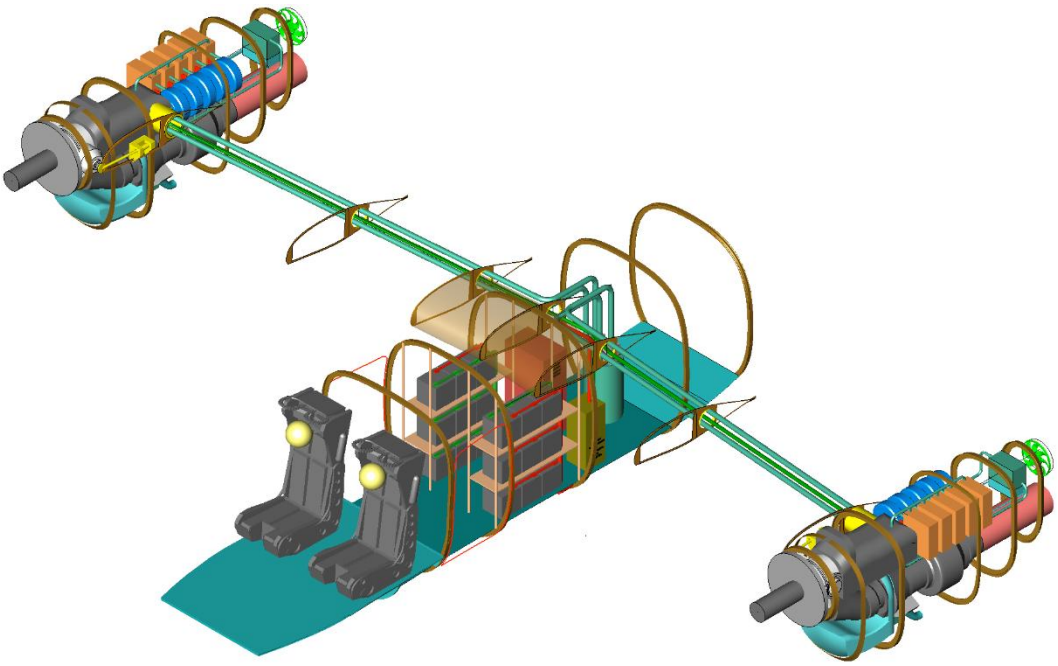

Figure 54. Isometric View of Powertrain Components in Nacelles and Fuselage.

4.5.4 Completed Hybrid XV-15 Solid Model

Figure 55 through Figure 59 show various views of the final Hybrid XV-15 solid model, and Figure 60 is a screenshot of the large-scale drawing.

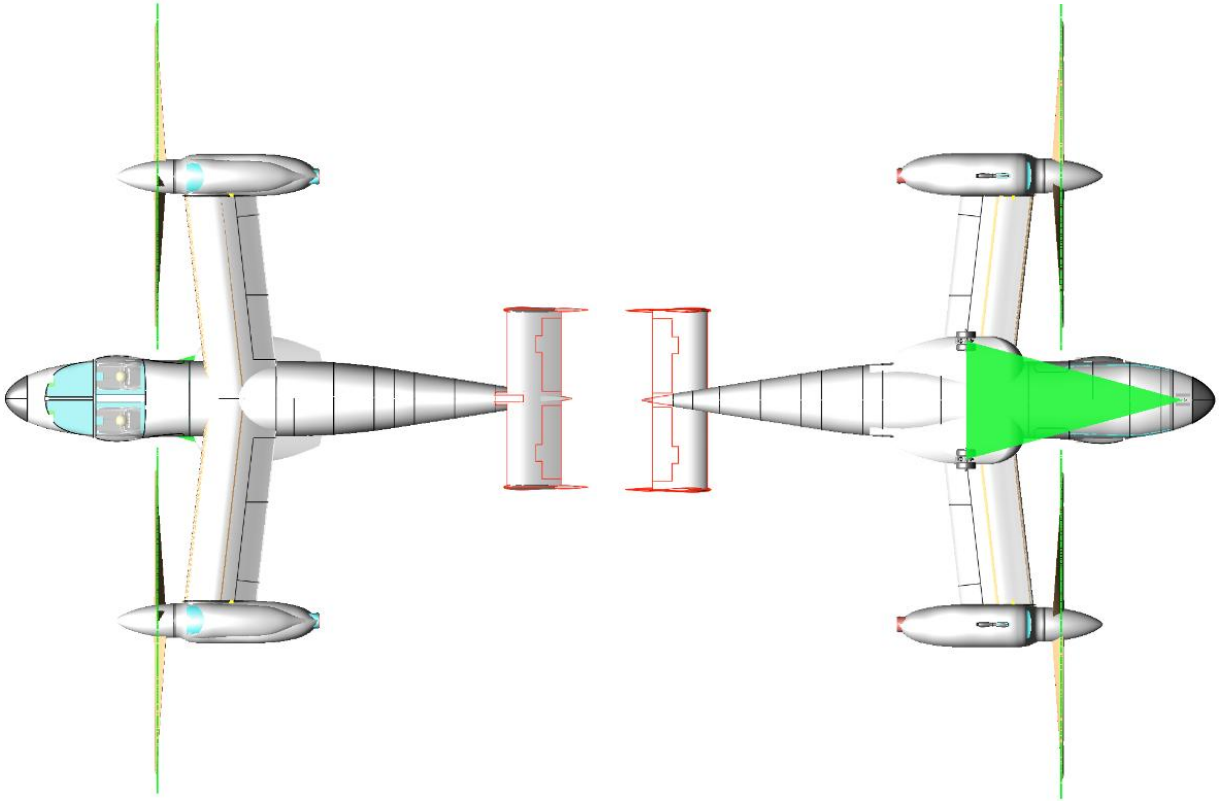

Figure 55. Top and Bottom Views of Hybrid XV-15 Solid Model.

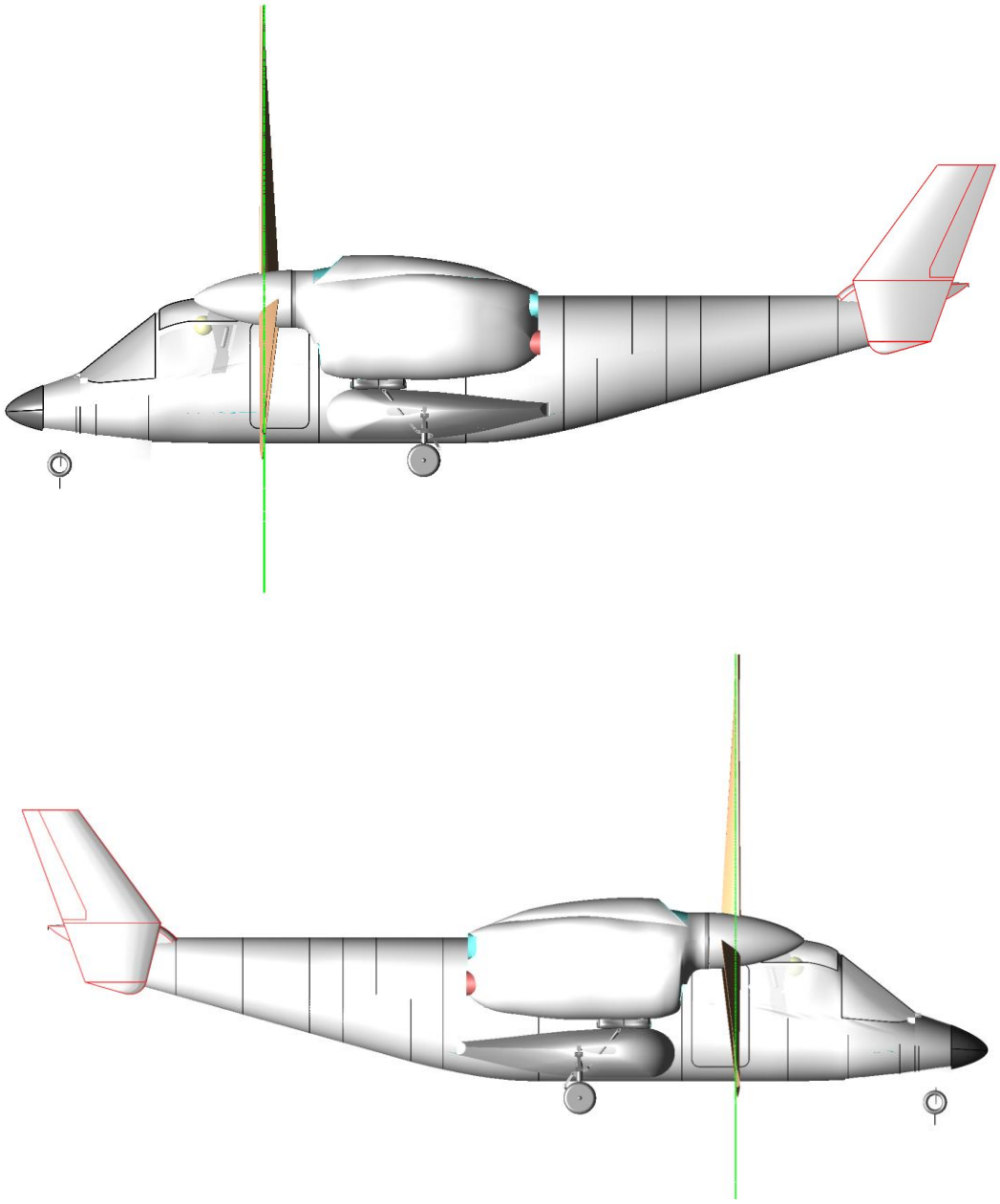

Figure 56. Left and Right Side Views of Hybrid XV-15 Solid Model.

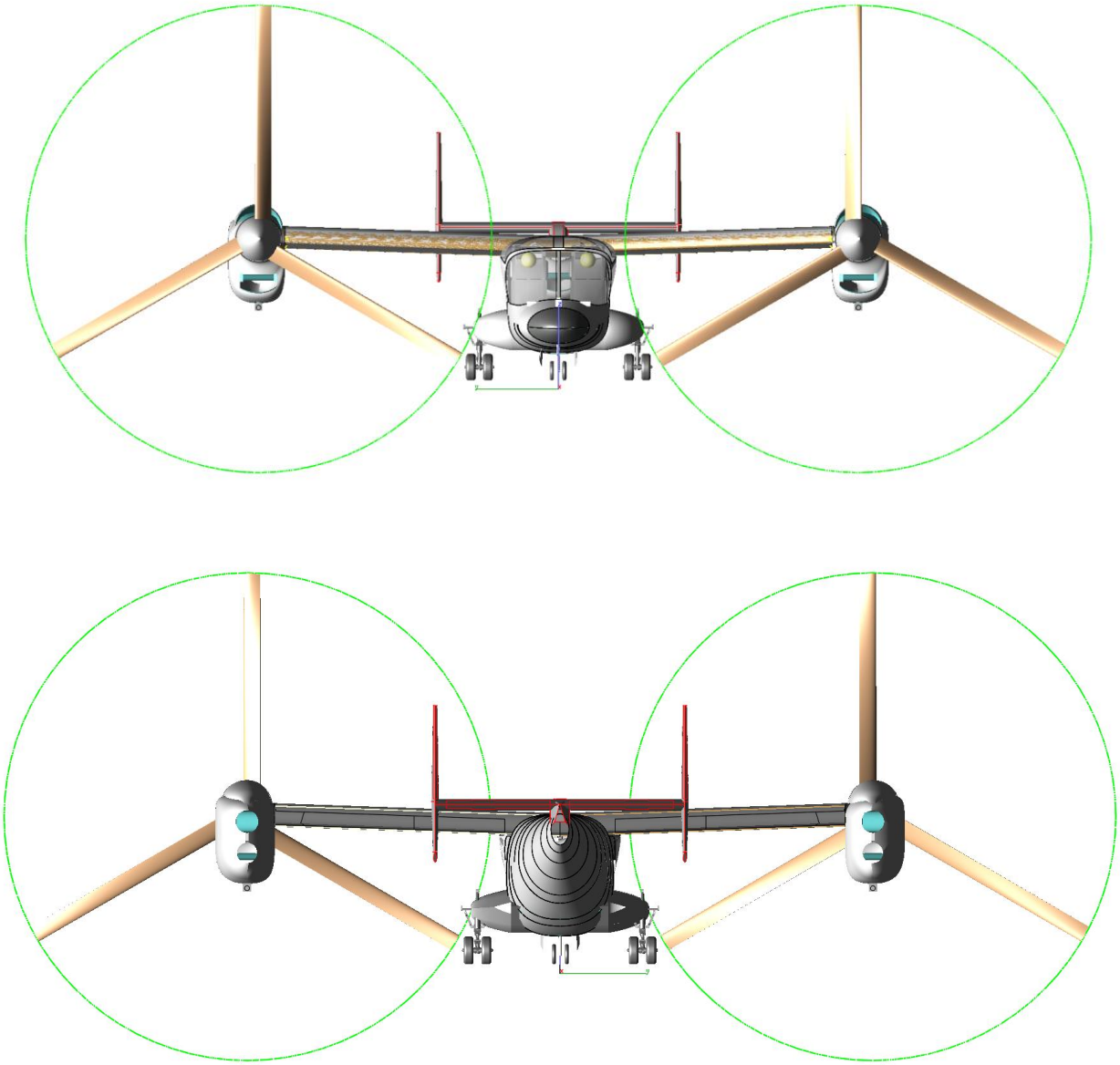

Figure 57. Front and Back Views of Hybrid XV-15 Solid Model.

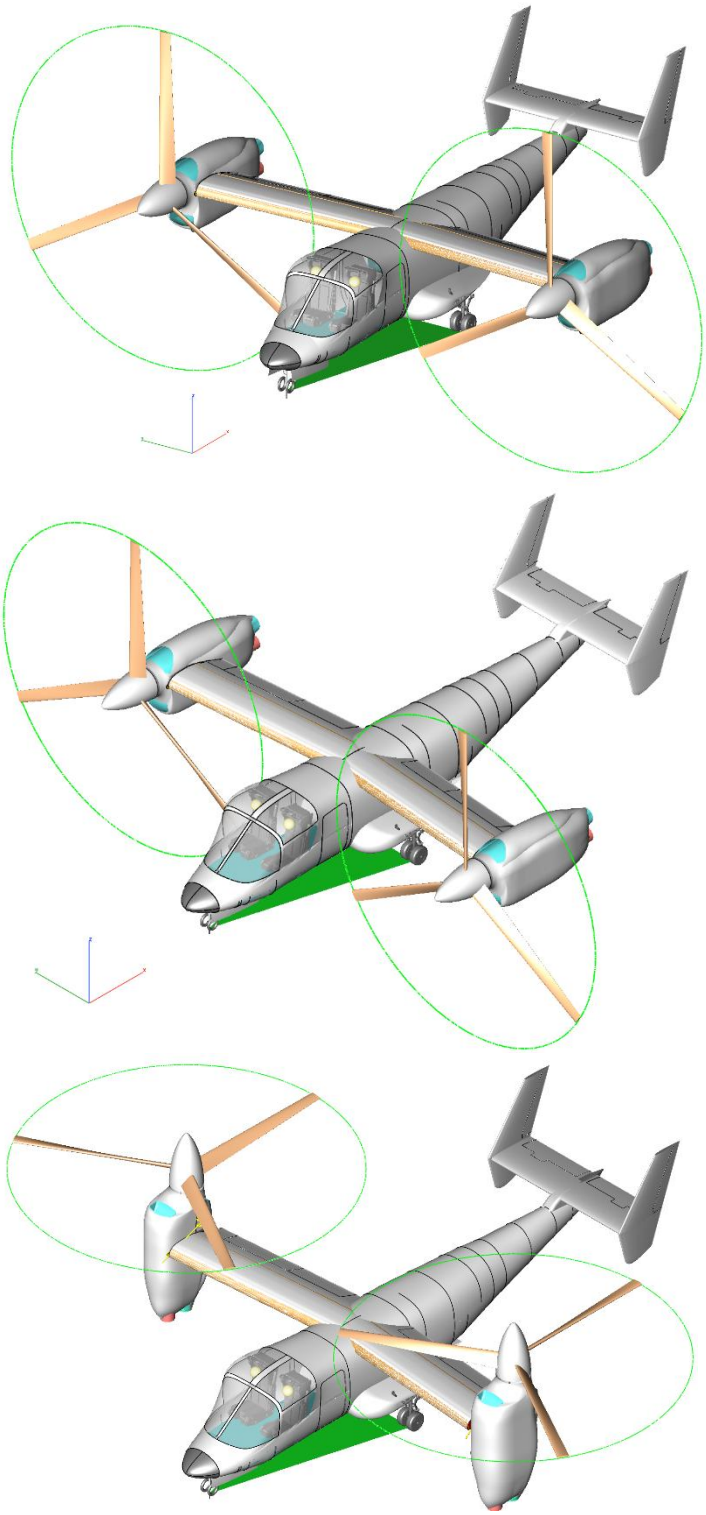

Figure 58. Trimetric and Isometric Views of Hybrid XV-15.

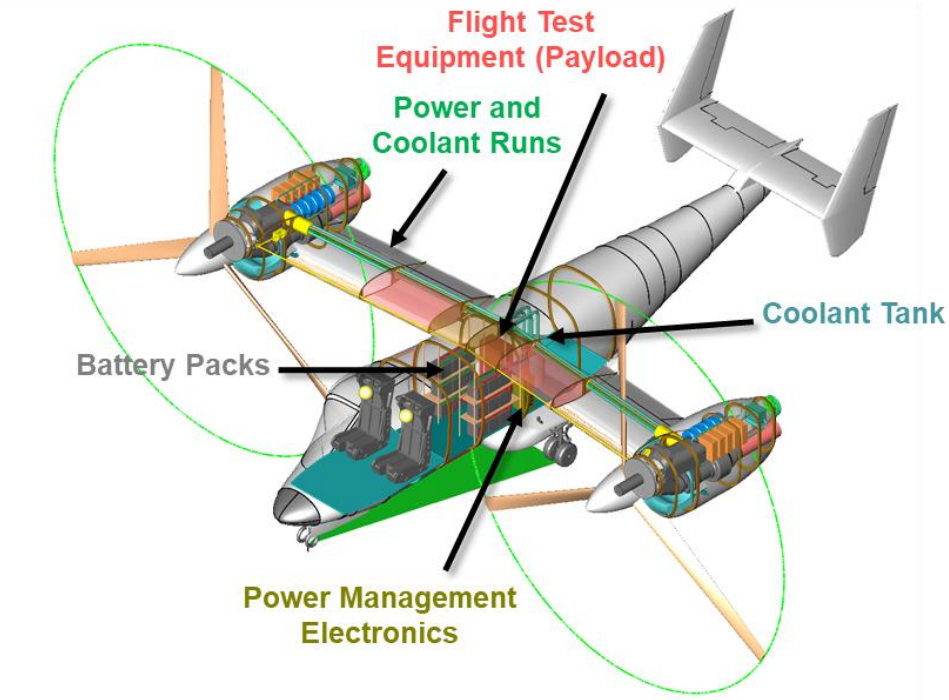

Figure 59. Isometric View With Labeling of Components in Fuselage.

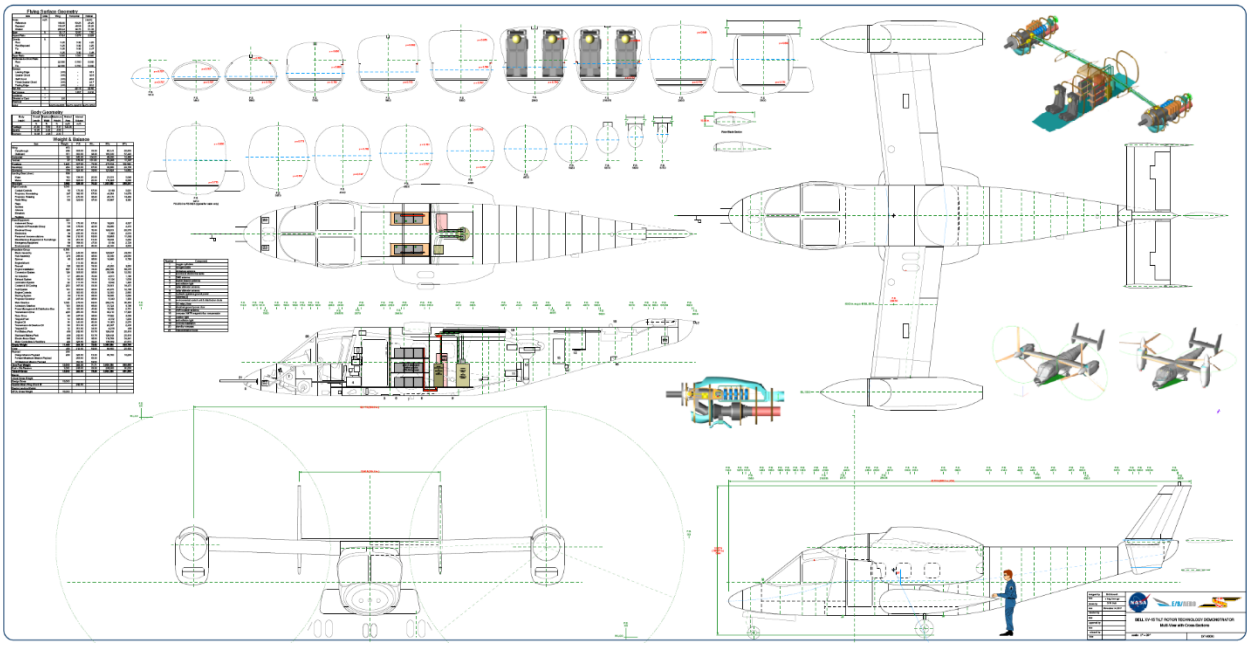

Figure 60. Screenshot of Hybrid XV-15 Large-Scale Drawing.

4.6 Lessons Learned

Progressing one of the trade study vehicles to a more detailed level of design allowed for the exploration of the impact of hybrid-electric propulsion systems on mission planning, thermal management, and airframe integration. This section lists several of the important lessons learned from development of the concept demonstrator.

4.6.1 Vehicle Mission Planning Complexity

The “worst case” engine failure mission scenario revealed a tight coupling between mission flight plan and fault mode performance of the vehicle, indicating a need for better tools for exploring how hybrid-electric propulsion architecture design affects vehicle mission planning methods. Full utilization of a hybrid vehicle’s capabilities will require the development of flight planning tools that can account for multiple onboard energy sources, internal power reconfiguration capabilities, and thermal endurance limits. This capability is important during both the design process and during operation of the vehicle. Energy and power management of some hybrid-electric vehicle designs may be complex to the point of requiring a highly automated onboard system to plot mission flightpaths for both nominal and contingency operation.

4.6.2 Thermal Management

One aspect of hybrid-electric TMS design noted during this initial sizing effort was the relative inefficacy of traditional vehicle liquid coolant loops. Most engine cooling systems are designed to operate at or above the unpressurized boiling point of the coolant through the use of a pressurized coolant loop. Allowing the coolant to operate at around 100–145°C greatly increases the ability of a coolant loop of given size to reduce the overall system size and weight. However, many COTS motors and controllers are limited to 65–85°C, which limits the maximum allowable coolant temperature and scales up radiator system size dramatically. Assuming a hot day, there could be as little as 30°C difference between the at-rest coolant temperature and the maximum allowable system temperature. This severely limits water-based coolants as a medium for heat transport or thermal capacitor material for electric aircraft propulsion.

A possible alternative thermal capacitor material would be phase change materials (PCMs). Rather than relying on a material’s single-phase heat capacity, PCMs absorb heat by changing phase from solid to liquid or liquid to gas. A wide variety of phase change materials exist, with different melting points, heats of fusion, and material densities. While PCMs have been used in a wide variety of applications, more research should be done into their potential use in aviation systems.

4.6.3 Airframe Integration Challenges

The development of a solid model of the Hybrid XV-15 revealed challenges with the airframe integration aspects of hybrid-electric aircraft propulsion systems. Many electrical powertrain components such as motors, generators, and batteries have a low power density compared to conventional mechanical powertrain components. As such, it can be challenging to fit a hybrid-electric propulsion system into an airframe OML designed for a conventional propulsion system. On the other hand, the use of an electrical bus and power cabling allows for some adaptability in the placement of electric powertrain components—for example, the Hybrid XV-15’s battery occupies a large volume, but the use of cabling to transfer power allows it to easily fit into the cargo bay of the baseline vehicle’s fuselage.

The cooling requirements of hybrid-electric propulsion systems also impose integration challenges, particularly for rotorcraft that may spend considerable time under a high-power, minimal-airflow flight condition. The challenge of cooling electrical powertrain components such as motors and inverters arises primarily from their relatively low operational temperature limits. The potential benefits of some hybrid-

electric propulsion schemes may be severely diminished if the electrical components require a complex, heavy cooling system. Additionally, cooling requirements may impose a need for large external heat exchangers with negative impacts on the vehicle's aerodynamics.

Finally, a challenge encountered with the propulsion system airframe integration of the concept demonstrator was the routing of power cabling and cooling lines through the nacelle pivot points. The current nacelle pivots impose two significant design risks. First, the primary power cables and cooling lines take up nearly all of the pivot's internal cross-sectional area but the diameter of the pivot cannot be further increased without modifications to the wing or pivot design. Additionally, the routing of water coolant lines through an actuation point directly next to 770 kW DC cables is concerning. Applying this integration challenge more generally, while the use of an electric bus for power distribution is often seen as a tool for improving the feasibility of intensively distributed propulsion systems, there are still integration restrictions that are not fully understood at this point.

5. Conclusion

ESAero used the in-house-developed PANTHER program to investigate the hybrid-electric rotorcraft trade space and design process. The ability to model complex hybrid-electric propulsion systems, including vehicles with different types of powerplants, revealed many situations where conventional conceptual design methods are inadequate. Many hybrid-electric propulsion architectures alter the fundamental relationship between a vehicle's weight, powerplant size, and energy storage requirements. The indeterminate nature of hybrid propulsion sizing represents a novel flexibility in design possibilities that may yield performance, efficiency, operational, or safety improvements. However, it also greatly complicates the initial design process. Some aspects of the conventional design process can be easily modified to work with hybrid systems; for example, this report derived the endurance indicator and range indicator metrics as the hybrid vehicle counterpart to the conventional propulsion specific endurance and specific range metrics. Other design methods, in particular methods of design optimization, require further development to fully extract the benefits that hybrid-electric rotorcraft have to offer.

The tools and concepts developed by ESAero were applied to a trade study of different hybrid-electric propulsion architectures. Assuming "cutting-edge" component-level performance and scaling, the hybrid vehicles exhibited marginal mission performance capability compared to the conventionally powered vehicles. However, the trade study process demonstrated the difficulty in fairly comparing hybrid and conventionally powered vehicles. Many of the benefits of hybrid-electric propulsion systems, such as reduced noise, reduced emissions, or reduced lifecycle costs, are more difficult to model. When accounting for future performance improvements, electrical components are predicted to greatly outpace conventional propulsion components, a factor that must be accounted for when designing next-generation hybrid vehicles.

Finally, a hybrid-electric tiltrotor demonstrator based on the XV-15 was developed. The design of this vehicle showcased and explored many of the features of hybrid-electric propulsion architectures including decoupled power and energy management, fault-tolerant hybrid-electric propulsion architecture design, distributed propulsion via electrical buses, and battery-boosted gas turbine propulsion. In-depth PANTHER sizing methods and mission simulations demonstrated that the development of a large hybrid tiltrotor is possible at the current level of performance of electric propulsion technology. This further level of design iteration revealed additional complications with hybrid-electric propulsion architectures, including thermal management system design, mission path planning complexity, and airframe integration challenges. However, the hybrid vehicle demonstrated that the battery-boost concept reduced cruise fuel consumption by more than 10 percent, highlighting the potential benefits offered by hybrid-electric propulsion architectures.

6. References

1. Gibbs, Y. (ed.): NASA Armstrong Fact Sheet: NASA X-57 Maxwell. Armstrong Flight Research Center, Nov. 2017. https://www.nasa.gov/centers/armstrong/news/FactSheets/FS-109.html
2. Workhorse. Surefly Personal Helicopter Brochure. http://workhorse.com/surefly
3. Aurora Flight Sciences, LightningStrike XV-24A Demonstrator Successfully Completes Subscale Flight Test Program. Press Release. Manassas, VA, April 2017.
4. Fredericks, W., McSwain, R. G., Beaton, B. F., and Klassman, D. W.: Greased Lightning (GL-10) Flight Testing Campaign. NASA/TM-2017-219643, Langley Research Center, July 2017.
5. Johnson, W.: NDARC Design and Analysis of Rotorcraft Validation and Demonstration. American Helicopter Society Aeromechanics Specialists' Conference, San Francisco, CA, Jan. 2010.
6. Department of the Army: Operator's Manual for UH-60A Helicopter. TM 1-1520-237-10, Oct. 1996.
7. Maisel, M.: Tilt Rotor Research Aircraft Familiarization Document, NASA Ames Research Center and U.S. Army Air Mobility R&D Laboratory, Jan. 1975.
8. Magee, J. P., and Alexander, H. R.: A Hingeless Rotor XV-15 Design Integration Feasibility Study. NASA Ames Research Center. NASA-CR-152310-1, March 1978.
9. Federal Aviation Administration: Certification of Transport Category Rotorcraft. Advisory Circular No. 29-2C, May 2014.
10. National Academies of Sciences, Engineering, and Medicine. Commercial Aircraft Propulsion and Energy Systems Research: Reducing Global Carbon Emissions (2016). Washington, D.C.: The National Academies Press. doi:10.17226/23490.
11. Dever, T. P., Duffy, K. P., Provenza, A. J., Loyselle, P. L., Choi, B. B., Morrison, C. R., and Lowe, A. M.: Assessment of Technologies for Noncryogenic Hybrid-Electric Propulsion. NASA/TP-2015-216588, NASA Glenn Research Center, Jan. 2015.
12. EMRAX. User's Manual for Advanced Axial Flux Synchronous Motors and Generators. Jan. 2017. www.emrax.com.
13. Emsiso. EmDrive 500 Motor Controller Datasheet V2.0. www.emdrive-mobility.com/emdrive-500
14. Welstead, J. R., and Felder, J. L.: Conceptual Design of a Single-Aisle Turboelectric Commercial Transport With Fuselage Boundary Layer Ingestion. Paper No. AIAA 2016-1027, 54th AIAA Aerospace Sciences Meeting, San Diego, CA, Jan. 4-8, 2016.